University of Southampton

Faculty of Medicine

<u>Human Development and Health</u>

Identification of Novel Structures in Term Human Placenta Using Serial Block Face Scanning Electron Microscopy

by

Eleni Palaiologou (BSc, MSc)

Thesis for the degree of Doctor of Philosophy

June 2019

University of Southampton

<u>Abstract</u>

Faculty of Medicine
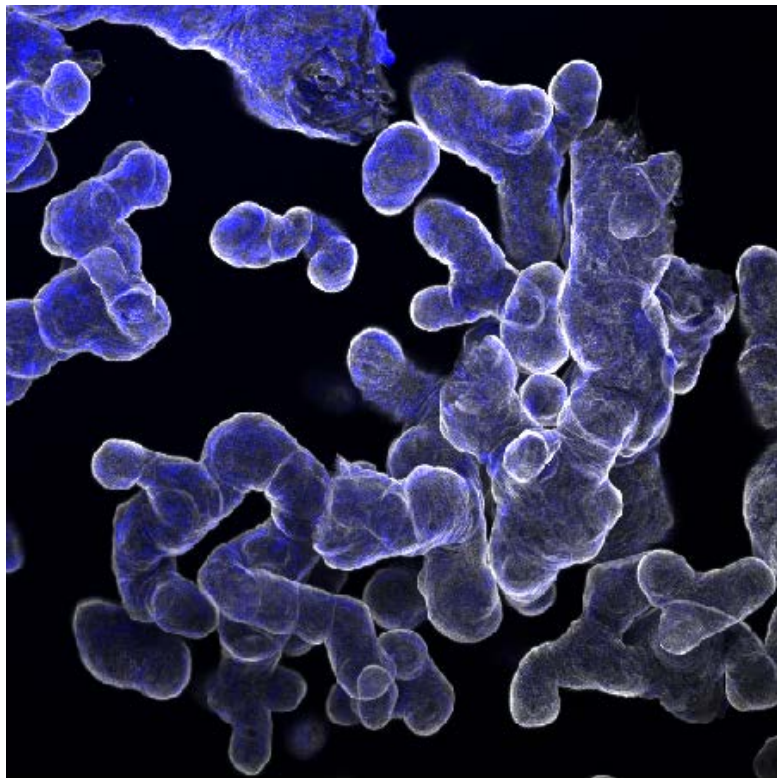Human Development and Health

Thesis for the Degree of <u>Doctor of Philosophy</u>

Identification of Novel Structures in Term Human Placenta Using Serial Block Face Scanning Electron Microscopy

by
Eleni Palaiologou

The placenta is a vital organ for the normal development and growth of the fetus. Inadequate placental function can result in poor fetal growth, which is associated with diseases in adult life. Understanding the structure and function of the normal placenta will enhance our understanding of the mechanisms underlying the placental dysfunction. Investigating the structure of the different cell types, the relationships between them and relating their structure to their function will result in a better understanding of the structures underlying placental function. Previous work on placental structure has primarily been based on 2D sections, however new 3D approaches are now available and this thesis has sought to use these to enhance our understanding of placental structure at different scales.

To investigate the placental structure new 3D imaging techniques have been utilised in this project. Serial block face scanning electron microscopy (SBFSEM) along with transmission electron microscopy and confocal laser scanning microscopy have been used to visualize in more depth the different cell types in the human placenta and also reconstruct cellular structures in 3D. A stereology approach was performed to allow quantifiable analysis of the different cellular structures.

SBFSEM revealed novel structures in the placenta that could not be observed in 2D. SBFSEM demonstrated a fetal erythrocyte protruding through syncytiotrophoblast, enabled the 3D reconstruction of a placental fibroblast and the interactions of fibroblast processes with other fibroblasts as a fibroblast network and in contact with giant extracellular vesicles. SBFSEM also revealed the existence of inter-endothelial protrusions (IEPs) found inside the endothelial cells in terminal villi of term normal placenta.

The existence of fibroblast networks, the interactions of fibroblast processes with giant extracellular vesicles and the identification of IEPs between endothelial cells demonstrate how 3D approaches allows us to better understand placental structure and the relationships between different cell types. Segmentation of thousands of slices generated by SBFSEM technique is a very time-consuming process and thus the development of automated segmenting techniques are necessary to reduce the amount of time and effort in segmentation.

Table of Contents

List of Tables

List of Figures

Declaration of Authorship

I, Eleni Palaiologou declare that this thesis and the work presented in it are my own and has been generated by me as the result of my own original research.

Identification of Novel Structures in Term Human Placenta Using Serial Block Face Scanning Electron Microscopy

I confirm that:

1. This work was done wholly or mainly while in candidature for a research degree at this University;

2. Where any part of this thesis has previously been submitted for a degree or any other qualification at this University or any other institution, this has been clearly stated;

3. Where I have consulted the published work of others, this is always clearly attributed;

4. Where I have quoted from the work of others, the source is always given. With the exception of such quotations, this thesis is entirely my own work;

5. I have acknowledged all main sources of help;

6. Where the thesis is based on work done by myself jointly with others, I have made clear exactly what was done by others and what I have contributed myself;

7. Either none of this work has been published before submission, or parts of this work have been published as: [please list references below]:

Chapter 3 has been published: (Palaiologou et al., 2017)

Signed: ……………………………………………………………………

Date: ……………………………………………………………………

Acknowledgements

Abbreviations

Abbreviations	Definitions
DOHaD	Developmental origins of health and disease
FGR	Fetal growth restriction
SGA	Small for gestational age
LGA	Large for gestational age
VEGF	Vascular endothelial growth factor
VE-cadherin	Vascular endothelial cadherin
MRI	Magnetic resonance imaging
Micro-CT	Micro computed tomography
TEM	Transmission electron microscopy
SBFSEM	Serial block face scanning electron microscopy
RT	Room temperature
PFA	Paraformaldehyde
TDE	Thiodiethanol
ECVs	Extracellular vesicles
STD	Standard deviation
SEM	Standard error of mean
IEPs	Interendothelial protrusions
ICM	Inner cell mass
BSA	Bovine serum albumin
DAPI	4'.6-diamidino-2-phenylindole

Chapter 1: General Introduction

1.1 Introduction

The placenta is a fetal organ, which forms the interface between the mother and the fetus. The placenta protects the fetus from harmful substances, ensures the transfer of nutrients from the mother to the fetus and serves as an endocrine organ, which produces hormones important for pregnancy. Failure of the placenta to support the fetus can result in poor fetal growth that is associated with higher rates of chronic diseases in adult life (Eriksson et al., 2011).

Placental structure is integral to placental function. Our understanding of placental structure is based largely on 2D imaging which has limitations, particularly in terms of visualizing the overall structure of the villous tree and the distribution of different cell types within the villi. This project will address questions about the relationship between placental structure and function utilizing 3D imaging techniques.

In this chapter, I will discuss how placental function affects fetal growth and lifelong health, outline placental development and structure at term, and discuss key aspects of placental structure, especially in relation to function.

1.2 Developmental Origins of Health and Disease

Epidemiological evidence, supported by studies in animals, suggests that suboptimal fetal growth is associated with lifelong health consequences (Gluckman et al., 2008). These observations led to the Developmental Origins of Health and Disease (DOHaD) hypothesis, which proposes that the fetal environment during pregnancy has consequences on the later health and well-being of the baby.

1.2.1 Epidemiological evidence for the DOHaD hypothesis in relation to birth weight

Epidemiological studies show an association between low birth weight and increased rates of chronic diseases in later life including heart disease, diabetes and cancer (Osmond and Barker, 2000, Gluckman et al., 2008). Studies of the Dutch Famine cohort suggest that the alterations to adult physiology are in response to fetal undernutrition (Roseboom et al., 2001). The Dutch Famine study used three periods of 16 weeks to distinguish between babies exposed to famine during late gestation (born between January and April 1945), mid gestation (born between April and August 1945) and early gestation (born between August and December 1945). This study showed that when there was severe food shortage the babies that were undernourished in late gestation had the highest mortality rate compared to the babies that were undernourished early and mid-gestation. It was also observed that babies undernourished in late gestation had reduced birth weight and increased risk of cardiovascular diseases, neurological defects and metabolic diseases (Roseboom et al., 2001).

Undernutrition during gestation can cause reduced fetal growth. However, there are other factors that can affect fetal development, among them is poverty, drug use, alcohol, smoking, maternal diseases, stress and environmental toxins (Lawn et al., 2005). Women in poverty are more likely to be undernourished during pregnancy leading to babies with low birth weight (Lawn et al., 2005).

1.2.2 Epidemiological evidence for the DOHaD hypothesis in relation to the placenta

As mentioned above the placenta is key to fetal development. While a number of early studies suggested relationships between placental weight and adult disease, these have not been supported by subsequent larger studies (Godfrey, 2002, Hemachandra et al., 2006). Instead, these larger studies suggest that there is a relationship between fetal/placental ratio and postnatal disease (Wallace et al., 2013, Matsuda et al., 2015). Placental/fetal ratio is a

marker of placental efficiency, i.e. how many grams of placenta you need to support a gram of fetus.

Studies in transgenic mice have shown that there are imprinted genes expressed in the placenta which can regulate placental growth and placental capacity to support fetal growth. In P0 IGF2 knockout mice there was reduced placental volume and surface area of the exchange barrier in the placenta (Fowden et al., 2011). These two structural alterations lead to reduced diffusion capacity of nutrients which in turn induced reduced fetal growth (Sibley et al., 2004). Studies of nutrient transfer across the P0 IGF2 knockout mouse placenta showed that initially small placental size was compensated for by expressing higher levels of glucose and amino acid transporters and enabling these placentas to meet fetal demand. However, as fetal demand increased towards the end of gestation the compensation was no longer able to meet fetal demand with a smaller placenta and fetal growth restriction (Constancia et al., 2005). The upregulation of placental nutrient transporters in this model is taken to suggest that the placenta is responding to fetal signals to regulate placental nutrient transfer in line with fetal demand.

A placenta's weight, size and shape may influence its ability to transfer nutrients to the fetus (Thornburg et al., 2016). Variations in the size and shape of the placenta reflect placental development including implantation, growth and expansion of the chorionic plate that in turn affect fetal growth (Barker et al., 2010). Lower placental weight predicts lower birthweight, and constraints in placental growth may influence the childhood growth (Baptiste-Roberts et al., 2009, Sibley et al., 2004). Combinations of the placental size and shape have been shown to predict coronary heart disease, hypertension and coronary heart disease in adulthood (Eriksson et al., 2011). However, these macroscopic measures are hard to relate to the underlying causes of poor placental function and fetal growth.

Most studies focus on the correlation between placental weight and macroscopic measures of placental size to lifelong health. However, macroscopic measures of the placenta do not provide good information on placental function. However, macroscopic measures cannot reveal the structures of specific cells that are responsible for the normal placental function, such as transfer of nutrients to the fetus, and how these cells interact with other cells or components in the villous stroma. To understand the normal placental function, we need to study the ultrastructural level of the normal placenta and identify how each cell type and the interactions between them contribute to the normal placental function. Little is known about the relationship between microscopic features of placental structure and how this is associated with lifelong heath. A better understanding of the placental structure is required to enhance our knowledge in the mechanisms underlying placental function as these are key to fetal development and lifelong health.

1.3 Embryonic Development

In humans the embryonic period starts at fertilization, when the egg is fertilized by the sperm and continues until the end of the 10th week of gestation (Vaillancourt and Lafond, 2009). The fetal development starts at the beginning of the ninth week of gestation, when the embryo is called fetus (Forgács and Newman, 2005).

1.3.1 Blastocyst formation

After fertilization, the zygote travels down the fallopian tube and it divides simultaneously three times (from the two-cell stage to the four-cell and then to the eight-cell stage) until it forms a ball of cells called the morula. The morula divides even further forming a cavity between the cells. This mass of cells with a cavity is called a blastocyst. The blastocyst consists of the inner cell mass (ICM) and the blastocyst cavity that are surrounded by

the trophectoderm cells (**Figure 1.1A**). The blastocyst reaches the uterus on the sixth day

after fertilization. On the seventh day, the trophectoderm of the blastocyst invade into the

endometrium of the uterus and implantation starts (**Figure 1.1B**). The trophectoderm cells

will give rise to the placenta and the embryonic membranes and the ICM to the embryo and

the extraembryonic mesenchyme layer (Wilcox et al., 1999). At later stages of gestation, the

extraembryonic mesenchyme layer forms the yolk sac (Castellucci et al., 1990b).
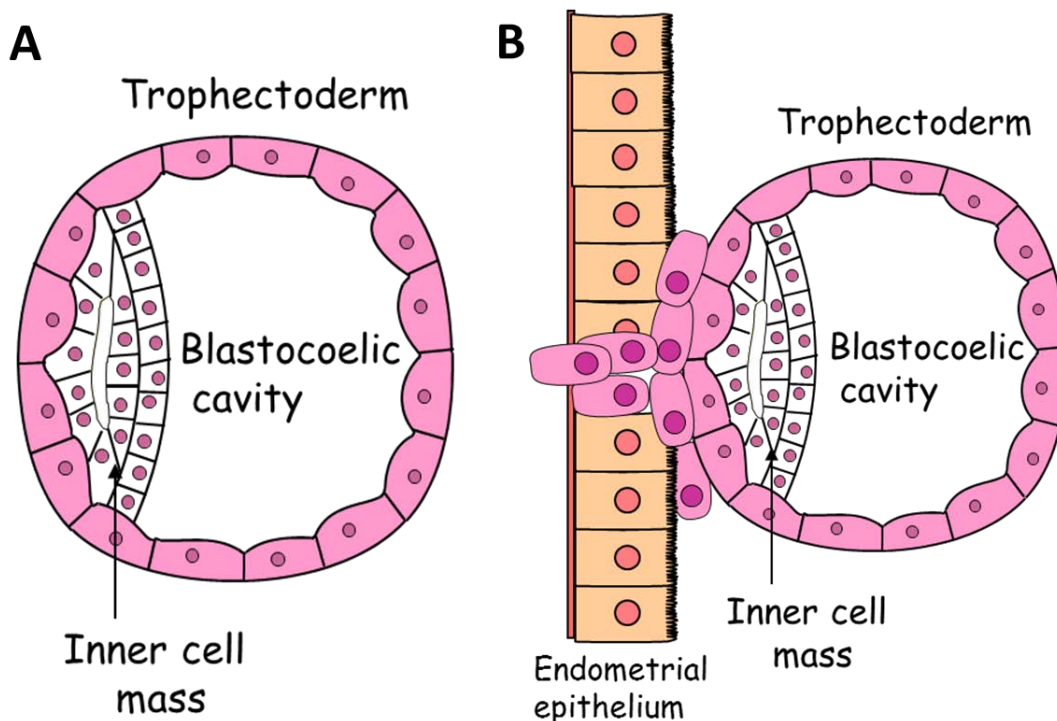
*Figure 1.1: **Blastocyst formation and implantation** A. The blastocyst consists of the inner cell mass, the cavity and the trophectoderm cells shown in pink that surround the cavity and the inner cell mass. **B**. Implantation of the blastocyst happens on the seventh day of gestation when the trophectoderm cells invade the endometrium.*

1.3.2 Different stages of the embryonic development

In the third week of gestation, neurogenesis begins with the formation of the noto-

chord. Following neurogenesis, the early embryonic vasculature begins to develop at the

onset of the fourth week. The heart, the liver and the lower limbs start to form on the fifth

week, while in the sixth week the development of the face begins. In the seventh week, the

6

head and the upper limbs of the embryo start to develop and the eight week is the last week of embryonic development (Vaillancourt and Lafond, 2009).

1.3.3 Fetal growth

Fetal development starts at the ninth week of gestation and continues until the end of pregnancy. During that period, the fetus is growing rapidly, its bones, skin, hair are growing, the digestive system is also developing and the baby's brain is growing fast. This fetal growth is supported by placental function, which is important to provide the oxygen and nutrients that are necessary for the normal fetal development. The placenta works as a filter to any harmful infections in the maternal bloodstream and allows the maternal blood to pass close to the fetal circulation allowing transport of oxygen, glucose and other nutrients (Siauve et al., 2015).

1.3.4 Abnormal fetal growth

Fetal nutrition plays a critical role in the development of the fetus. Suboptimal maternal nutrition or placental dysfunction during gestation can reduce the fetal nutrition and fetal growth (Bell and Ehrhardt, 2002).

Fetal growth restriction (FGR) occurs where a baby's growth in the womb falls below its initial growth trajectory, suggesting that it is growth restricted rather than just genetically small. The FGR babies fail to achieve their potential size at birth, but they may undergo postnatal catch up growth. Placental dysfunction, maternal vascular disease and early preeclampsia could also account for FGR babies (Odegard et al., 2000). FGR babies are at increased risk of mortality and in order to diagnose FGR serial ultrasound measurements are required (Resnik, 2002, Froen et al., 2004).

Small for gestational age (SGA) babies are those whose birth weight is below the 10th percentile for the gestational age (Xu et al., 2010, Resnik, 2002). SGA babies can either be constitutionally small or may be the result of FGR (Clayton et al., 2007). Approximately 70%-90% of SGA babies undergo postnatal catch up growth, which mainly occurs from 6 months to 2 years (de Ridder et al., 2008).

Although infants who grow well in the womb are less likely to suffer from chronic disease in adult life, large for gestational age (LGA) babies are also at increased risk of disease. LGA is defined as being above the 90th percentile for birth weight (Xu et al., 2010). LGA babies can have problems being born and may be at increased risk of obesity and diabetes in later life (Xu et al., 2010). LGA babies may occur where there is increased placental transfer of nutrients and are particularly common in diabetic pregnancies. It is important to note that some LGA and SGA babies may be genetically large or small and have grown normally for their genetic potential while others will be LGA or SGA because of altered placental nutrient supply (Xu et al., 2010).

1.4 Placental function

The placenta performs multiple roles in pregnancy helping the fetus to develop normally. The placenta is the barrier between the fetal and maternal circulations, mediates the exchange of nutrients, protects the fetus from xenobiotic molecules and serves as an endocrine organ by producing hormones essential to support pregnancy.

1.4.1 The Placental Barrier

The maternal and fetal circulations are separated by the syncytiotrophoblast, stroma and fetal capillaries of the placental villi, which form a physical barrier preventing mixing

of the two circulations. The syncytiotrophoblast is the main structure that determines which substances cross the placenta; e.g., nutrients and oxygen to the fetus and waste products back to the maternal circulation. A major role of the placenta is to protect the fetus against maternal hormones, toxins, infectious diseases and bacteria (Arechavaleta-Velasco et al., 2002). Even though most bacteria and xenobiotic molecules do not cross the placenta, some potentially harmful molecules are transferred across to reach the fetus. Certain drugs can diffuse across the placenta and in some cases are transported by placental transport proteins. One large molecule that can cross the placenta, via transcytosis, is maternal IgG, providing the fetus with passive immunity (Fouda et al., 2018).

1.4.2 Placental Nutrient Transport

One of the main functions of the placenta is the transfer of nutrients (amino acids, minerals, lipids, vitamins, glucose), to ensure normal fetal growth and development (Gude et al., 2004). Nutrients reach the fetal circulation through crossing each of the two membranes of the syncytiotrophoblast (the microvillous membrane facing the maternal circulation, and basal membrane facing the fetal circulation) and the fetal capillary epithelium. After crossing the fetal capillary epithelium, nutrients enter the fetal circulation (Walker et al., 2019). Transfer of oxygen and carbon dioxide occurs by simple diffusion and transfer of nutrients through transporter-mediated mechanisms which includes transporters located in the microvillous and basal plasma membranes of the syncytiotrophoblast. Glucose is transported through the transporter GLUT proteins (Stanirowski et al., 2017) and amino acids are transported through either accumulative, exchange or facilitated amino acid transporters all of which are members of the SLC (solute carrier) gene family (Simner et al., 2017).

1.4.3 Endocrine Function

The placenta also serves an endocrine function by producing hormones essential for maternal adaptation to support the pregnancy, these include progesterone, oestrogen, placental growth factor, placental lactogen and cytokines. Progesterone and oestrogen are two important hormones produced by the placenta and the corpus luteum. Progesterone is essential for suppressing the menstrual cycle and inhibiting the uterine contractions before the baby is ready to be delivered. Oestrogen is important for the regulation of fetal growth, placental steroidogenesis and onset of parturition. Human placental lactogen is another hormone produced by placenta that regulates embryonic development and metabolism and along with placental growth hormone, stimulates an increase in the availability of maternal glucose and amino acids. Human chorionic gonadotropin (hCG) is another important hormone that regulates the secretion of luteinizing hormone at around the eighth day after ovulation, taking over from the corpus luteum, and the secretion of progesterone and oestrogen during the first six weeks of pregnancy (Costa, 2016).

1.4.4 Metabolism of nutrients

The concentration of the amino acids in the fetal blood is determined by the fetal metabolism. Any change in the fetal metabolism may result in changes in the concentration gradient for facilitated diffusion of amino acids, which may have an impact on the transport of amino acids to the fetus. The placenta is responsible for the fetal amino acid supply, through interconversion of amino acids, or using them for protein synthesis, energy production and pathways for biosynthesis (Cleal et al., 2018a). Placental interconversion of amino acids results in the breakdown of one amino acid and the production of another, thus altering the composition of amino acids available for transport to the fetus. Placental metabolism

will therefore affect the concentration gradient of individual amino acids, which in turn affects the activity of the amino acid transporters (Lewis et al., 2013).

To conclude the placenta is an organ that plays a major role during pregnancy, ensuring normal fetal development and growth.

1.5 Development of the human placenta

Placental development starts following implantation, with the invasion of the trophoblast inside the endometrium and continues throughout gestation. The ability of the placenta to transport nutrients needs to increase throughout pregnancy to match increasing fetal demand. The capacity of the developing placenta must always match or exceed fetal demand otherwise fetal growth restriction will occur. Placental growth in early pregnancy exceeds the growth of the fetus, in the second and third trimester of the pregnancy though, placental weight increases at a much slower rate and it reaches a plateau around 95th day of gestation (**Figure 1.2**). This slow increase in placental weight is compensated by significant structural changes in the placenta, which result in an increase in the placental functional ability and more importantly transport of nutrients from the mother to the fetus (Schneider, 1996).
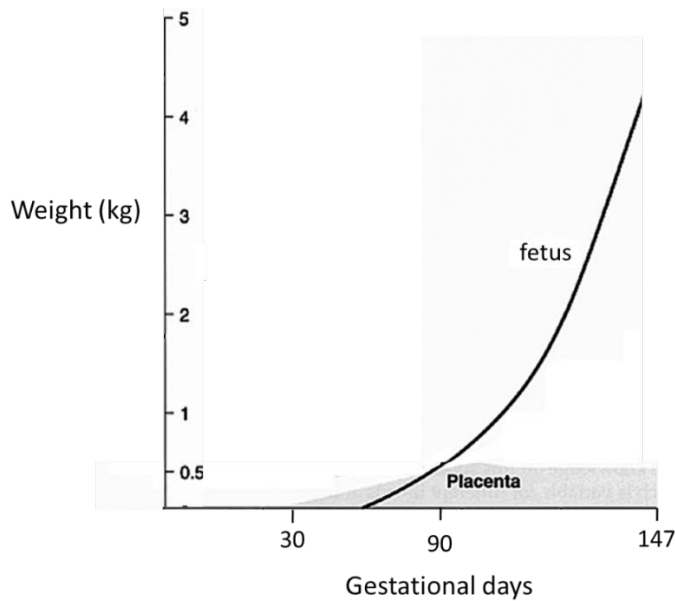
*Figure 1.2: **Human fetal growth compared to placental growth per gestational days.** Graph showing the increase of fetal growth getting closer to the end of gestation compared to the placental growth, which reaches a plateau after around 95th day of pregnancy. Figure modified from (Schneider, 1996).*

1.6 Placental structure at term

The normal full-term human placenta is usually a discoid organ, on average 22 cm diameter, 2.5 cm thick and weighing 500 g. The placenta has two external surfaces; the chorionic plate facing the fetus and to which the umbilical cord containing two umbilical arteries and one vein is attached, and the basal plate that abuts the maternal endometrium (**Figure 1.3A**) (Burton, 2006).

1.6.1 Stem villi at term

In term placenta, stem villi account for 20 - 25% of the total villous stroma and form the base of the villous trees, which in turn branch repeatedly to create a cotyledon 2 - 6 cm in diameter (**Figure 1.3 B**). The syncytiotrophoblast layer of the stem villi is uniformly thick and there are no vasculosyncytial membranes as in terminal villi.

Figure 1.3: *Diagram of the different scales of placentas used for different microscopes. A. maternal side of the placenta, the diameter is around 22 cm. B. a whole cotyledon around 2-6 cm in diameter which is perfused with a fluorescent agent. This image is produced from a micro-CT. C. a small piece of a cotyledon ranging 1-3 mm³ in size used to be observed under the confocal microscope. D. a smaller piece less than 1 mm³ in size is used to be processed for the scanning electron microscope. PE: pericyte, CA: capillary, CO: collagen in stroma, ST: syncytiotrophoblast, CT: cytotrophoblast, BS: basement membrane, EC: endothelial cell, MV: microvilli*

13

The stem villous stroma is characterized by condensed collagen fibres within which there are fibroblasts, macrophages and myofibroblasts. The fetal vessels in the stem villi are composed of arteries, veins and capillaries, which are large vessels with thick vessel walls. Stem villi have a mechanical role to support the villous trees and because they have large vessels, it makes it possible to regulate the distribution of the fetal circulations into fetal vessels. The presence of myofibroblasts in the stem villous stroma may potentially provide a contractile system in regulating the maternal circulation in the intervillous space (Farley et al., 2004).

The villous trees are surrounded by the intervillous space which contains maternal blood (Castellucci et al., 1990b). Maternal blood coming from the dilated maternal spiral arteries enters the intervillous space, bathes the villi and drains back through the endometrial veins. Therefore, there are no maternal blood vessels in the intervillous space. The villi, which are covered by the multinucleated syncytiotrophoblast, are lined with the intervillous space.

1.6.2 Intermediate villi at term

Immature intermediate villi are characterised by their bulbous structure and are continuations of stem villi. Intermediate villi have loose stroma consisting of macrophages (Hofbauer cells), more prominent vessels compared to stem villi, and a discontinuous cytotrophoblast layer. These villi are believed to be the main sites of exchange during the first and second trimester, since terminal villi are not yet differentiated (Castellucci et al., 1990b). Mature intermediate villi are long and peripheral branches of the villous trees, which lack fetal vessels in the stroma. Mature intermediate villi differentiate into terminal villi (Castellucci et al., 1990b).

1.6.3 Terminal villi

Terminal villi are the terminal branches of the stem villi and are linked to the later ones through the intermediate villi. They constitute nearly 40% of the villous volume in term placenta. These villi are characterised by a high degree of vascularization and highly dilated sinusoids (**Figure 1.4**). Terminal villi have less stroma compared to intermediate and stem villi and contain fetal capillaries. The fetal capillaries oppose against thin layers of syncytiotrophoblast forming vasculosyncytial membranes. The distance between the fetal vessels and the basement membrane of the syncytiotrophoblast is approximately 3.7 μm. This small distance makes terminal villi the most appropriate villi for diffusive exchange. Therefore, terminal villi constitute the fundamental functional units of the placenta through which the transfer of oxygen, electrolytes, carbon dioxide and nutrients occurs between the mother and the fetus (Castellucci et al., 1990b).
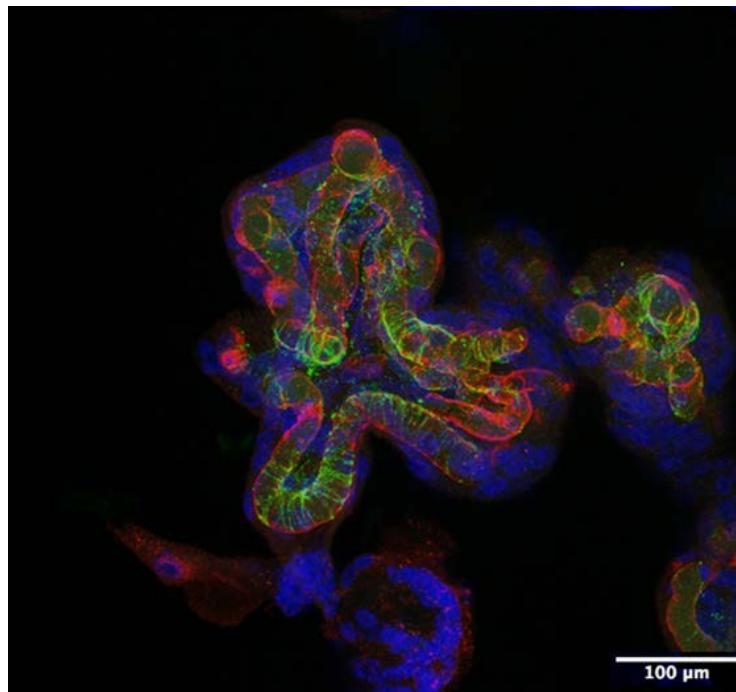
__Figure 1.4: Terminal villi in term placenta.__ Representative image showing the structure of fetal capillaries in chorionic villi. Blue: DAPI staining nuclei. Red: lectin staining the endothelial cells of the capillaries. Green: smooth muscle actin staining pericytes surrounding the capillaries. Figure produced by Professor Rohan Lewis.

1.7 The placental vascular system and blood flow

1.7.1 Fetal-placental vasculature

Fetal-placental vasculature is not only important for enabling the fetal blood flow through the placenta, which constitutes the major role of the placental function, but angiogenesis is also important for the development of the villous trees.

The formation of placental vessels is divided into two stages; vasculogenesis and angiogenesis. Vasculogenesis is the *de novo* formation of blood vessels, which in the placenta starts from the extra-embryonic layer of the blastocyst. The *de novo* formation of the blood vessels follows the development of the villous trees. After day 35 of gestation, vasculogenesis occurs only in the mesenchymal villi (Robin et al., 2009). Angiogenesis is the expansion of the vascular network from existing blood vessels by 'sprouting of endothelial cells and constitutes the creation of new vessel branches and also longitudinal growth of the pre-existing vessels (Kaufmann et al., 2004).

Fetal vessels in the placenta are derived from hemangioblastic cells derived from the mesenchymal cells of the trophoblast (Burton, 2006). The first vascular network that appears in the mesenchymal villi has no distinction between arteries, veins and capillaries. Around the eighth week of gestation, the *de novo* fetal vessels which are derived from the mesenchymal cells, fuse with the existing vascular nets, establishing the feto-placental circulation, which starts around the 12th week of gestation (Burton, 2006).

The effective feto-placental circulation commences at the end of the first trimester, when the number of fetal erythrocytes reduces dramatically, thus reducing the resistance to blood flow (Burton and Jauniaux, 2018). The reduction in the resistance of blood flow is followed by accumulation of connective tissue cells around the endothelial cells, which

results in transformation of primary fetal vessels into arteries and veins. After this transformation, one artery and vein are formed in immature intermediate villi and from this artery and vein a whole capillary network is formed (Burton, 2006).

Stem villous arteries are encircled by layers of smooth muscle cells. The arteries and veins are predominant in the stem villi. In mature intermediate villi, the fetal vessels constitute continuations of the large arteries and veins of the stem villi but in these villi fetal vessels have only pericytes and no smooth muscle. In mature intermediate villi, smaller arterioles and venules appear with smaller diameters and fewer layers of smooth muscle cells. The terminal ends of the arterioles and venules continue into capillaries. Capillaries are predominately found in terminal villi and are characterized by a capillary diameter ranging from 5-10 μm (for non-dilated capillaries), loss of smooth muscle, one layer of endothelial cells and formation of loops and coils (Kaufmann et al., 2004). The veins are characterized by thinner walls and less smooth muscle than arteries. Venules have a larger endothelial lumen, thus increased blood volume compared to arterioles, and thinner walls compared to veins (Kaufmann et al., 2004).

Initially the fetal capillaries are not surrounded by a basement membrane. By the third trimester, though, a few strands of basement membrane may surround the pericytes and may be in between the pericytes and the endothelial cells (Demir et al., 1989). The basement membrane is composed of proteins including laminin, fibronectin and collagen. The proteins that the basement membrane consists of are thought to be secreted by endothelial cells and pericytes (Myren et al., 2007).

1.7.2 Maternal blood flow

There are no maternal blood vessels in the placenta but blood is released from spiral arteries directly into the intervillous space. It then drains into the maternal veins whose localisation remains unclear. In the first trimester there is no blood flow as the spiral arteries are blocked by cytotrophoblast plugs. This means early placental and fetal development has to occur in a low oxygen environment (Burton, 2006). During this period, nutrients are secreted by uterine glands into the intervillous space, from where they can be taken up by placental villi (Burton et al., 2002).

Once the implantation process is completed, at the 11th week of gestation, the maternal blood flow begins. The removal of the cytotrophoblast plugs from the openings of the maternal spiral arteries defines the onset of the maternal-placental circulation (Burton et al., 2009). When the maternal-placental circulation is established, the exchange of oxygen and nutrients begins in the placental villi. The fetal oxygen uptake is regulated by the uterine and umbilical blood flow and the transplacental oxygen gradient (Jauniaux et al., 2003).

1.8 Placental cell types

1.8.1 Syncytiotrophoblast and cytotrophoblast

The placental villi consist of an outside layer of syncytiotrophoblast and inside this layer are the cytotrophoblast (**Figure 1.5**). In the first trimester there is a continuous layer of cytotrophoblast under the syncytiotrophoblast but by term they are reported to cover 44% of the basal surface of the syncytiotrophoblast (Jones et al., 2008). Beneath the trophoblast, lies the basement membrane, which separates the trophoblasts from the stroma.

The syncytiotrophoblast is a multinucleated syncytium, which forms a continuous layer that extends over the surfaces of all the villous trees. The syncytiotrophoblast is derived from cytotrophoblast fusion (Benirschke, 2012). The maternal facing surface of the

syncytiotrophoblast is covered in microvilli increasing its surface area by a factor five to sevenfold (Teasdale and Jean-Jacques, 1985). The syncytiotrophoblast is continually renewed by cytotrophoblast fusion. There are some regions where the syncytiotrophoblast becomes damaged and is replaced by fibrin deposits (Brownbill et al., 2000). The role of the syncytiotrophoblast is to act physiologically as an endothelium and it is involved in a majority of activities such as hormone synthesis, transports, metabolic regulation and immune defence (Benirschke, 2012).

The cytotrophoblast sits beneath the syncytiotrophoblast. Cytotrophoblast are considered to be the trophoblast stem cells since they continuously proliferate throughout gestation and differentiate into syncytiotrophoblast (Castellucci et al., 1990b). During the first trimester, cytotrophoblast cells appear to have a cuboidal shape and form a less complete layer. During the second trimester, the cytotrophoblast cells have a flatter shape (Mori et al., 2007a). A recent study revealed that the cytotrophoblast cell bodies and their processes cover 44% of the normal term placental villi (Jones et al., 2008).

1.8.2 Non-cellular components of the stroma

The villous core of the terminal villi, the stroma, consists of everything from the basement membrane under the trophoblast to the basement membrane surrounding the feto-placental blood vessels. In more detail, the stroma consists of loose connective tissue containing macrophages, fibroblasts and the trophoblast basement membrane. The trophoblast membrane consists of loose connective tissue and separates the trophoblast from the stroma. Among the fibroblast and macrophages, there are collagenous fibres, which form unorientated meshworks (Benirschke, 2012). The fibres differ in diameter ranging from less than 5 µm up to 20 µm. The amount of collagenous fibres increases from the mesenchymal stroma which is in mesenchymal villi to fibrous stroma found in stem villi (Benirschke, 2012).

There are distinct changes in the stroma in different parts of the villous trees. Mesenchymal villi have primitive stroma, immature intermediate villi have fluid filled stromal channels, stem villi have dense fibrous stroma, mature intermediate villi have less dense stroma, while terminal villi have capillaries that cover more than 50% of the stromal core (Benirschke, 2012).

1.8.3 Fibroblasts

Fibroblast is a cell type of the stroma that is characterized by its long and thin processes that create a branched cytoplasm, which surrounds the nucleus (**Figure 1.5**). Due to their star-like shape fibroblasts are also known as active stellate fibroblast cells (Ravikanth et al., 2011). Fibroblasts play an important role in synthesizing the extracellular matrix and producing collagen (Avery et al., 2018).

Many fibroblasts are not isolated cells but can form complex networks (Langevin et al., 2004). Fibroblast networks may be more likely to withstand the stress caused from mechanical forces compared to loose individual fibroblast cells (Kessler et al., 2001). Therefore, fibroblast networks may play an important role in a body-wide signalling system responding to mechanical forces and induce pathways that influence other physiological processes (Langevin et al., 2004). In placenta the role of fibroblast networks is unclear but according to the above mentioned fibroblast networks may play a role in coordinating the movements of the placenta villi and may respond to the mechanical stresses from the mother and the baby. However, in some diseases like Alzheimer's, fibroblast networks may impair cell migration and cell viability (Chirila et al., 2013).

In human placenta, stromal fibroblasts are first observed at the beginning of the third month of gestation at the same time as the formation of immature intermediate villi. They are derived when fetal mesenchymal cells start to acquire desmin as a cytoskeletal filament

and then differentiate into fibroblasts (Burton, 2006). The newly formed fibroblasts found in stem and immature villi have elongated stellate cell bodies, sparse cytoplasm and long, thin processes (Castellucci et al., 2000). In terminal and mature intermediate villi fibroblasts have shorter processes and more abundant cytoplasm (Sati et al., 2008).

There is limited research on the existence of placental fibroblasts networks and even though the role of placental stromal fibroblasts is unclear, they are believed to be important in the production of collagen fibres found in the stoma.

1.8.4 Macrophages

Placental macrophages are referred to as Hofbauer cells. Like stromal fibroblasts the Hofbauer cells are derived from the differentiation of hemangioblastic cells from the mesenchymal cells. The role of Hofbauer cells in the placenta is unclear. Histological studies have shown that placental macrophages have large numbers of lysosomes, mitochondria, rough and smooth endoplasmic reticulum and abundant Golgi bodies. Hofbauer cells *in vitro* have an active phagocytic ability and immunological role against pathogens (Ingman et al., 2010).

1.8.5 Pericytes

Pericytes were first called as "Rouget cells" and then as pericytes describing their close proximity to endothelial cells (Bergers and Song, 2005). Pericytes are periendothelial mesenchymal cells that surround blood vessels and capillaries (Birbrair et al., 2017). Pericytes are thought to belong to the same lineage as vascular smooth muscle cells, macrophages and fibroblasts. However, there is no single molecular marker to identify the pericytes and distinguish them from other cell types (Armulik et al., 2011). Pericytes surround endothelial cells forming long finger like processes, which encircle many capillaries (**Figure**

1.5). Placental pericytes differentiate from the same hemangioblastic progenitor cells as the endothelial cells. Placental pericytes are easily distinguished from endothelial cells since they contain a less-electron dense cytoplasm and fewer microfilaments compared to endothelial cells and also by the fact that they are on the outside of the endothelial cells (Bergers and Song, 2005). Pericytes communicate with endothelial cells with paracrine signalling or physical contact and are believed to regulate blood flow (Bergers and Song, 2005, Fakhrejahani and Toi, 2012). The density of pericytes as well as the proportion of pericytes coverage to the endothelial abluminal surface varies between different organs. The central nervous system has the highest pericyte coverage vasculature with a 1:1-3:1 ratio between endothelial cells and pericytes and a 30% coverage of the pericytes in the abluminal surface (Mathiisen et al., 2010). The density of pericytes in other tissues is significantly lower. The human skeletal muscle has a 100:1 ratio between endothelial cells and pericytes (Diaz-Flores et al., 2009).

An important role of the placental pericytes may be to allow endothelial cells to differentiate and multiply from vascular branches, thus promoting angiogenesis (Bergers and Song, 2005). Pericytes also promote endothelial cell survival through the secretion of proteins, which encourage the secretion of vascular endothelial growth factor (VEGF) (Franco et al., 2011). The proportion of vessels that are surrounded by pericytes, increases as gestation advances (Challier et al., 1999), thus implying that as the vascular network advances, the plasticity of the vessels is reduced. Pericytes may also have a contractile role in regulating vessel diameter in the placenta (Challier et al., 1999). The strongest evidence for pericyte constriction comes from work in rat renal tubules where pericytes were shown to constrict potentially regulating blood flow (Crawford et al., 2012). However, whether or not pericytes have a contractile role has not been determined in the placenta.

1.8.6 Placental Endothelial cells

Endothelial cells in the placenta are derived from hemangioblastic cells during vasculogenesis in the first trimester (Jones and Fox, 1991).

In the placenta, the fetal capillary endothelium is non-fenestrated, i.e. there is absence of transcellular pores, and any diffusion of hydrophilic solutes would need to occur through the endothelial interface between adjacent endothelial cells. In the placenta, endothelial interfaces between adjacent endothelial cells are thought to have similar permeability to those in skeletal muscle (Leach and Firth, 1992). Frequently, the cell membranes of the endothelial cells form leaf-like folds into the endothelial lumen of the capillary (Leach, 2002). The feto-placental endothelial cells contain many cisternae of rough endoplasmic reticulum, mitochondria, Golgi bodies and some secretory droplets (Jones and Fox, 1991).
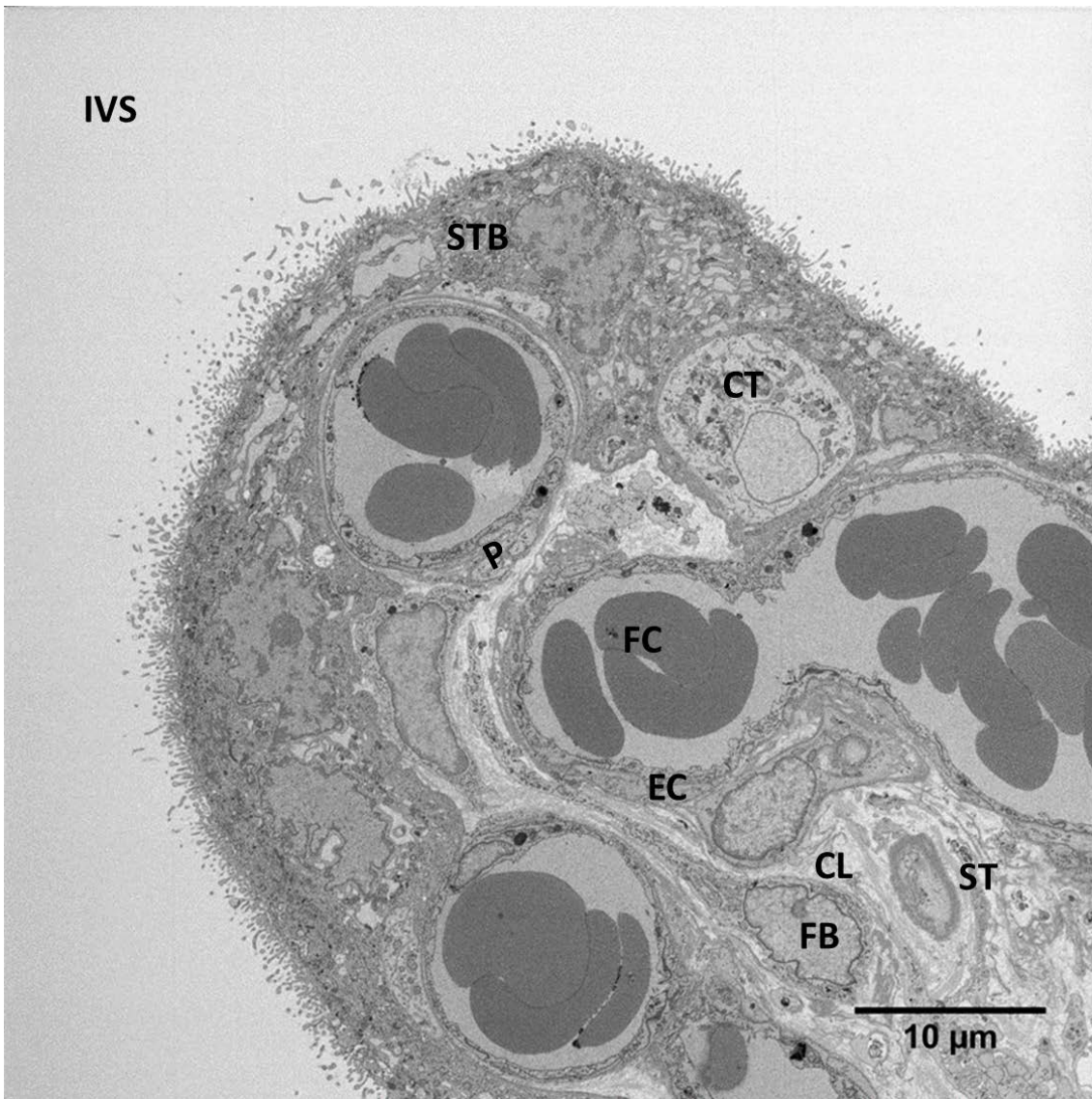
Figure 1.5: ***A diagram showing the arrangement of different cell types in placental villi.*** *The first layer is the syncytiotrophoblast (**STB**), then the cytotrophoblast (**CT**), the stroma (**ST**), the fetal capillary (**FC**) and the endothelial cells (**EC**). The fetal capillaries are surrounded by pericytes (**P**). In the stroma there are the fibroblasts (**FB**) collagen fibres (**CL**).* ***IVS****: intervillous space.*

Endothelial cells are important in maintaining the barrier function of the vasculature. Endothelial cells seal the vessel wall by junctional complexes within the endothelial interface between adjacent endothelial cells. The junctional complexes maintain the connection between neighbouring endothelial cells. These junctional complexes may include tight junctional molecules, components of adhesion junctions such as vascular endothelial cadherin (VE-cadherin), platelet endothelial cell adhesion molecule, leukocyte cell adhesion mole-

cule and also intercellular adhesion molecule (Dejana et al., 2009b). Endothelial cell junctional molecules play crucial role in inflammation and pathological conditions, since there is evidence that in response to injury or infection, there is controlled opening or loosening of endothelial cell interface between adjacent endothelial cells (Reglero-Real et al., 2016). Endothelial cells adhere to one another through cell junctions (Lievano et al., 2006).

The two main types of endothelial interface between adjacent endothelial cells that are present in the placental capillary endothelium are tight junctions and adherens junctions. The tight junctions help maintain cell polarity between the luminal and abluminal side of each endothelial cell and regulate the tightness of the junction which determines the rate of paracellular diffusion between two neighbouring endothelial cells. The tight junctions consist of transmembrane adhesive receptors which are different claudins that define the selective permeability of solutes through tight junctions and cytoplasmic adaptors some of which are occludin, cingulin and ZO-1 which contribute to the adhesion of the neighbouring endothelial cells as shown in (**Figure 1.6**) (Bazzoni and Dejana, 2004). Tight junctions restrict the leakage of transported solutes and water and allow the passage of small ions. Adherens junctions are thought to serve as a bridge connecting the actin cytoskeleton of neighbouring cells through direct interaction (Leach, 2002). The adherens junctions also consist of transmembrane adhesive receptors such as VE-cadherin and cytoplasmic adaptors some of which are catenin and plakoglobin as shown in (**Figure 1.6**). Adherens junctions could also serve in the remodelling of the vascular endothelium and as mechanotransducers since they contain VE cadherin which may act as a transducer of shear stress signal in combination with the VEGFR factor (Bazzoni and Dejana, 2004).

A recent study in rat arteries demonstrated that ageing impaired the activity of adherens junctions by reducing the activity of VE- cadherin. Impaired role of adherens junctions resulted in a reduced endothelial barrier, endothelial dilation dysfunction, increased

inflammatory activity and formation and expansion of atherosclerotic plaque (Chang et al., 2017). Another recent study (Yamazaki et al., 2019) associated the loss of tight junctions in the brain endothelium with the Alzheimer's disease. The study also showed that the loss of tight junctions resulted in the blood-brain barrier disruption, which can impair neuroinflammation and changes in the neurovascular unit.

In the human placenta, both tight and adherens junctions exist in the vascular bed but in vitro study has shown that there is molecular heterogeneity in tight and adherens junctions which is dependent on the position in the villous tree (Leach et al., 2000). There is absence of occludin and plakoglobin in the tight and adherens junctions respectively, in the terminal villous capillaries compared to the arteries, veins and arterioles which have occludin and plakoglobin. This suggests that the junctions in the fetal capillaries in the terminal villi are less stable and so there is increased plasticity for remodelling and exchange of solutes in the fetal capillaries compared to the bigger vessels (Leach et al., 2000).
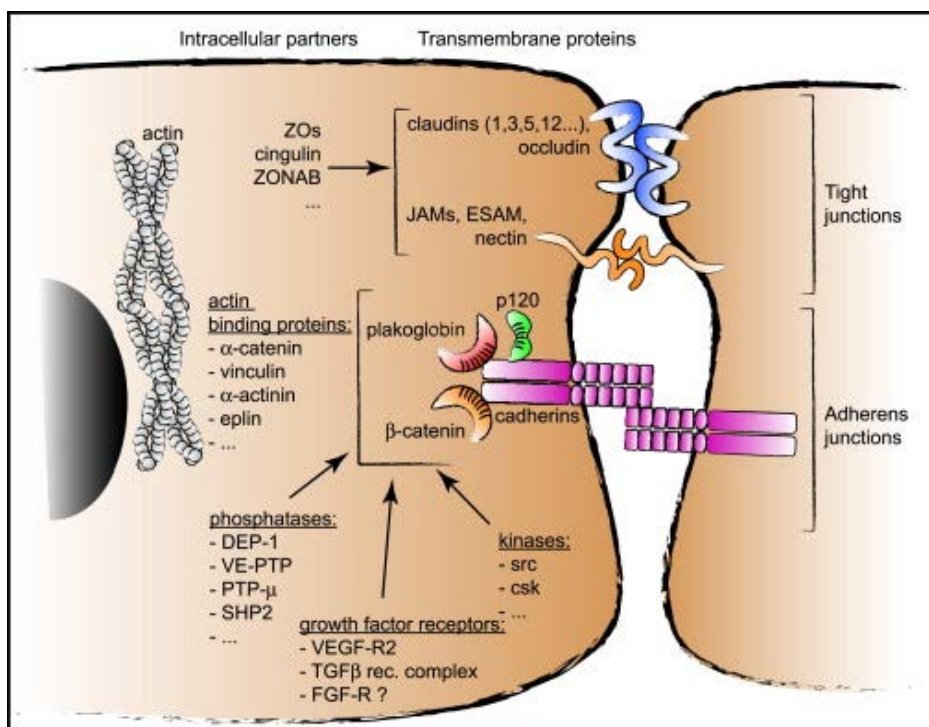
Figure 1.6: ***Endothelial interface between adjacent endothelial cells.*** *The two endothelial cells can be connected by adherens junctions that connect the cytoskeleton of the neighbouring cells or by tight junctions, which are responsible to maintain cell polarity and the tightness of the junction determining the rate of paracellular diffusion. Figure reproduced from(Dejana et al., 2009a).*

Endothelial cells can also connect with adjacent cells via interdigitations at the borders of the adjacent endothelial cells in cornea capillaries (Masterson et al., 1977) and in umbical vein endothelial cells (Kurzen et al., 2002) (**Figure 1.7**). These endothelial interdigitations have tight and adherent junctions and increase the tightness of the endothelial barrier by reducing the rate of paracellular diffusion (Kurzen et al., 2002). In lymphatic vessels, these interdigitations are known as overlapping flaps. These flaps contain adherens and tight junctions and can open and close without disrupting the structural integrity of the endothelial cells (Baluk et al., 2007).
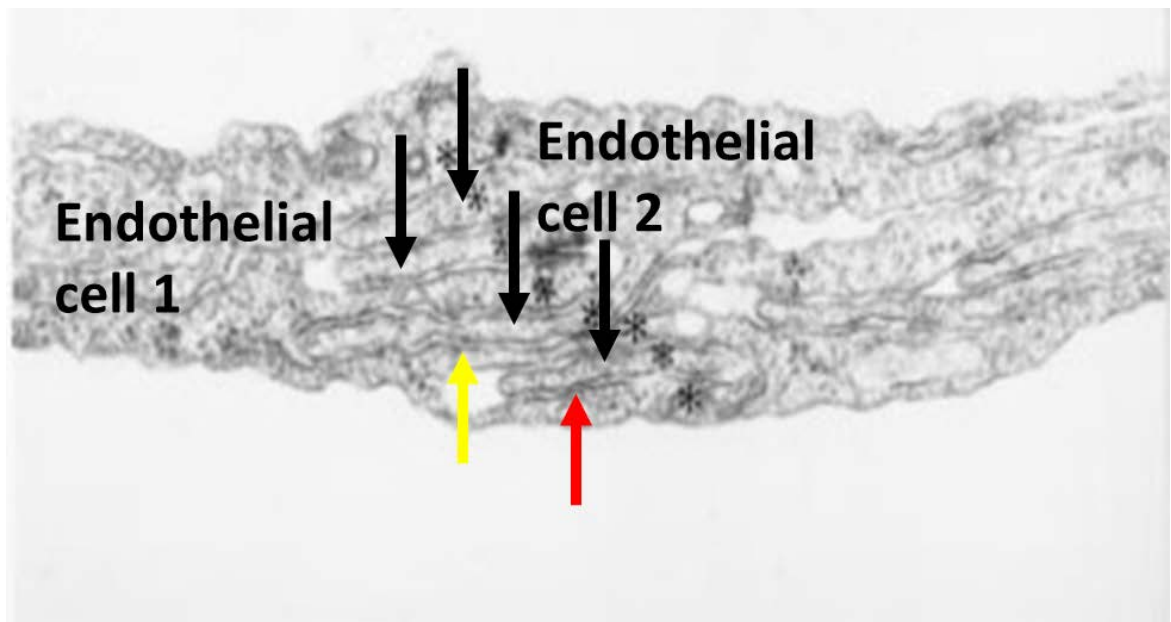
*<u>Figure 1.7:</u> **Interdigitations between adjacent endothelial cells.** The adjacent endothelial cells are in contact via the interdigitations shown with black arrows. The red arrow points to a tight junction and the yellow to an adherens junction. Figure reproduced from (Kurzen et al., 2002).*

Fibroblasts can communicate with other fibroblasts via similar junctional complexes. In rat tendon fibroblast networks are formed via gap junctions (McNeilly et al., 1996). Fibroblast networks are also formed in the junctional region of the zebrafish heart. Serial block face scanning electron microscopy (SBFSEM) has shown that in zebrafish the cardiac myocytes with each other via adherens junctions or desmosomes (Lafontant et al., 2013). Fibroblast networks have also been found in human heart, and it has been shown that

fibroblasts communicate with neighbouring fibroblasts via connexins and cadherins (Banerjee et al., 2006).

Evidence of endothelial heterogeneity in terms of their structure and function has been reported recently in four different organs heart, liver, lung and kidney (Marcu et al., 2018). A study has suggested endothelial heterogeneity in placenta between different vascular beds. This study showed that umbilical vein endothelial cells had a more polygonal phenotype compared to the microvascular endothelial cells that appear to be more elongated (Aird, 2012). There is also heterogeneity with different response of arterial endothelium to shear stress with an increase of expressing arterial markers, compared to the vein endothelial cells (Casanello et al., 2014). It has also been reported that there is different response of microvascular endothelial cells to vasoactive drugs compared to the umbilical vein endothelial cells (Lang et al., 2003). Another study also demonstrated that there is heterogeneity in microvascular and macrovascular endothelial cells in term human placenta regarding different immunoreactivity to diverse molecular markers (such as IgG and transferrin) suggesting functional endothelial heterogeneity in human placenta (Lang et al., 1993).

While a report (Nikolov and Schiebler, 1973) suggests that there is endothelial heterogeneity in placenta based on electron microscopy imaging of organelles, other researchers do not see this and suggest that it may have arisen due to sampling (Karimu and Burton, 1995). Investigation of the different types of placental endothelial cells could be achieved through microscopy using 3D imaging techniques. 3D imaging enables the 3D reconstruction of endothelial cells, which in turn enables the visualization of different types of cells if there are, and the relationships between neighbouring endothelial cells. This will tell us whether there are different endothelial cell populations and if so, whether there are regional variations in distribution inside each cell or between cells throughout the villous tree.

1.9 Imaging techniques

Various techniques have been utilized to image placental structure at different scales either in 2D or 3D (Siauve et al., 2015). So far, most of the studies have investigated the placental structure utilizing 2D imaging techniques. Advances in technology have enabled the use of 3D imaging techniques which can provide in depth visualization of placental structure. 3D imaging techniques available now include magnetic resonance imaging (MRI), Doppler ultrasound, micro-CT, light sheet microscopy, confocal microscopy and serial scanning electron microscopy.

1.9.1 Traditional imaging and stereology

Traditional microscopy used thin sections from wax embedded tissue, resin embedded tissue, or cryo-sections under the light microscope or resin embedded sections under the electron microscope. These approaches only provided 2D information but summary 3D information could be derived using morphometry. Stereology is a way of analysing 2D histological images to generate 3D data. Stereology uses random systematic sampling to provide quantitative analysis of size, shape and number of objects. More specific, stereology uses specific sampling techniques and mathematical approaches to estimate volumes, surface areas, and lengths of tissue features (Mouton, 2002). In placenta, morphometry allows quantitative 3D information to be determined from a 2D image (thin tissue section) in which the volume and dimensions of the capillaries and villi are estimated (Mayhew et al., 2004). To achieve systematic random sampling in the placenta, one approach could be to place a transparent sheet with quadratic pattern of holes on top of the placenta and take placental samples where the holes overlie the placenta. Then these samples could then be cut into smaller pieces and every other slice could be visualized under the microscope. The images produced by the electron microscope could be randomly overlaid by a grid consisting of four vertical

and four horizontal lines. The points of the grid count the volumes of the different cellular structures, while the sites where the horizontal lines intersect with a cellular compartment count the surface areas of these compartments (Mayhew, 2006). However, stereology provides limited information of the branching of villi, and length of capillaries (Mayhew et al., 2008).

1.9.2 Wholemount confocal microscopy

Wholemount confocal microscopy provides a high optical resolution (the shortest distance between two points so that they can be distinguished by either the observer or a camera as two different points and not as a single dot). This microscope uses a point illumination and a pinhole in an optical plane in front of the detector to eliminate the out-of-focus signal and allowing optical sectioning into the tissue. In confocal microscopy the beam scans across the sample in horizontal plane by using oscillating mirrors and the scan speed is as slow as to provide better signal-to-noise ratio, leading to increased contrast and higher resolution. Confocal laser scanning microscopy enables the reconstruction of a 3D structure from the obtained images by collecting sets of images at different depths of the sample (Wright and Wright, 2002). These stacks of images provide a high resolution and an in depth discrimination of the sample, thus enhancing the study of cellular and to a limited extent sub-cellular structures, and also the subpopulations of different cell types in the tissue (Jonkman and Brown, 2015). Therefore, confocal microscopy provides a direct, non-invasive, serial optical sectioning of thick, living specimens with a minimum of sample preparation. However, this technique is useful only in small pieces of tissue around 1-3 mm^3 and the z depth cannot be lower than 200 nm (Takizawa and Robinson, 2006).

1.9.3 Transmission Electron Microscopy

Transmission electron microscopy (TEM) is a high-resolution type of microscope in which an electron beam is transmitted through thin sections around 100 nm thick. The electron beam travels from the electron gun through a condenser lens creating a small and thin beam which hits the thin specimen. When the beam hits the specimen, some of the electrons are transmitted depending on the thickness and electron transparency of the specimen. The transmitted electrons are focused by the objective lens into an image which is captured by a digital camera (Goggin et al., 2016).

1.9.4 Serial scanning electron microscopy approaches

Serial scanning electron microscopy approaches allow the generation of big datasets of serial images of the specimen. In the past researches used to cut serial sections by hand, then scan them in the transmission electron microscopy (TEM) and line all the TEM images up in order to make a 3D reconstruction of the sample (Heppelmann et al., 1989). There are currently four ways generating stacks of electron microscopy images; serial section transmission electron microscopy (ssTEM), automated tape-collecting ultramicrotome scanning electron microscopy (ATUM-SEM), serial block face scanning electron microscopy (SBF-SEM) and focused ion beam scanning electron microscopy (FIBSEM).

In serial section transmission electron microscopy sections are cut by hand in an ultramicrotome and then collected onto grids. Sections are imaged in a TEM and then a camera can acquire images. Even though the sample is not completely destroyed and part of the sample can be re used, this manual sectioning is prone to errors and is also labour intensive. Moreover, some sections may be lost or get folded or wrapped, which limits the number of sections (Bock et al., 2011, Takemura et al., 2013, Atasoy et al., 2014). In the auto-

mated tape-collecting ultramicrotome scanning electron microscopy sections are cut automatically and collected on an electrically opaque tape (Hayworth et al., 2014). This allows the cutting of thousands of slices as thin as 30 nm. These sections are then stored on silicon wafers and imaged in a scanning electron microscope. In focused ion beam scanning electron microscopy, slices are cut using a focused ion beam (Knott et al., 2008). This allows ablation of sections as thin as 5 nm with a resolution of less than 5 nm. It also provides a large number of consecutive images since sections do not suffer from wrapping or getting lost. However, focused ion beam scanning electron microscopy provides limited field of view less than 0.1 mm^2 (Knott et al., 2008).

SBFSEM allows the generation of high-resolution image stacks of small areas of tissue allowing 3D reconstruction. This microscope consists of an ultramictorome mounted inside the vacuum chamber of a scanning electron microscope. Samples are fixed, stained with heavy metals and finally infiltrated in an epoxy resin. The electron beam scans the surface of the block face of the sample, an image is generated, the sample is lowered down and then the ultramicrotome cuts a thin section (usually around 50 nm) from the block face (**Figure 1.8**). After the section is cut, the block face is raised to the focal plane and imaged again. SBFSEM can cover large fields of view around 1 mm^2, generate thousands of serial high-resolution 3D images and large datasets (Goggin et al., 2016).

SBFSEM has been widely used to study cellular structures at the nanoscale and reconstruct different cell types in 3D in a range of tissues including kidney, bone, brain and liver. Research has been conducted in studying the kidney and more specific the complicated cellular structure of the podocytes (Ichimura et al., 2015). Another study has emphasized the significance of using SBFSEM to enhance the visualization of the glomerulus and especially the novel podocyte protrusions into the glomerular basement membrane in the glomerular disease (Randles et al., 2016). This study revealed that SBFSEM enabled the 3D

construction of the diseased glomerulus basement membrane which has not been observed previously. This 3D reconstruction enabled to understand structural differences in the disease compared to the normal glomerulus, enhancing the understanding of the mechanisms of the glomerular barrier dysfunction in the glomerular disease. SBFSEM has also been used to study the bone structure and more specific the osteocytes (Goggin et al., 2016). This study identified novel microstructural phenotypes in the osteocytes that could not be observed before using other imaging techniques, and SBFSEM also revealed the complex osteocyte and lacuna-canalicular network. The identification of the novel osteocyte processes suggested the importance of the SBFSEM to study more in depth the structure of osteocytes which will enhance the understanding of the role of the osteocytes in bone development and aging. SBFSEM has also been used to visualize thin axons and synapsis in rodent brain tissue, suggesting the possibility of completely reconstruct in 3D the connectivity of neuronal circuits (Denk and Horstmann, 2004). SBFSEM has also been used to visualize the shape and the 3D arrangement of the parenchymal cells, the hepatic sinusoids and the bile canalicular network in the rat liver (Shami et al., 2016). This study emphasized the significance of SBFSEM in providing large volumetric information in a relatively timely and automated manner and enabling the 3D reconstruction of novel structures with a higher detail than confocal microscopy. SBFSEM successfully demonstrated how the parenchymal cells interact with the novel 3D complex bile canalicular network and enhanced our knowledge in visualizing the complicated microarchitecture of the liver which has not been observed before. The study concluded that understanding the complex structure of normal liver tissue will enable the comparison to the diseased one.
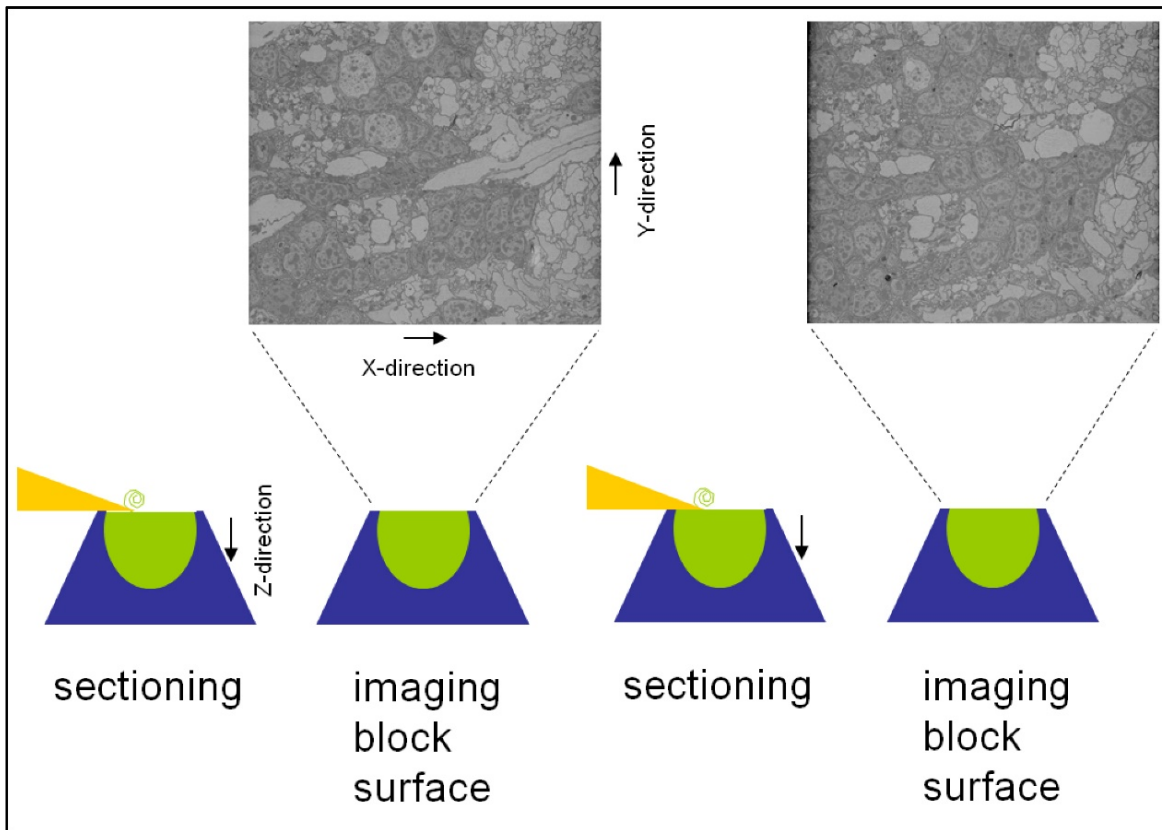
Figure 1.8: ***Serial block face scanning electron microscopy****. The image displays the process of serial block face scanning electron microscope. At first, the blade shaves the surface of the block face, then the electron beam scans the block face and an image is produced. This process keeps going on until the end of the block face of the sample.*

The major advantage of the focused ion beam scanning electron microscopy and SBFSEM techniques is that the sections are not folded or wrapped, which affect the data quality and the subsequent data analysis. Thus, these techniques allow the generation of large datasets. However, in both FIBSEM and SBFSEM the samples are destroyed and cannot be used again (Lichtman and Denk, 2011). In contrast, the major advantage of both the ATUM-SEM and ssTEM is the fact that the sample is not completely destroyed and therefore part of the sample can be re used, more sections can be cut and observed under different microscopes and different resolution and in multiple times, or even at the same time. Thus, ATUM-SEM and ssTEM reduce the acquisition time of images compared to the SBFSEM and FIBSEM techniques. However, ATUM-SEM and ssTEM are both labour intensive and

there is always an increased risk of sections get lost or folded, which in turn reduces the number of dataset (Lichtman and Denk, 2011).

1.10 Aims and objectives

In order to understand placental dysfunction we first need to investigate the normal placenta. A key determinant of placental function is structure, which can be assessed through visualising overall villous structure and relationships between different cell types. Placental structure has traditionally been studied using 2D imaging techniques. However, 2D imaging provides limited information about the interactions of different cells and how these cells are distributed within the villous tree. New 3D imaging techniques enhance our knowledge in studying more in depth the structure of the human placenta, since 3D imaging can demonstrate how placental cell types are distributed in relation to the structure of the villus tree itself and the different cells within the villous tree. This 3D picture of the villi will allow us to develop hypotheses about how these cells may interact and the functional implications of this. Developing a better understanding of the placental cellular relationships will provide an improved basis for us to understand how these cells interact and their function within the placenta.

The overall aim is to use 3D imaging techniques to study the placental cellular "Interactome". The cellular interactome is the whole set of cellular interactions in a particular tissue and how these contribute to its overall function. Once we know how these cells relate to each other, we will be better placed to understand their function. My objectives are to:

- Identify novel structures in the human placental syncytiotrophoblast and its basement membrane

To achieve this a placental sample was collected, fixed and processed for SBFSEM. Segmenting the stack generated from the SBFSEM, allowed the visualization of a novel structure which demonstrated the stretching abilities of the syncytiotrophoblast and the loose connection with the basement membrane.

- Identify novel structures in the placental stroma and the relationships between them

To achieve this novel 3D reconstruction of the placental fibroblast structure was followed by 3D reconstruction of fibroblast networks. The fibroblast networks were quantified in eight different placentas. High-resolution TEM images of giant ECVs to describe their structure was followed by calculations of their length and width and quantification analysis in eight different placentas.

- Identify novel structures within placental endothelial cells

To achieve this 3D reconstruction and high resolution TEM images were provided to study the structure of novel interendothelial protrusions. Quantification analysis of both the endothelial interface between adjacent cells and protrusions was performed in eight different placentas.

Chapter 2: General Methods

2.1 Contributions

The work presented in this study would not have been achieved without the contribution of many other people. The research team of the midwives helped consenting patients at Princess Anne Hospital and Dr. Emma Lofthouse and Brogan Ashley helped collecting human term placentas. Patricia Goggin (Electron Microscopist at the Biomedical Imaging Unit at Southampton General Hospital) imaged most of the placental samples under the SBFSEM microscope and also trained me to perform the imaging.

2.2 List of reagents

Reagent	Company
0.03 M aspartic acid	Analar, UK
1 M NaOH	BDH, UK
0.1 M sodium cacodylate buffer	Agar Scientific, UK
0.23 M sucrose	BDH, UK
2 mM CaCl$_2$	BDH, UK
2% Aqueous uranyl acetate	Diagnostic lab, UK
4% Paraformaldehyde (PFA)	Sigma, UK
2% Bovine Serum Albumin (BSA)	Fisher Scientific, UK
2% Osmium tetroxide	BDH, UK
4'.6-diamidino-2-phenylindole (DAPI)	Sigma, UK
Absolute Ethanol, MW 46.069 g/mol	Fisher, UK
Acetonitrile 99% pure, MW 41.053 g/mol	Fisher, UK

Gluteraldehyde	BDH, UK
0.1 M sodium cacodylate buffer	Agar Scientific, UK
Lead nitrate	Analar, UK
Osmium ferrocyanide	Argos Organics, UK
Potassium ferrocyanide	Agar Scientific, UK
0.3 M cacodylate buffer plus 4 mM calcium chloride	BDH, UK
Phosphate buffer saline (PBS) consisting of 0.0027 M potassium chloride, 0.137 M sodium chloride pH 7.4	Sigma, UK
Spurr resin	Agar Scientific, UK
Thiocarbohydrazide	Acros Organics, UK
Thiodiethanol (TDE)	Sigma, UK
Triton X 100	Sigma, UK
Walton's lead aspartate consisting of 0.066 g of lead nitrate and 10 ml of 0.03 M aspartic acid	Analar, UK

2.3 Placental Collection

Term human placentas from uncomplicated pregnancies were collected with written informed consent and ethical approval from the Southampton and Southwest Hampshire Ethics Committee B (11/SC/0529) from Princess Anne Hospital at Southampton. After delivery and within a few minutes one small piece from the periphery of a peripheral cotyledon

was selected and placed into the fixative buffer. There were 8 placentas used for SBFSEM and another 8 used for TEM. The total number of placentas used for this study was 16. From the 16 placentas, 63% of them were collected from normal delivery and 37% of them were from a C-section. The numbering of the placenta does not refer to the actual placenta number of the study due to patient confidentiality. Unfortunately, information about gestational age and ethnicity was not available as patient information is not routinely collected. Information about the confocal placentas was not accessible to me as it was not routinely collected. Placentas were screened for the presence of vacuoles in the syncytiotrophoblast layer under the TEM. Those placentas that appear to have vacuoles in the syncytiotrophoblast and had become hypoxic, were excluded from this study. Those placentas that had no vacuoles were then processed for either TEM or SBFSEM.

Placenta number	Rejected or processed for TEM and 3view	Number of SBFSEM stacks
1	Processed	8
2	Processed	1
3	Processed	1
4	Processed	2
5	Processed	5
6	Processed	1
7	Processed	3
8	Processed	6
9	Rejected (vacuolated)	0
10	Rejected (vacuolated)	0
11	Rejected (vacuolated)	0

12	Rejected (vacuolated)	0
13	Rejected (vacuolated)	0
14	Rejected (vacuolated)	0
15	Rejected (vacuolated)	0
16	Rejected (vacuolated)	0
17	Rejected (vacuolated)	0
18	Rejected (vacuolated)	0
19	Rejected (vacuolated)	0
20	Rejected (vacuolated)	0
21	Rejected (vacuolated)	0
22	Rejected (vacuolated)	0
23	Rejected (vacuolated)	0
24	Rejected (vacuolated)	0
25	Processed for TEM	0
26	Processed for TEM	0
27	Processed for TEM	0
28	Processed for TEM	0
29	Processed for TEM	0
30	Processed for TEM	0
31	Processed for TEM	0
32	Processed for TEM	0

2.4 Transmission Electron Microscopy

Transmission electron microscopy (TEM) was used to obtain high-resolution images of 2D sections of placental samples. TEM uses a thin (90-100 nm thick specimen) resin infiltrated slice of specimen that sits in a vacuum chamber in the microscope. An electron beam fires down through a gun passing through electromagnetic coils that accelerate the

electrons to higher speed and focus the electron beam onto a certain part of the specimen. The electron beam hits the specimen and the image is formed from the interaction of the electrons with the specimen, more electrons pass through less electron dense regions of the specimen while fewer electrons pass through more electron dense regions of the specimen. Those electrons that pass though the specimen hit the camera and then an image is captured by the camera (Ruska, 1980).

2.4.1 Fixing placentas for TEM

Placentas were collected within 30 min of delivery and small pieces of villous tissue (from 1 to 5 mm^3) were placed into the fixative buffer consisting of 3% glutaraldehyde in 0.1 M sodium cacodylate buffer at room temperature (RT). The placental fragments were stored at 4°C for at least 18 h and until processing for TEM (**Figure 2.1**).

2.4.2 Tissue processing for TEM

Following fixation, placental fragments were rinsed twice for 10 min using the fixation buffer consisting of 0.1 M sodium cacodylate buffer at pH 7.4 plus 0.23 M sucrose and 2 mM $CaCl_2$. After that, the specimens were left for 60 min in 2% osmium tetroxide in 0.1 M sodium cacodylate buffer at pH 7.4. Again, the specimens were rinsed twice for 10 min and after a wash with distilled water, samples were treated with aqueous uranyl acetate for 20 min. Samples were cleared using different concentrations of ethanol starting from 30% until absolute ethanol. At the end, specimens were treated with 50:50 Spurr resin and acetonitrile overnight. The following day fresh resin was changed with the previous one and left for 6 h. Finally, specimens were infiltrated in fresh resin and left for 24 h in the oven at 60°C to enable the resin to polymerise (**Figure 2.1**).

2.4.3 Ultracutting of placentas for TEM

An ultramicrotome (Ultracut Reichert-Jung, UK) was used to cut ultrathin sections of placental fragments (ranging 90-100 nm). The slices were placed on a grid, immersed briefly in 1 M NaOH and left to dry out for 60 min. Then, the samples were treated with Reynolds lead citrate to enhance the density and then observed under the TEM (**Figure 2.1**).

2.4.4 TEM imaging

Placental samples were visualized under the TEM (Tecnai T12, ThermoFisher, Eidhoven, Netherlands). The copper grid was placed under the TEM, the electron beam voltage was set for 80 KV, condenser aperture at 1 and spot size at 1. Copper grids were preferred because they are cheaper and stronger than gold and platinum grids and they do not tarnish (Harris, 2000). In these studies the objective aperture was three and the magnification ranged from X 5000 to X 85000.

2.4.5 Screening out the vacuolated placentas

Placentas were screened by TEM for the presence of vacuoles in the syncytiotrophoblast which indicate the tissue has become hypoxic. In the absence of oxygen ATP levels fall, and the inhibition of active transport leads to osmotic swelling of organelles, creating vacuoles that distort the consistency of syncytiotrophoblast as shown in **Figure 2.2 A.** Those placentas that appeared non-vacuolated in the syncytiotrophoblast were selected to be processed for TEM and SBFSEM (**Figure 2.2 B**).
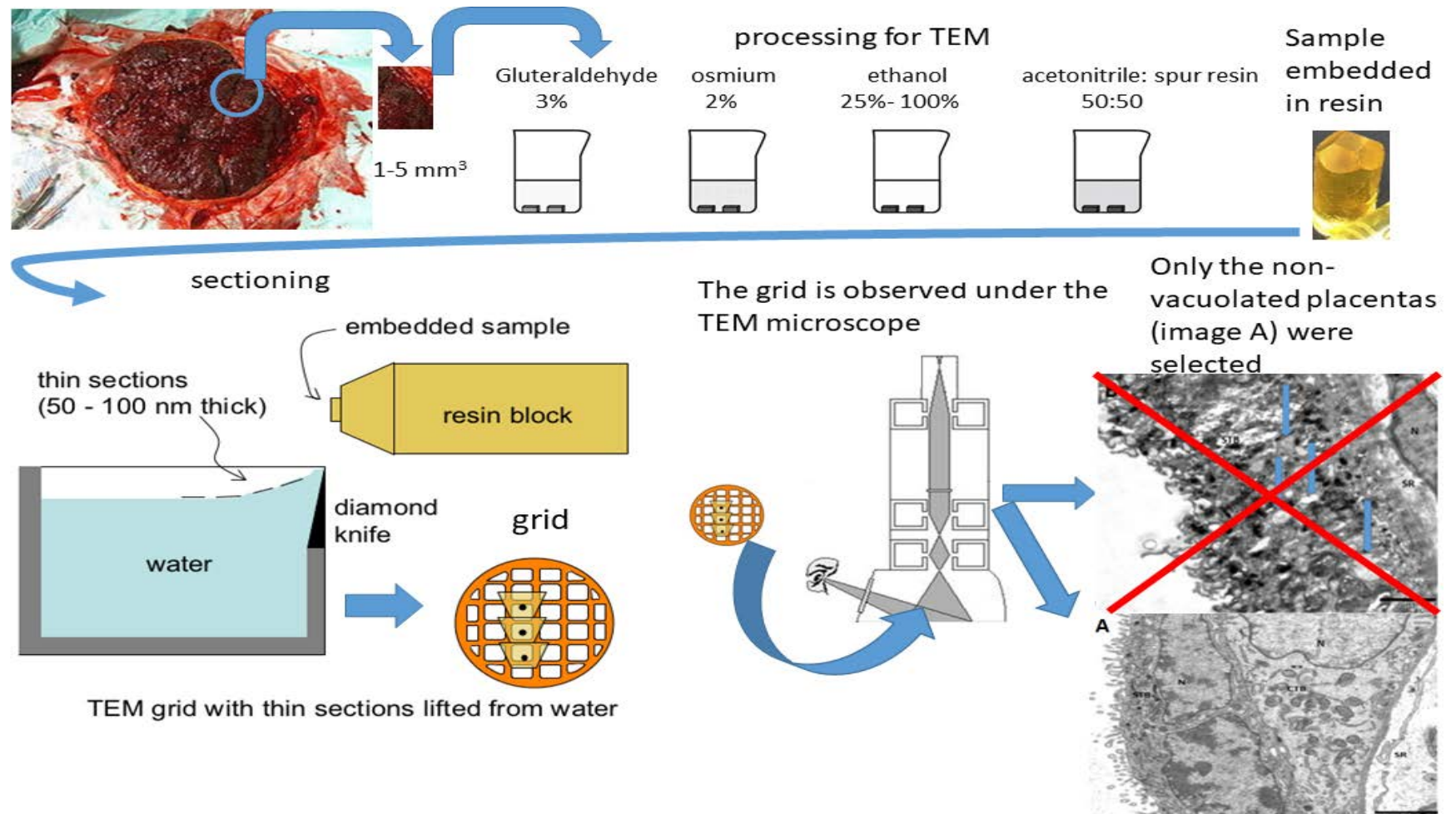
***Figure 2.1:** **Diagram showing the workflow of processing samples for TEM.** Placentas were collected, a small 1mm thick slice was cut, then placed into fixative, processed for TEM, embedded into resin, cut with an ultramicrotomy knife and observed under the TEM. Those placentas that appear to have vacuoles in the syncytiotrophoblast as shown in the figure with the red cross were excluded from the TEM and SBFSEM imaging.*
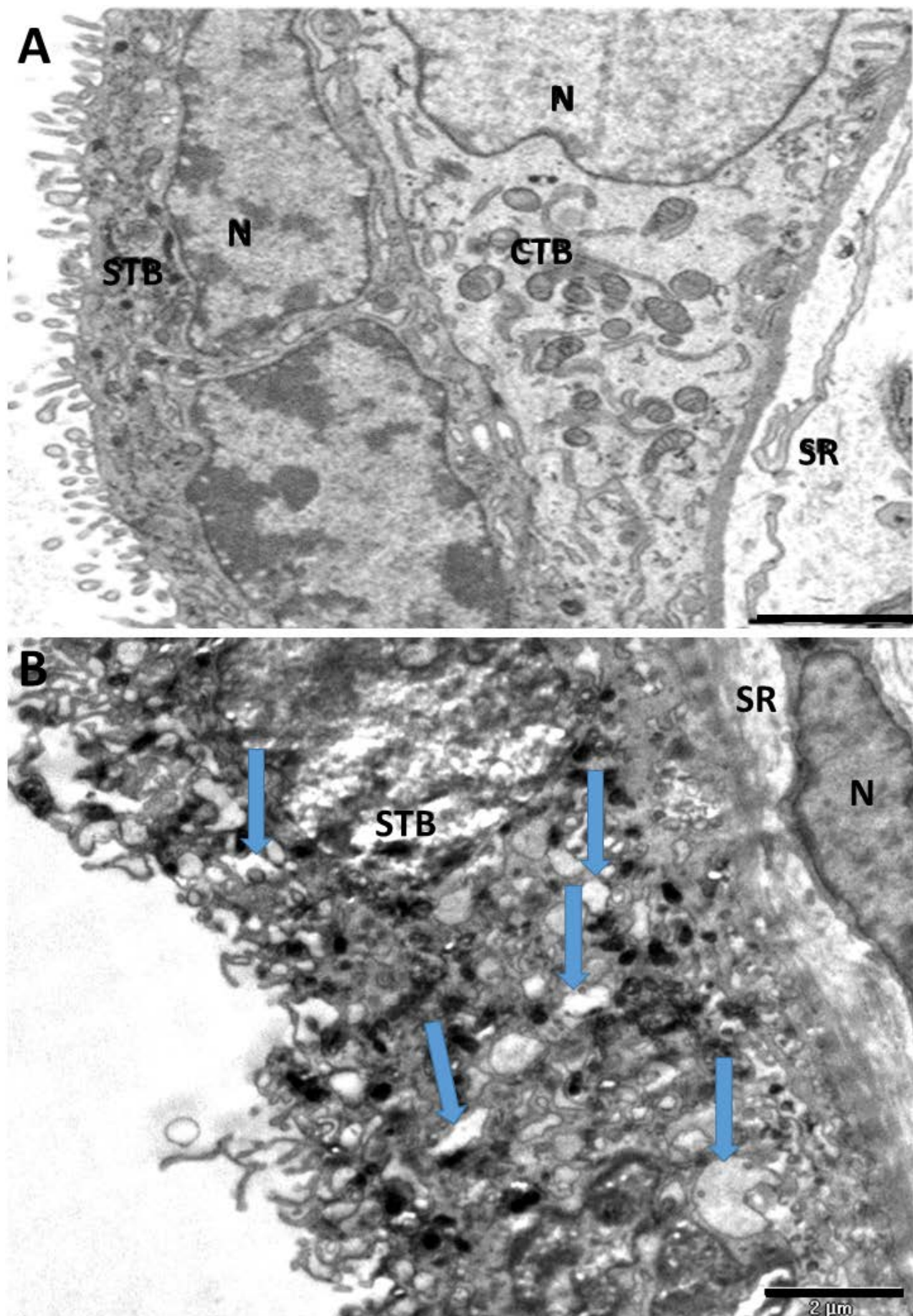
Figure 2.2: TEM images of normal human term placentas*. **A**. Image showing the structure of normal placenta without any vacuoles. Scale bar: 3 µm **B**. Image showing the structure of normal placenta with vacuoles (blue arrows) distorting the consistency of the syncytiotrophoblast. Scale bar: 2 µm. STB: syncytiotrophoblast, N: nuclei, CTB: cytotrophoblast, SR: stroma.*

2.5 Serial Block Face Scanning Electron Microscopy (SBFSEM)

SBFSEM allows the generation of high-resolution image stacks consisting of thousands of slices. This microscope consists of an ultramictorome knife inside the vacuum chamber of a scanning electron microscope. The electron beam scans the surface of the block face of the sample, an image is generated by the detection of the back scattered electrons, the sample is then lowered down and the ultramicrotome cuts a thin section (usually around 50 nm) from the block face. After the section is cut, the block face is raised to the focal plane and imaged again. SBFSEM can generate thousands of serial high-resolution 3D images and large datasets.

2.5.1 Processing placentas for SBFSEM

Non-vacuolated placentas were processed for SBFSEM. Placental tissue was placed into fixative buffer consisting of 3% glutaraldehyde in 0.1 M sodium cacodylate buffer for at least 24 h before processing for SBFSEM utilizing Ellisman's protocol (Deerinck et al., 2010). Fixed placental tissue was cut into less than 1 mm thick pieces, rinsed twice for 10 min using 0.1 M sodium cacodylate buffer at pH 7.4 plus 0.23 M sucrose and 2 mM $CaCl_2$. The placental fragments were then immersed into osmium ferrocyanide, fixative containing 3% potassium ferrocyanide in 0.3 M cacodylate buffer plus 4 mM calcium chloride. Then the samples were rinsed 5 times for 3 min with water and left for 60 min on ice in thiocarbohydrazide. After rinsing 5 times for 3 min with water, samples were immersed for 30 min in 2% osmium tetroxide in 0.1 M sodium cacodylate buffer at pH 7.4. Then the specimens were treated with 2% aqueous uranyl acetate to enhance the density in the placental fragments. Aqueous uranyl acetate was followed by Walton's lead aspartate solution. Samples were left for 30 min in Walton's solution and were dehydrated using a series of ethanol concentrations starting from 30% up to absolute ethanol. Dehydration is important in order

for the resin, which is hydrophobic, to infiltrate in the sample. Specimens were then infiltrated in 50:50 Spurr resin and acetonitrile, and left for 24 h. Specimens were then infiltrated in fresh resin for 6 h and then placed in the oven at 60˚C for 48 h to allow the resin to polymerise.

After the polymerisation, the specimens were trimmed to less than 1 mm^2, mounted on an aluminium pin with conductive glue and coated with gold and palladium to make the specimen conductive and reduce the charging of the specimen that would otherwise happen due to the accumulation of static electric fields created by the electrons. Charging makes the image distorted and stripy (**Figure 2.3**).

2.5.2 Imaging in the SBFSEM

The aluminium pins with the resin-infiltrated placental tissue on the top, were placed on the stage of a 3 view Gatan microscope (Gatan, Abingdon, UK) inside an FEI Quanta 250 field emission gun scanning electron microscope (Thermofisher, Eindhoven, Netherlands). For this study, the accelerating voltage of the microscope was set in 3 KV, spot size 3 and the pressure in 40 Pa. The diamond knife inside the microscope was slicing every 50 nm thick slices. Stacks of images were generated at voxels (voxel is the 3D pixel) ranging 2.6-14 nm in the X and Y axis and 50 nm in the Z axis, and the number of slices was typically 300-2000. The total image size (the number of pixels in the X and Y axis) was ranging between 3000 X 3000 and 8192 X 8192 pixels. Gatan Microscopy Suite Software (GMS version 3, UK) was used to collect digitised images of each stack (**Figure 2.3**).

2.5.3 Analysis of the SBFSEM images

The high-resolution 3 view stacks were first processed in Fiji software (version 2.0.0-rc-43) and then analysed using Amira (version 6.0; ThermoFisher, Eindhoven, Netherlands) software to produce the 3D reconstruction of placental tissues. The stacks were converted from DM3 files to tiff files using Gatan Microscopy Suite Software (GMS version 3, UK). The tiff files were then uploaded into the Fiji. The tiff stacks were processed using the filter Gaussian blur filter 2.00 sigma radius to enhance the smoothing of the image, enhanced contrast 0.4% saturated pixels to improve the contrast of the image and downsized to 3000 X 3000 pixels. The processed stacks were saved as image sequence and then loaded into Amira. Segmentation of cell features was performed in Amira to allow 3D reconstruction of cellular structures. Every single cell or feature was manually drawn with a specific colour using the pencil tool as shown in (**Figure 2.4**). This process was repeated in every slice of the stack until all the slices are drawn (**Figure 2.5**). A 3D image can then be generated from the stack using the volume-rendering tool. Volume-rendering adds every segmentation on each slice together and reconstructs the surface creating the 3D image.

processing for SBFSEM

Sodium Cacodylate buffer | Osmium ferrocyanide | Thiocarbo-hydrazide | 2% osmium | 2% uranyl acetate | Walton's lead aspartate | Ethanol dehydration | Spur: acetonitrile 50:50

1-5 mm³

Sample embedded in resin → Coating with gold and palladium → Diamond knife (Cutting → Imaging) Electron beam → Stack generated by the 3 View

X-axis, Y-axis, Z-axis
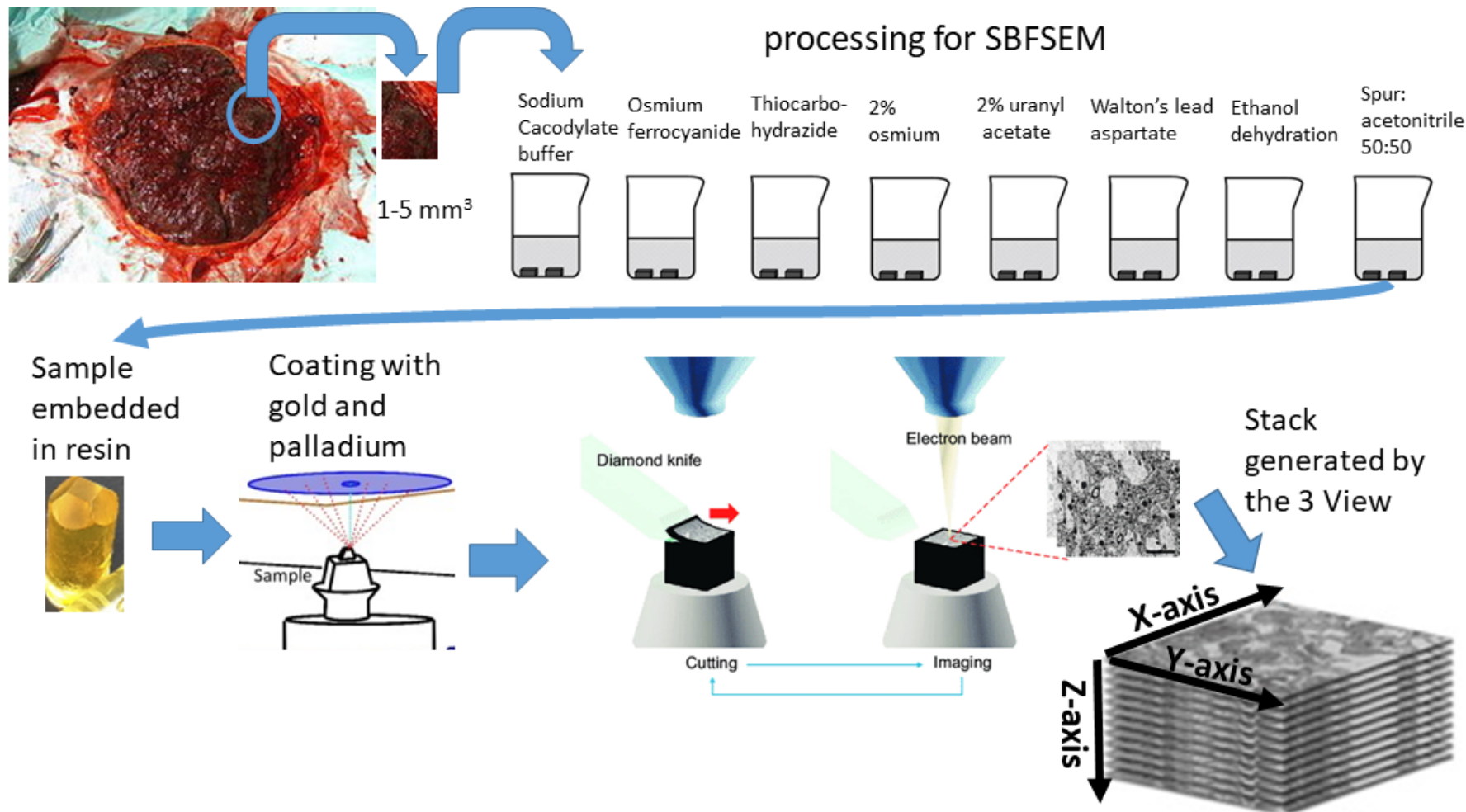
*Figure 2.3: **Diagram showing the workflow of the processing samples for SBFSEM.** Placental samples were cut into small pieces, fixed, processed for SBFSEM, embedded in resin, coated with gold and palladium and observed under the 3 view microscope. The stack of images was produced by the Gatan micrograph software.*

51
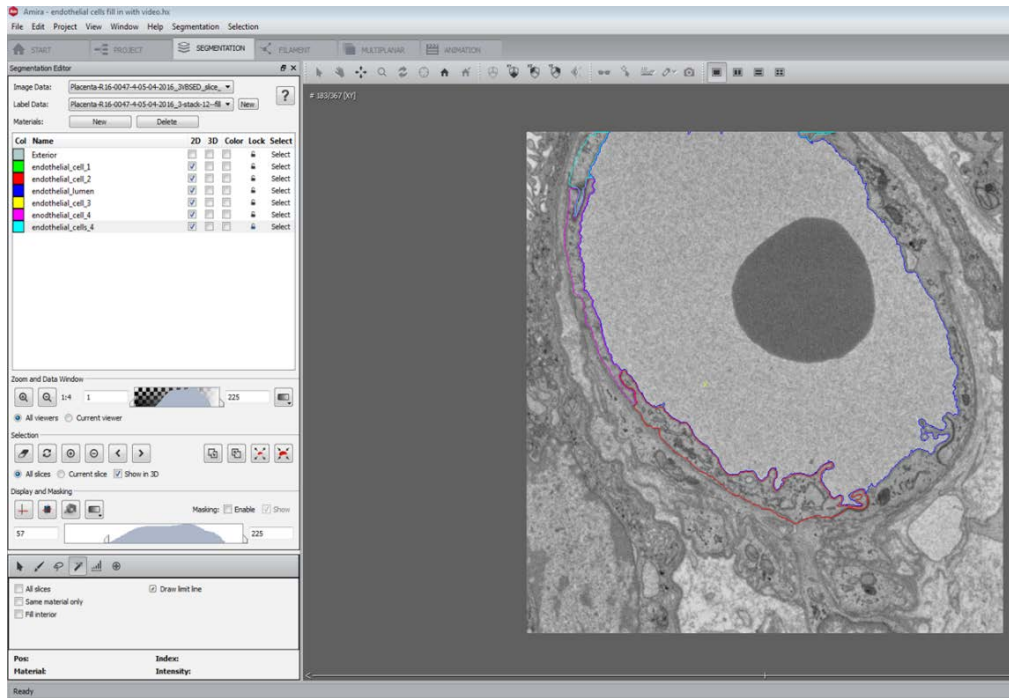
Figure 2.4: ***Segmentation in Amira****. Software analysis for the 3D stacks produced from the serial block face electron microscope. On the left, there is the toolbar where the individual should name its material and pick a specific tool (showing at the end of the toolbar) to draw the different cell types. On the right is the stack, showing one representative slice out of thousands that may consist of. In that slice each endothelial cell is drawn with a different colour.*

2.6 Wholemount confocal laser scanning microscopy

Placental fragments of 1-3 mm^3 size were placed on the stage of the confocal micros-copy (SP5, Leica, UK). A laser beam is focused into a small area on the surface of the sample and in a tight focal plane, which allows the laser beam to go in depth inside the sample compared to a normal fluorescent microscope. When the laser beam hits the specimen in the focal plane, the photons emitted from the fluorophores that are on the specimen pass through the objectives and are detected by the camera to generate the image. The high-quality images produced by the confocal microscopy are used to visualize the placental vasculature and villous tree.
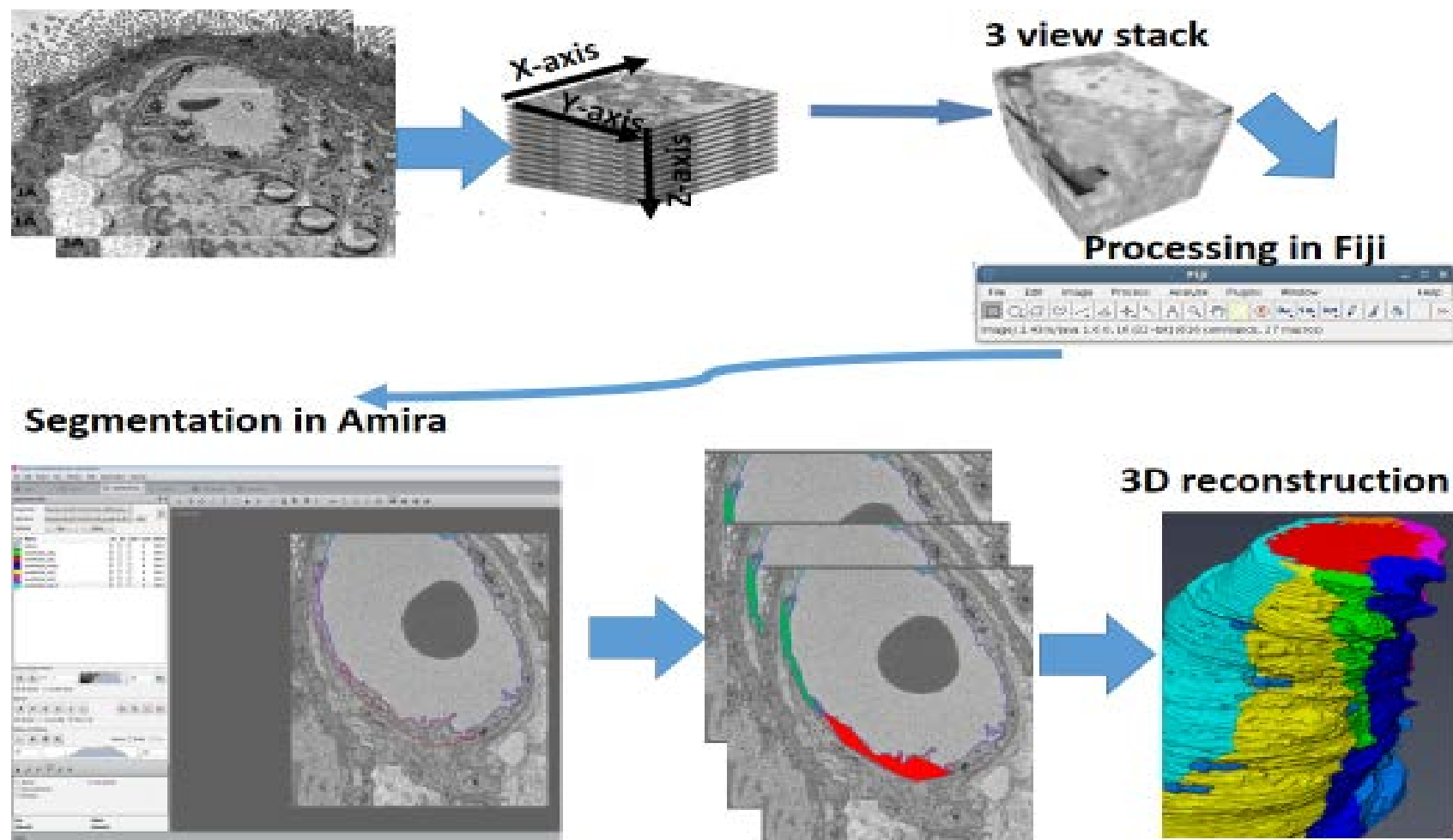
Figure 2.5: ***Diagram showing the workflow of the segmentation of SBFSEM stacks in Amira.*** *The SBFSEM stack was first processed with filters in Fiji, then the processed stack was uploaded into Amira and each slice was manually segmented.*

53

2.6.1 Fixing placental tissue for immunostaining

Tissues were fixed overnight in 4% (PFA), 32g PFA in boiling 800 ml of 1 M PBS

pH 7.4 (0.01 M phosphate buffer, 0.0027 M potassium chloride, 0.137 M sodium chloride).

PFA fixative was made up fresh, aliquoted in 20 ml volumes and frozen at -20°C until use.

Defrosted fixative was used within one week. After overnight fixing, the fixative was poured

off, leaving a few drops in the tube and replaced with PBS (0.01 M phosphate buffer, 0.0027

M potassium chloride, 0.137 M sodium chloride). Samples were then stored at 4°C until use.

2.6.2 Immunostaining

For the immunostaining, the fixed placental samples were washed with PBS, cut into

smaller pieces and incubated for 60 min in 1% Triton-X 100 in PBS to permeabilise the

tissues. Then the samples were incubated in 2% BSA diluted in PBS to block non-specific

binding. Samples were then washed with PBS 3 times for 10 min each and primary antibod-

ies diluted in PBS were added to the samples and incubated overnight at 4°C. The next day

the samples were washed 3 times for 10 min each, and secondary antibodies were added and

incubated for 2 h on the roller with 0.4% 4',6-diamidino-2-phenylindole (DAPI) and then

washed with PBS 3 times for 10 min each. Samples were then cleared with Thiodiethanol

(TDE), starting from 10% TDE in PBS for 30 min, then 25% TDE for 30 min, then 50%

TDE for another 30 min, and finally 3 x in 97% TDE for 30 min each time. Samples were

stored at 4°C until they could be observed under the confocal microscope.

2.6.3 Imaging on the confocal microscopy

Placental samples $\approx$ 1-3 mm^3 were placed on the microscope slide of a 4-channel

confocal laser scanning microscope (SP5, Leica, UK) and then the Leica software was used

to visualize the samples under confocal. First, the Argon laser was switched on and adjusted

to 30%, and the X 10 objective was selected to identify the sample on the focal plane. Once the sample was identified, the other lasers were switched on and adjusted according to the emission spectra of the dyes that were used on the placental samples. Once the lasers were set up, then the fluorescence setting of the microscope was switched on and the x, y, and z axis were used to select the appropriate focus plane. The z step was set (typically ranging between 1 and 2 µm), the number of slices were ranging 50-70, the sequential stack was chosen to eliminate spectral bleed, with 4-line averaging to reduce random noise and a stack of confocal images was acquired from sequential focal planes (**Figure 2.6**).

2.6.4 Image analysis of the confocal images

The 3D confocal stacks were uploaded into the Fiji, the split channel setting was selected and each channel was saved separately as tiff image sequence. Each channel was then uploaded into Amira in order to produce the 3D reconstructions (**Figure 2.6**).

2.7 Quantification of volumes and diffusion barriers

To measure volumes and surface areas of the different cell types in the terminal villi of human term placentas and assess the potential cellular barriers to diffusion a stereological approach was adapted for SBFSEM stacks (Mayhew, 2006). Stereology was applied to 27 stacks from eight different placentas in total. It is important to note that nearly all the stereological measurements were applied to stacks from terminal villi which are believed to be the primary exchange area within the villi and not the villi as a whole. All the stereological analysis was performed by one person (EP) and my supervisor reviewed selected images to ensure the validation of the analysis. In order to calculate the volume of every cell type/area of interest in a stack, I selected every 50 slices starting from a random starting slice determined using the random number generator in Excel.
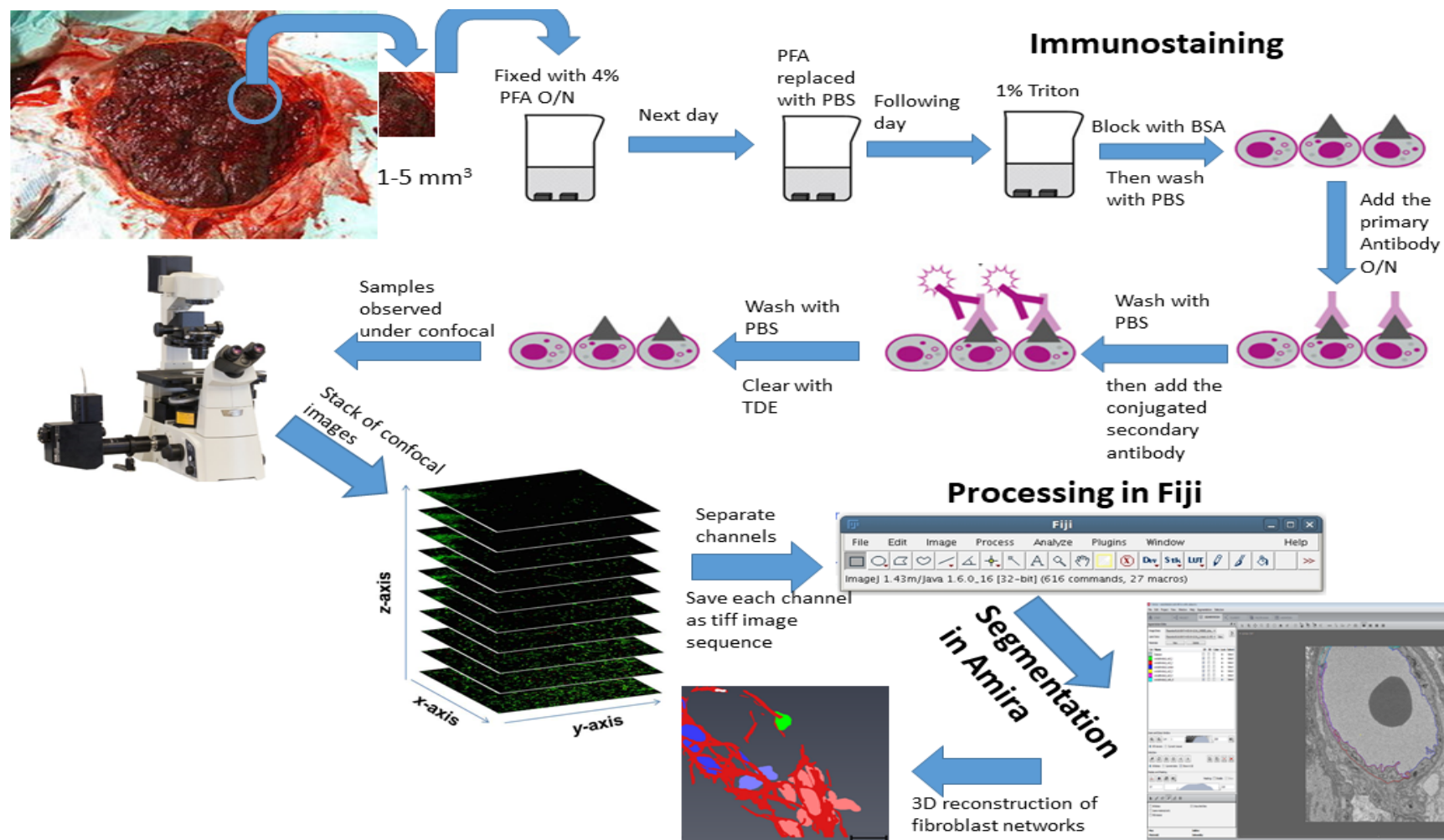
Figure 2.6: ***Diagram showing the workflow of processing samples for confocal imaging****. Placenta samples were placed into PFA and then immunostaining was performed. The samples were observed under confocal, the stack of images were first processed in Fiji and then uploaded into Amira to achieve the segmentation.*

56

A randomly offset 4 by 4 grid (giving 16 points where lines intersect) was applied to each of the selected slices using the random offset function in Fiji (Gundersen et al., 1988). To calculate proportional volumes of villous features the number of points where the lines intersected falling in each cell type or area of interest (syncytiotrophoblast, cytotrophoblast, stroma, fibroblasts, macrophages, pericytes, endothelial cells, endothelial lumen and intervillous space) as shown in **Table 2.1**, were counted and expressed as the proportion of the total number of points falling on villous tissue, excluding the points falling on the intervillous space which is not placental tissue. The total tissue volume was determined from the number of points falling on tissue as a proportion of total points times the volume of the region analysed as shown in **Figure 2.7**.

To assess the extent to which cell types within and around the stroma may act as barriers between the syncytiotrophoblast and endothelium I determined i) the proportion of syncytiotrophoblast covered by cytotrophoblast, ii) the proportion of fetal capillary endothelium covered by pericytes and iii) the proportion of the stroma between trophoblast and endothelium which contain fibroblasts. For these calculations, the randomly selected slices and the randomly offset grids described above were used counting intersections on the horizontal lines. To determine the proportion of syncytiotrophoblast basal membrane covered in cytotrophoblast in the terminal villi, the number of intersections with syncytiotrophoblast basal membrane in direct contact with cytotrophoblast (**Figure 2.8 black arrows**) was divided by intersections with syncytiotrophoblast basal membrane (**Figure 2.8 blue arrows**). To determine the proportion of capillary covered in pericytes in terminal villi, intersections with endothelial basal membrane in direct contact with pericytes (**Figure 2.8 white arrows**) were divided by the total intersections with endothelial basal membrane (**Figure 2.8 pink arrows**). To determine proportion of pathways across the villous stroma that are blocked by fibroblasts the number of times that a line intersected both syncytiotrophoblast basal mem-

brane and endothelial basal membrane with fibroblast in between (**Figure 2.8 yellows arrows**) was divided by the total number of times the line intersected both syncytiotrophoblast basal membrane and endothelial basal membrane (**Figure 2.8 blue and pink arrows**).
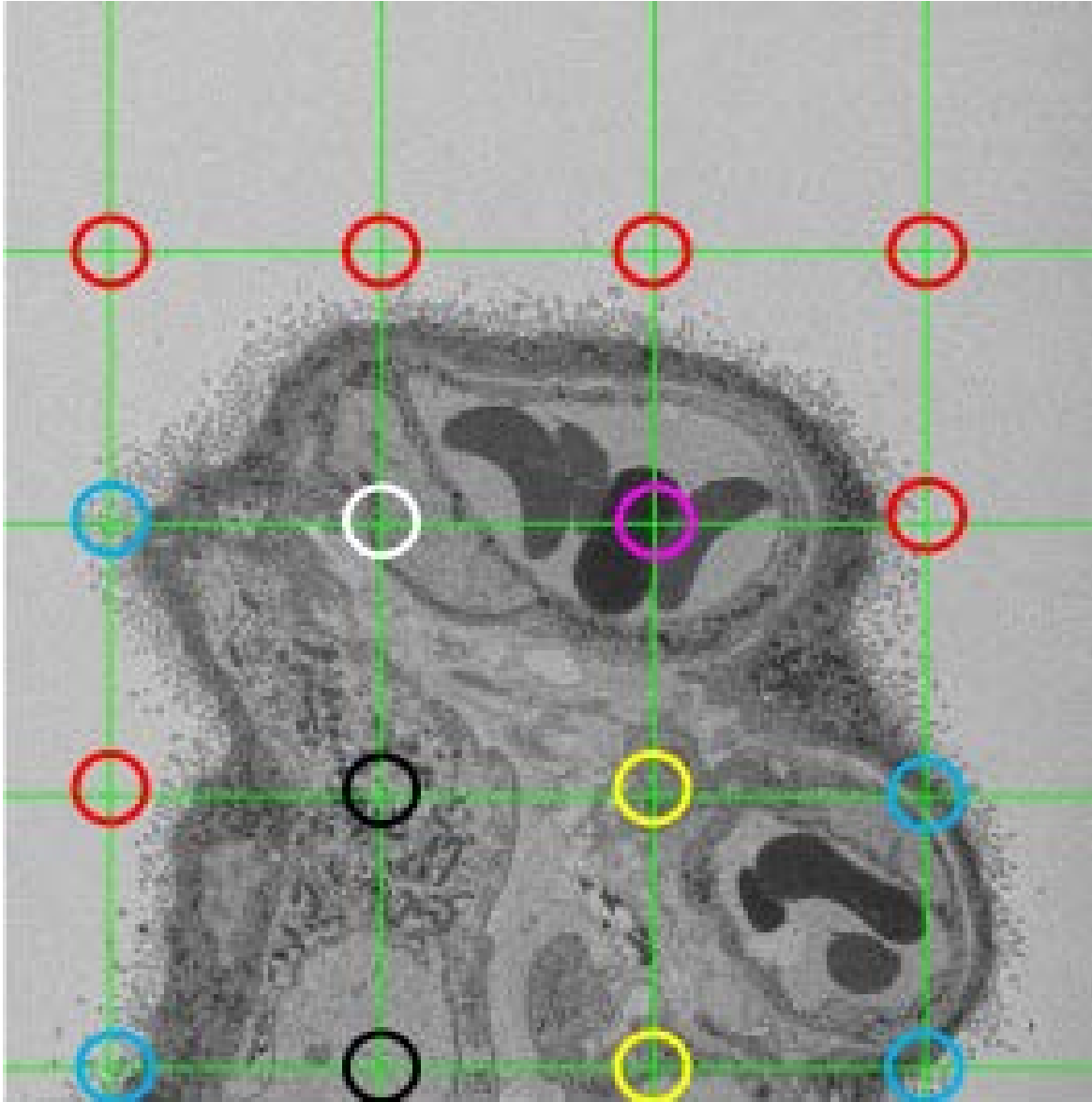
Figure 2.7: ***Example of a grid on a SBFSEM image****. The circles show the 16 points on the grid. The red circles show the points falling on the intervillous space. The blue circles are points falling on the syncytiotrophoblast, the black circles are cytotrophoblast, the yellow are fibroblasts, the white is pericyte and the pink is endothelial lumen.*

Table 2.1: Counts of the features identified by point counting on Figure 2.7.

Feature	Count
Intervillous space (red)	6
Syncytiotrophoblast (blue)	4
Cytotrophoblast (black)	2
Fibroblasts (yellow)	2
Pericytes (white)	1
Stroma	0
Extracellular vesicles	0
Macrophages	0
Endothelial cells	0
Endothelial lumen	1
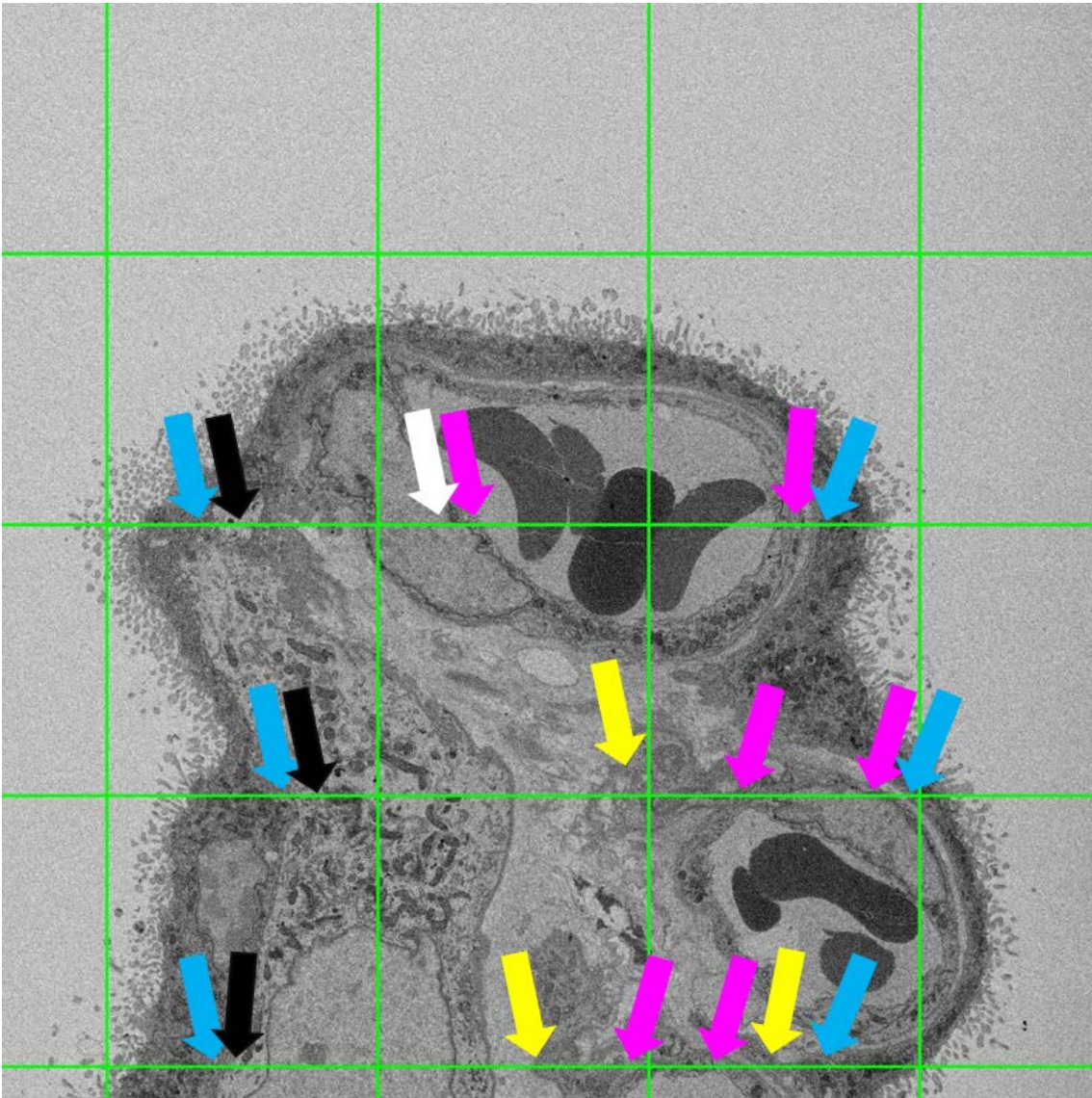
Figure 2.8: ***Arrows showing the intersections on the grid.*** *Blue arrows show the intersections with syncytio-trophoblast basal membrane, black arrows depict the number of intersections with syncytiotrophoblast basal membrane in contact with cytotrophoblast. Pink arrows are for the intersections with endothelial basal membrane, white arrows are for the intersections with endothelial basal membrane in contact with pericytes. Yellow arrows are for the intersections of syncytiotrophoblast basement membrane in contact with fibroblasts.*

Table 2.2: **Example of the surface area percentages of the components as shown in Figure 2.8.**

Feature	Count
Intersections with syncytiotrophoblast basal membrane	6
Intersections with syncytiotrophoblast basal membrane in contact with cytotrophoblast	3
Intersections with endothelial basal membrane	6
Intersections with endothelial basal membrane in contact with pericytes	1
Intersections with syncytiotrophoblast basement membrane in contact with fibroblasts	3

2.8 Data analysis

The sample size of this study was eight distinct normal human term placentas from which I had 27 stacks as shown in the appendix. For stereological analysis running means were plotted to assess the adequacy of the sample size. Data are presented as mean and SEM or median (range) and STD as appropriate. Data analysis was performed in excel. The graphs were made in excel and GraphPad Prism software (version 7.0, UK). Student t-test was used as for normally distributed values, while Mann Whitney test was used where non-parametric analysis was required. Statistical significance was considered to be when $p \leq 0.05$.

Chapter 3: Serial block-face scanning electron microscopy of fetal erythrocytes protruding through the placental syncytiotrophoblast

3.1 Introduction

The outer layer of placental villous tree is the syncytiotrophoblast. The syncytiotrophoblast constitutes the barrier between the maternal and fetal circulation. Even though the syncytiotrophoblast layer should form a continuous barrier, there are studies showing that there is size selective transfer of solutes across the syncytiotrophoblast through paracellular routes (Sibley, 2009, Bain et al., 1990). It has been proposed that denudations of the syncytiotrophoblast may serve as paracellular routes for proteins or hydrophilic molecules to pass through (Brownbill et al., 2000). Syncytiotrophoblast denudations are areas covered with fibrin-type fibrinoid deposits. The paracellular routes allow the permeability of substances with low molecular size.

Even though cells should not be able to pass through the syncytiotrophoblast layer, a study has shown that fetal blood cells pass into the maternal bloodstream, and persist in the maternal blood for up to 27 years, a condition known as microchimerism (Bianchi et al., 1996).

The aim of this chapter is to investigate a novel ultrastructural feature which shows the passage of a fetal cell through the syncytiotrophoblast layer and consider the implications this observation may have for our understanding of the nature and properties of this layer.

3.2 Methods

Placental tissue samples were collected as described in Chapter 2.1 and processed for SBFSEM as described in 2.2.3.2. Placental samples were aldehyde fixed, infiltrated in resin, trimmed in the ultramicrotome, mounted on an aluminium pin with conductive glue and sputter coated with gold/palladium. SBFSEM was carried out on the processed block using a Gatan 3View microscope inside an FEI Quanta 250 FEGSEM at 3.0 KV accelerating voltage and with a vacuum level of 40 Pa. A stack of 426 sequential slices of placental tissue with a Z resolution of 50 nm was generated. The voxel size was 22 x 22 x 50 nm, while the total image size of each slice was 3000 x 3000 pixels.

Images of the stack were processed in Fiji (version 2.0.0-rc-43) using the filter Gaussian blur (sigma radius 2) and enhanced contrast (0.4%-saturated pixels) (Schindelin et al., 2012). To estimate the size of the holes in the syncytiotrophoblast, from which fetal erythrocytes were protruding, the maximal diameter of the hole in the X-Y axis of the image was measured in Fiji. This was repeated in images from 3-5 slices either side to ensure it was the maximum point. The maximal diameter of the hole in the Z-axis was estimated by counting the number of 50 nm slices in which it appeared. The high-resolution 3D stacks were segmented using Amira (Avizo version 6.1.1, UK) software to produce the 3D reconstruction of each placental cell type in the section.

The most prominent protruding erythrocyte and the surrounding region of syncytiotrophoblast were manually segmented in Amira. To calculate how much the syncytiotrophoblast layer was stretched from the basement membrane, the surface area of the syncytiotrophoblast layer and the cross-sectional area of the first slice were measured in Amira. Before calculating the surface area of the syncytiotrophoblast, smoothing of the syncytiotrophoblast surface area was performed to make it comparable to the flat surface of the base, which was considered the cross-sectional area of the first slice. The calculations of the surface areas were performed in Amira with the generate surface area application tool, while

the calculations of the average diameter and circumference of the base were performed in

Fiji using the ruler tool.

3.3 Results

This study demonstrated a novel feature where fetal erythrocytes had pooled under the syncytiotrophoblast of normal human term placenta. In one case a large proportion of a fetal erythrocyte had passed through a small hole in the syncytiotrophoblast layer. In several others cases a small proportion of an erythrocyte had passed through small holes in the syncytiotrophoblast layer.

3.3.1 Fetal erythrocytes protruding through the placental syncytiotrophoblast

SBFSEM on a stack of 426 sequential slices of placental tissue with a Z resolution of 50 nm demonstrated a thin region of the syncytiotrophoblast, which was detached from the underlying basement membrane (**Figure 3.1A**). Syncytiotrophoblast is detached from the underlying structures in this region of villi not that it is detached form the villi itself (in which case it would most likely have been washed away during processing). As the syncytiotrophoblast can be observed but the basal lamina and stromal tissue cannot be observed this indicated that it is detached in this region. The space under the syncytiotrophoblast contained 78 erythrocytes and one unidentified cell of low electron density. The majority of blood cells were erythrocytes, but there were also some platelets, one of them is shown in (**Figure 3.5**).

There were 17 erythrocytes observed partially protruding through the syncytiotrophoblast at 25 sites (**Figure 3.1 B & C**) all located on the side of the structure where the syncytiotrophoblast was thinnest. The median diameter of the holes was 0.56 μm (range 0.34 - 1.41 μm) in the X - Y plane and 0.50 μm (range 0.20 - 1.85 μm) in the Z plane. In 20 cases the protrusion was covered by syncytiotrophoblast membrane on the maternal side suggesting that it may have pushed through a relatively weaker area rather than a pre-existing hole. The holes disappear after part of the cell has come out. The syncytiotrophoblast layer is apparently thinner compared to the normal trophoblast layer in the normal placentas as shown in **Figure 3.3**, but unfortunately the thickness of the layer could not be measured

accurately due to the resolution of the image. The surface area of the whole syncytiotroph-oblast as shown in **Figure 3.1 B**, was 5415 μm^2 vs. the cross-sectional area of the base of the structure was 1628 μm^2 suggesting a 3.3-fold stretch (actual stretch may be less if syn-cytiotrophoblast is pulled in from adjacent regions). The base of the structure was considered the first slice of the stack. The syncytiotrophoblast basal membrane is apparent but due to the fact that there are no high-resolution EM images it cannot be determined that the syn-cytiotrophoblast basal membrane is indented. No endothelium or stroma was apparent un-derlying the syncytiotrophoblast. This is clearly demonstrated by another image (**Figure 3.2**) showing the absence of syncytiotrophoblast in some damaged villi. The structure was 19 μm at its deepest point, with an average diameter at the base of 42.9 μm and a circumference of 144.4 μm.

3.3.2 Observations in the basement membrane

TEM images of the interface between the basal and basement membrane showed loose connection of the syncytiotrophoblast with the basement membrane. The existence of folds inside the basal membrane implies that the basal and basement membrane are not fully adjacent and so they can be disconnected (**Figure 3.3A, B**).

3D reconstructions of these folds based on SBFSEM imaging are presented in (**Figures 3.4 A**).
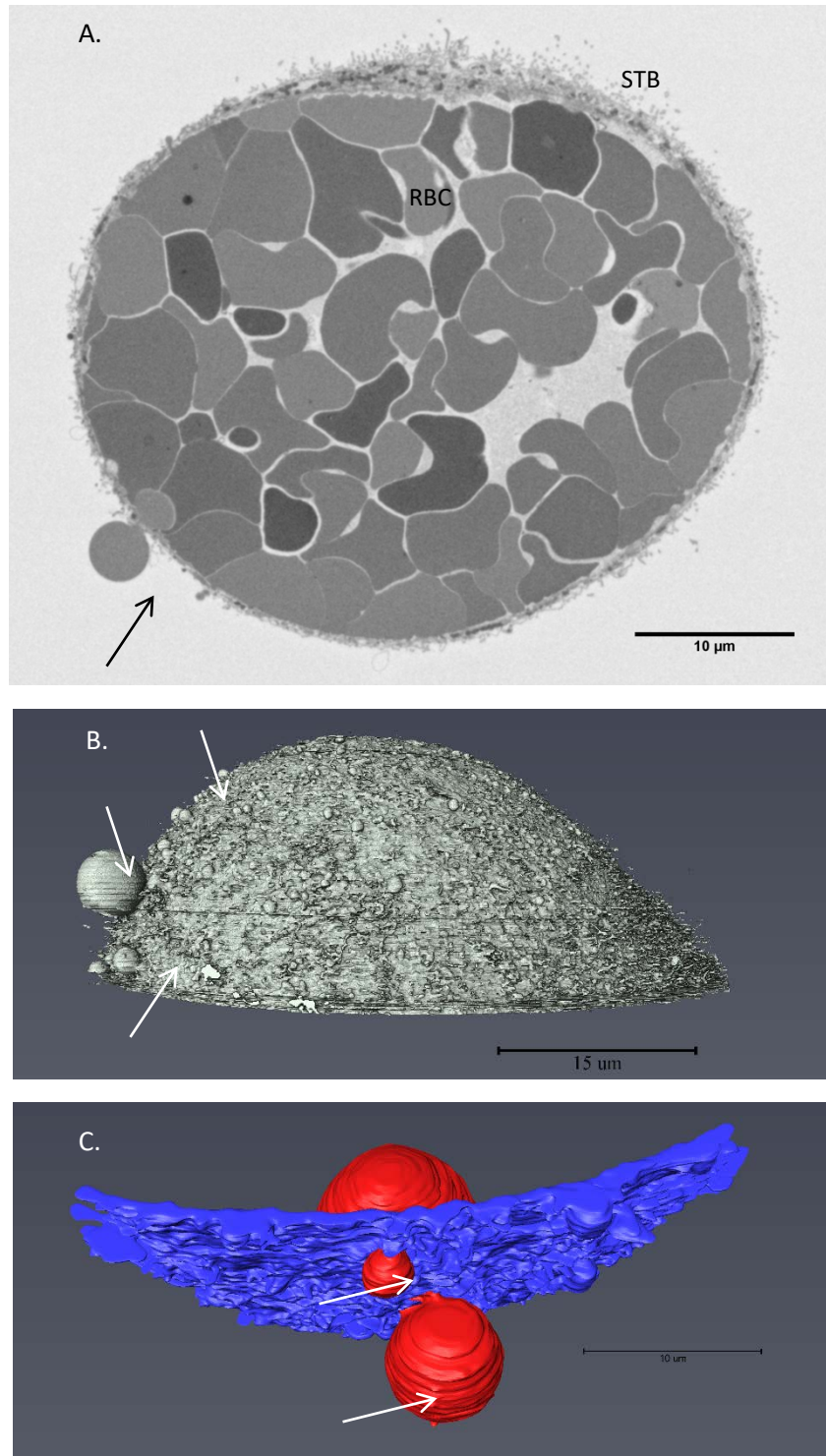
Figure 3.1: Electron microscopy image of the structure and 3D reconstructions of the stack. A, An image from the SBFSEM showing the syncytiotrophoblast (STB), the erythrocytes (RBC) and the main protruding erythrocyte (arrow), B, The segmented structure showing the surface of the syncytiotrophoblast and the protruding erythrocytes (arrows), C, segmentation of the largest protruding erythrocyte (red) pushing through the syncytiotrophoblast (Blue) in two places (arrows). Videos of the image stack and the segmented images rotated can be seen in the supportive information section in the following link: https://onlinelibrary.wiley.com/doi/full/10.1111/joa.12658
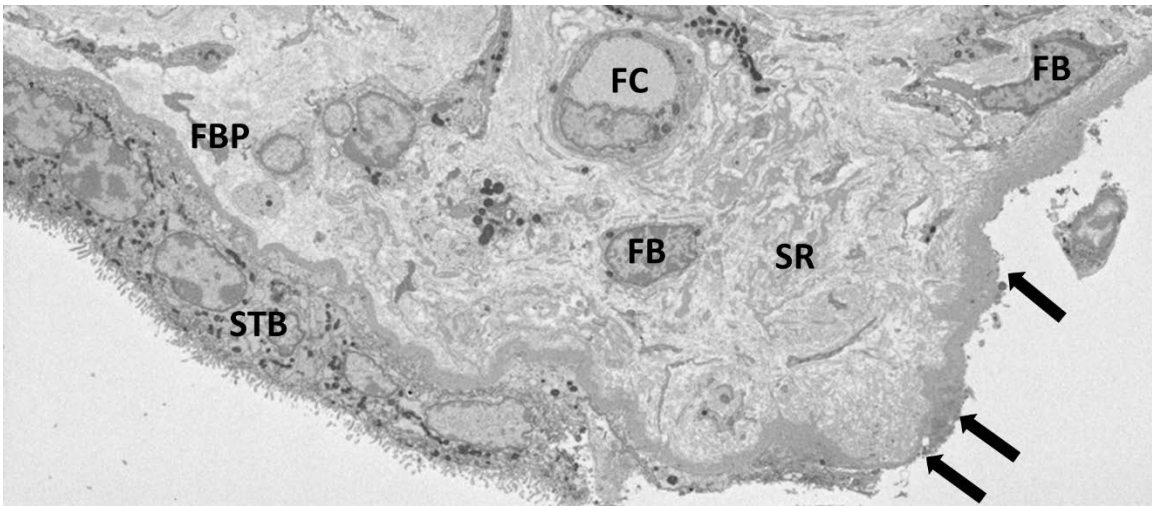
***Figure 3.2:** **TEM image showing the surface of a placental villi with a denuded region that has lost its syncytiotrophoblast** (shown with black arrows).In the denuded region the underlying basement membrane appears intact and may be thicker than in regions covered by syncytiotrophoblast. **FBP**: fibroblast process, **FC**: fetal capillary, **FB**: fibroblast, **SR**: stroma, **STB**: syncytiotrophoblast. Scale bar: 10 µm.*
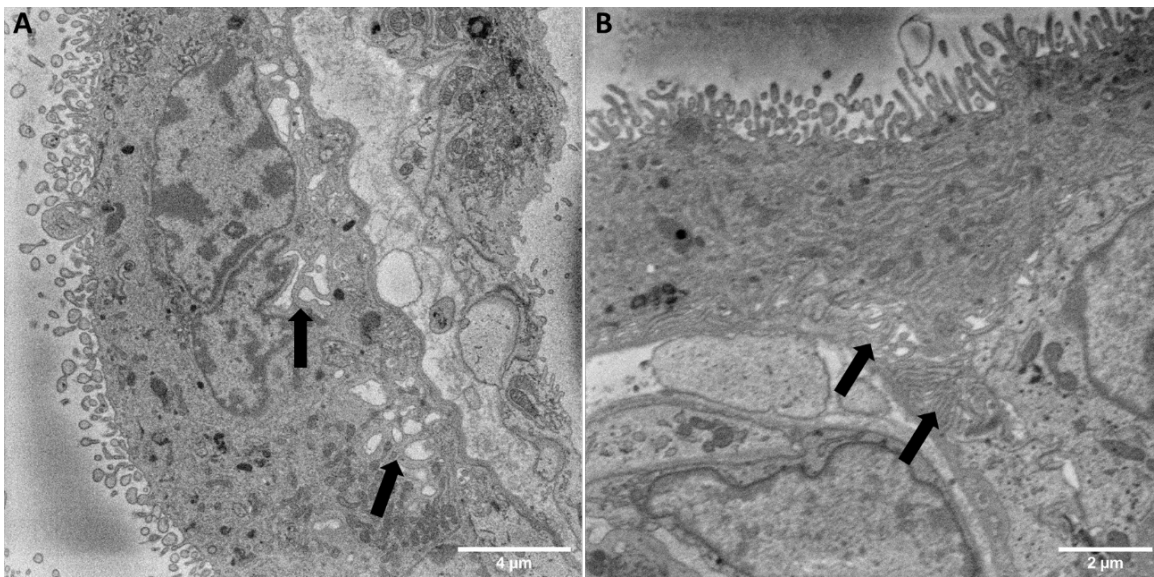
***Figure 3.3:** **High-resolution electron microscopy images of the folds inside the syncytiotrophoblast basement membrane.** **A** and **B** show the folds of the basal membrane (indicated by black arrows) inside the basement membrane.*
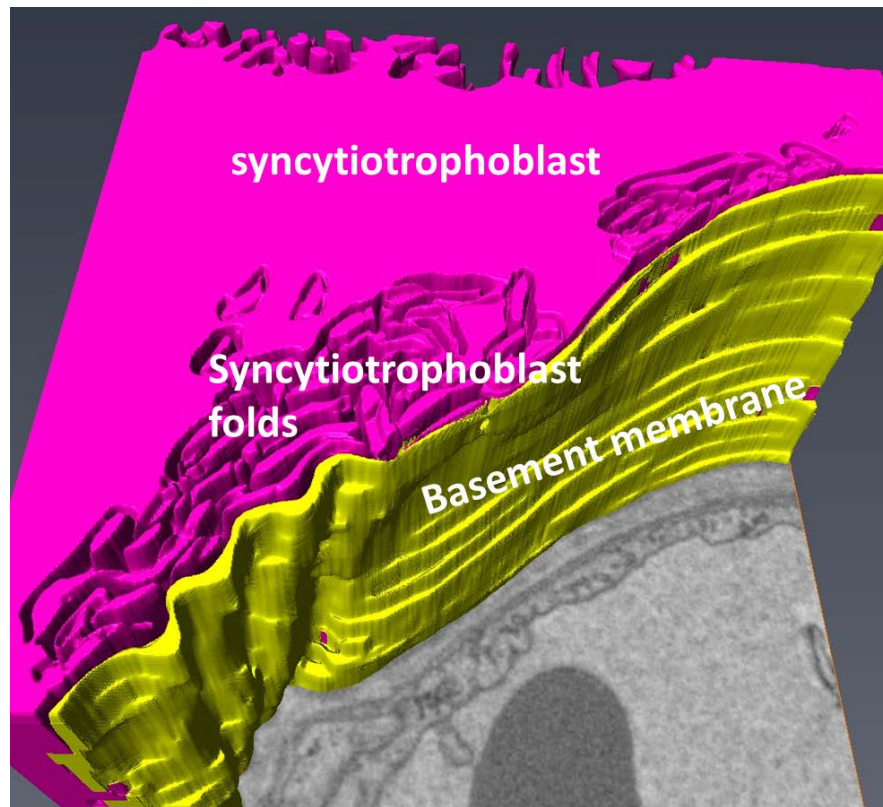
Figure 3.4: 3D reconstruction of syncytiotrophoblast folds. *Image showing the 3D visualization of the syn-cytiotrophoblast folds. Basement membrane is shown in yellow and the syncytiotrophoblast is shown in pink. Figure produced by medical student Daisy Parsons using SBFSEM stacks produced for this thesis.*
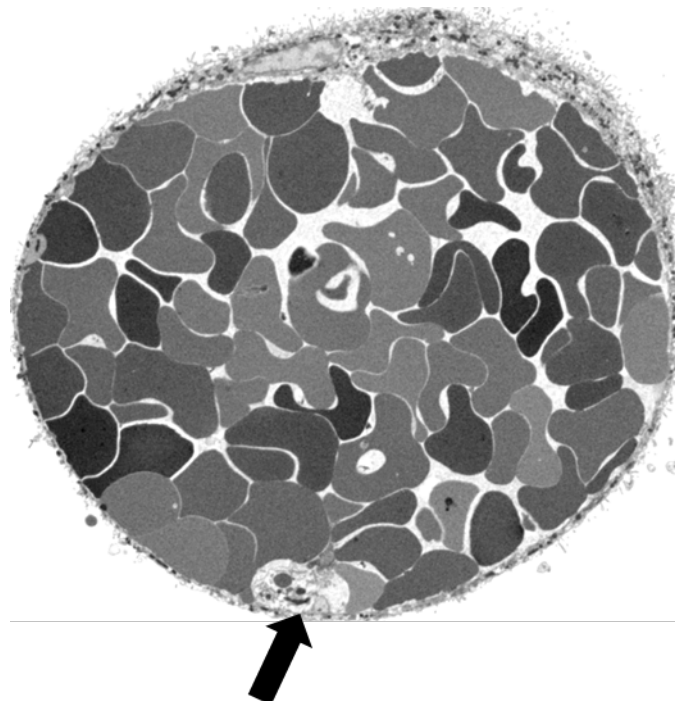
Figure 3.5: A representative slice of the SBFSEM stack showing a platelet. *The platelet is shown with a black arrow.*

3.4 Discussion

Fetal cells would not be expected to be able to pass through the placental syncytio-trophoblast layer, however previous studies suggest that fetal blood cells can pass into the maternal bloodstream. In this chapter, I investigated a region of tissue which suggests that fetal cells may, under specific pathological conditions such as microtraumatic rupture of the fetal vessels, cross the syncytiotrophoblast (Dawe et al., 2007, Schroder, 1975). This feature suggests a potential pathway of fetal blood cells passing through the syncytiotrophoblast layer. Even though it was not obvious, this feature is likely to have been the result of a leakage of the fetal capillary which may have resulted in fetal hydrostatic pressure pushing erythrocytes through weaker areas in the stretched syncytiotrophoblast. The fetal blood pooling is likely to have caused the syncytiotrophoblast to stretch away from the basement membrane.

This study suggests that when there is a breach on a fetal capillary, the hydrostatic pressure created can push fetal erythrocytes to pass through the syncytiotrophoblast layer and cross it without ripping it apart. This transfer of cells across the syncytiotrophoblast is different from the known process of transendothelial migration of immune cells, like leuko-cytes (Muller, 2014). In this process, leukocytes interact with molecules in the endothelial cell border such as platelet endothelial cell adhesion molecule, CD99 and CD 155. Then kinesin moves the leukocyte's membrane along the microtubules and the leukocyte moves through the endothelial interface of adjacent endothelial cells (Muller, 2014). Therefore, the leukocyte requires interaction with molecules that are found in the membrane of endothelial cells, which may not be the case in this study, since it is likely that the fetal erythrocytes have been pushed via the hydrostatic pressure created rather than interact with molecules such as cell adhesion molecules expressed in cells. Moreover, the transmigration of leuko-cytes across the endothelial cells requires kinesin in order for the cell to roll over and signals

72

so that the cells can make space for the immune cells to pass. In this study however, the syncytiotrophoblast shows a plasticity, which enables the membrane to stretch, compared to the transmigration of leukocytes, where the endothelial cells membrane has no plasticity, does not stretch, rather the leukocyte rolls over in between the cells with the assistance of kinesin.

The data generated from this stack of placental images raises questions about the strength and permeability of the syncytiotrophoblast. This pathological structure suggests the association between the syncytiotrophoblast and basement membrane is relatively weak and the syncytiotrophoblast can stretch, potentially allowing movement of villi.

The only holes observed in the syncytiotrophoblast in this study were those with protruding erythrocytes, suggesting that they only open under pressure. The holes were smaller than the protruding regions of erythrocyte indicating that they had sufficient structural integrity to prevent a rip occurring as the erythrocyte pushed through. These holes could represent regions of damage, trans-syncytial channels or a structural feature making the syncytiotrophoblast locally weak.

While this observation probably represents a pathological feature, it does demonstrate a potential route for transfer of fetal cells to the mother through the syncytiotrophoblast. This could explain maternal microchimerism where fetal lymphoid cells persist in the mother's body (Bianchi et al., 1996, Dawe et al., 2007). Therefore, it is worth examining in more detail the structure of the syncytiotrophoblast in order to enhance our understanding in the mechanisms underlying the exchange of cells between fetal and maternal circulation.

The loose connection between the trophoblast basal membrane and the basement membrane of the syncytiotrophoblast has also been observed in other studies that depict that there are regions of syncytiotrophoblast damage across the placental villi (Nelson et al., 1990). These regions are also known as denudations of syncytiotrophoblast layer and are

regions where the syncytiotrophoblast is detached from the basement membrane and re-placed by fibrin deposits. These denudations could form where the trophoblast is sheared off directly from the basement membrane, leaving a very thin layer of basement membrane, or in regions where blood has pooled below the trophoblast and clotted before the overlying trophoblast died. While there is no evidence of fibrin deposits in this image, it is possible that this represents an early stage in the evolution of fibrin deposits, where the syncytio-trophoblast layer starts to become thinner compared to the normal trophoblast layer. Under-standing the pathogenesis of these regions is important as they may mediate paracellular diffusion of small solutes (Brownbill et al., 2000). Shedding of epithelial cells from the base-ment membrane has also been observed in the renal tubules in the pathological condition of acute tubular renal necrosis (Racusen, 1998). In acute renal injury, the tubular epithelial cells detach from the renal tubules causing tubule obstruction and leakage of the glomerular fil-trate (Rosen and Stillman, 2008).

The loose connection between the trophoblast basal membrane and the basement membrane could also be supported by the existence of the syncytiotrophoblast folds inside the basement membrane showing in 3D. The existence of folds in the basal membrane may suggest that the regions where there are folds, the basal membrane and the basal lamina will not be in direct contact, and their connection between them will be weak. Syncytiotropho-blast folds have also been reported before but only in 2D EM images, showing regions of trophoblast basal membrane presenting some irregularities and some occasional caveolae or interdigitation abutting the thin basement membrane (Jones and Fox, 1991). A looser con-nection would be consistent with the way in which the syncytiotrophoblast has been pushed away from the basement membrane in my observations and with the regions of denudation observed in villi. However, future work is essential in order to investigate in depth these

syncytiotrophoblast folds and define their structure and potential role in the transport of nutrients.

A limitation of this study is that it is a single event and that the underlying stroma was not observed. This is an inherent limitation of relatively low throughput techniques such as SBFSEM but the image may help the interpretation of such structures when they are observed in 2D. Another issue is whether shrinkage could have caused the erythrocytes to push through the membrane. However, it is unlikely that shrinkage caused the cells to push through the syncytiotrophoblast since this shrinkage would primarily occur during dehydration which occurs after the tissues are fixed and relatively rigid.

This study raised many questions as to how the syncytiotrophoblast layer has the ability to stretch so much without any breaching of the layer, the ability of fetal erythrocytes to squeeze through small holes and pass through the syncytiotrophoblast, and the existence of folds inside the syncytiotrophoblast. Whether this constitutes one unique observation or there is a chance that this can occur in normal placentas, is of great interest and requires further research in the future. Future work could include further investigation of the structure and function of the syncytiotrophoblast layer. Investigating the surface area that these folds constitute to the total surface area of the syncytiotrophoblast may provide evidence for the structure of the syncytiotrophoblast, which was not known so far. Investigate these folds in more placentas and try to reconstruct them in 3D will give more evidence for the existence of these folds. Quantification analysis should follow the segmentation to reveal the surface area that these folds cover in the syncytiotrophoblast. Investigating the function of these folds is also important in order to enhance our knowledge in the better understanding of the transport pathway through the basal membrane. To study the function of the folds immuno-histochemistry could be used for instance for Ca^{+2} transporters, Na^+/K^+ exchange regulatory proteins to see if there are more transporters/proteins in these folds and so facilitate the

transport of Ca^{+2}, Na^+/K^+ exchange through the placenta. It has been shown that the transport of calcium is increased in FGR babies compared to normal pregnancies but is unaltered in diabetes pregnancies (Strid et al., 2003). Therefore, studying the function of these folds may enhance our understanding in the number of calcium transporters. Investigating the properties of the syncytiotrophoblast layer in normal placentas would be interesting in order to see whether the syncytiotrophoblast can stretch under pressure and if so how much is the stretch from the bottom of the basement membrane. Moreover, try to study more in depth the mechanism through which the fetal erythrocytes pass through the syncytiotrophoblast layer is very important, since this can explain whether other fetal cells can also pass through the syncytiotrophoblast layer.

To conclude, this study successfully generated 3D images of a previously undescribed feature within the placenta. The structure that raises questions about the elastic properties of the syncytiotrophoblast and the potential passage of fetal erythrocytes through the syncytiotrophoblast layer.

Chapter 4: The placental villous stroma contains giant extracellular vesicles associated with fibroblasts networks

4.1 Introduction

Placental function underpins the development of the fetus in the womb and establishes the foundations for health in postnatal life (Burton and Fowden, 2015). The nutrients and waste products that cross the placenta, except those that cross the vasculosyncytial membranes where there is limited if any stroma, must also cross the placental villous stroma which lies between the trophoblast and the fetal capillaries (Castellucci et al., 2000). However, relatively little research has focused on the villous stroma, its contents and their contribution to placental function.

In other tissues, the stroma constitutes a fundamental component of the tissue and its maintenance and remodelling is essential for health (Bonnans et al., 2014). The connective tissue, or stroma, contains extracellular matrix, cells including fibroblasts and macrophages. Extracellular matrix consists of collagens surrounded by glycoproteins and proteoglycans which form a gel-like material that determine many of the physical properties of the connective tissue (Yue, 2014). These extracellular matrix proteins are produced by fibroblasts, that also maintain and remodel the extracellular matrix.

Other components of the extracellular matrix are stromal extracellular vesicles (ECVs) (Rilla et al., 2019). These small membrane bound vesicles have been observed in a number of different tissues and are thought to contain mediators that help regulate stromal remodelling and processes such as angiogenesis (Rilla et al., 2019). In bone, ECVs of different sizes (from 20 - 300 nm) and different types have been reported in association with particular tissues or roles) (Rilla et al., 2019). ECVs can be made in a number of different ways, exosomes (20 - 250 nm) are thought to be made inside the cell and secreted, while microvesicles (100 - 1000 nm) are thought to be made by folding and pinching off of the plasma membrane (Tong and Chamley, 2015).

In the placenta, the villous stroma lies between the trophoblast which forms the primary barrier between the mother and the fetus, and the fetal capillaries which transport the maternal nutrients to the fetus (Kaufmann et al., 2004). The villous stroma, is a loose connective tissue consisting of extracellular matrix, stellate cells and macrophages (Kohnen et al., 1996). The villous stroma is permeable to the diffusion of solutes while providing a supportive structural matrix for surrounding cells (Chen and Aplin, 2003). As the stroma increases the diffusion distance for gasses and other solutes, the value of its biological role within the placenta must offset any reduction in transfer efficiency.

Extracellular matrix proteins in the placenta have been shown to be altered in response to maternal infections such as in Chagas' disease, and in idiopathic fetal growth restriction (Duaso et al., 2012). The role of fibroblasts and macrophages within the villous stroma are not well understood. Fibroblasts in the villous stroma have a stellate structure with sparse perinuclear cytoplasm, and there is evidence that they produce collagen and so maintain the structural architecture of the extracellular matrix (Sati et al., 2008, Ilic et al., 2008). Changes in extracellular matrix composition are reported when cultured placental fibroblasts are exposed to hypoxia raising questions about the role of fibroblasts and extracellular matrix in disease (Chen and Aplin, 2003). Fibroblasts may also regulate the vascular development, for instance via fibroblast growth factors that stimulate angiogenesis (Auguste et al., 2003). Placental villous macrophages (Hofbauer cells) are phagocytic and may play immune roles but more research is required to establish their role in the villous stroma (Seval et al., 2007, Jones et al., 2015a).

As mentioned above, stromal cells are known to secrete membrane-bound ECVs into the extracellular matrix. These vesicles contain bioactive compounds which interact with ECM proteins and are thought to act as signposts for the remodelling of stroma (Rilla et al.,

2019). There is only one report of stromal ECVs associated with pericytes in the placenta (Jones and Desoye, 2011).

The role of the villous stroma in health and disease is poorly understood. This study uses multiscale and 3D imaging at the nano and micro scales to provide an insight into the role of elements of the stromal matrix, including placental fibroblasts and ECVs.

4.2 Methods

Term placental tissue was collected after delivery from uncomplicated pregnancies with written informed consent as described in Chapter 2.3.

4.2.1 Tissue collection and fixation

Placental tissue samples from eight different placentas were collected as soon as possible after delivery (samples left more than a few minutes before fixation will show vacuolation within the syncytiotrophoblast) and small pieces ($\approx$ 2 mm^3) fixed in glutaraldehyde at RT and then placed at 4°C overnight until processing as described in Chapter 2.4.1.

4.2.2 SBFSEM processing and imaging

SBFSEM samples were aldehyde fixed, immersed in potassium ferrocyanide, and then in osmium tetroxide, in thiocarbohydrazide, aqueous uranyl acetate, lead aspartate and aspartic acid. The samples were then dehydrated using a series of increasing ethanol concentrations and infiltrated in resin. Polymerised blocks were trimmed (< 1 mm^2), mounted on an aluminium pin with conductive glue and sputter coated with gold/palladium (Deerinck et al., 2010) as described in Chapter 2.5.1.

Blocks were imaged using a Gatan 3View inside a FEI Quanta 250 FEGSEM at 3.0 kV accelerating voltage, spot size 3 and with a vacuum level of 40 Pa as described in Chapter 2.5.2. The voxel size of the stack that was used to segment the placental fibroblast in 3D was 7 x 7 x 50 nm, while the total size of the imaged region was 21 x 21 x 47.05. The regions chosen for imaging were those which appeared to be terminal villi and the field of the first slice was set to include the syncytiotrophoblast which was the initial focus of the study.

4.2.3 TEM processing and imaging

Fixed placental fragments were washed twice with cacodylate buffer, placed in osmium tetroxide, treated with aqueous uranyl acetate, dehydrated using an ethanol series starting from 30% until absolute ethanol, and then infiltrated in resin to enable the resin to polymerize, as described in Chapter 2.4.1 and 2.4.2.

Ultrathin sections (ranging 90 - 100 nm) were cut using an ultramicrotome as described in Chapter 2.4.3. The sections were placed on a grid, stained with Reynolds lead citrate to enhance contrast, and then observed under the TEM.

4.2.4 Preparation of placental tissue for observation under the wholemount confocal microscope

Placental tissue was collected from normal pregnancies and fixed in PFA as described in Chapter 2.6.1. After overnight fixing, the specimens were washed in PBS and then stored at 4°C.

Prior to labelling the placental samples were again washed in PBS, cut into 2 - 3 mm^3 blocks and permeabilised in Triton X-100. The samples were then incubated in BSA to block non-specific binding, and primary antibodies and/ or lectins diluted in PBS were added to the samples and incubated overnight at 4°C as described in Chapter 2.6.2. The primary antibodies and lectins that were used were; polyclonal rabbit anti human SLC22A11 (Abcam ab76385) was used at a dilution of 1:200, was shown to bind fibroblast like stellate cells in the villous stroma. Polyclonal mouse anti human CD136 (ABD Serotec MCA1853T) was used at 1:500, FITC-Aleuria Aurantia Lectin (AAL, Vector labs FL-1391) at 1:150 and rabbit anti human vimentin monoclonal (Clone SP20, Abcam ab16700) used at 1:500. Samples were then washed for 3 times 10 min, and incubated with secondary antibodies for 2 h on

the roller with 0.4% DAPI and then washed with PBS 3 times for 10 min as described in Chapter 2.6.2. Secondary antibodies were supplied by Thermo Fisher and used at 1:200.

Samples were cleared through an increasing series of Thiodiethanol starting from 10% up to 97% TDE and then stored at 4°C until imaging as described in Chapter 2.6.2.

Samples were imaged using a 4-channel confocal laser scanning microscope as described in Chapter 2.6.3. Stacks of 50 - 70 images were generated using sequential imaging (to eliminate spectral bleed through) with 800 by 800 pixels with 4-line averaging (to reduce random noise) using x 63 objective magnification and x 3 optical zoom. Each stack consisted of between 50 and 70 sequential images with a z axis spacing of 1 or 2 µm.

4.2.5 Image processing and analysis

The 27 SBFSEM image stacks of terminal villi from eight placentas were processed in Fiji (version 2.0.0 - rc - 43) using Gaussian blur (sigma radius 2) and enhanced contrast (0.4% saturated pixels). Selected regions were manually segmented in Amira (Version 6.0) as described in Chapter 2.5.3. SBFSEM stacks were analysed/segmented in Amira (version 6.0) to produce 3D reconstructions of each placental cell type. Confocal laser microscopy image stacks were also analysed using Amira (version 6.0), to reconstruct in 3D the networks of fibroblast-like stellate cells as described in Chapter 2.6.4.

TEM images were all adjusted for brightness (+ 75%) and contrast (+ 17%) in Photoshop.

4.2.6 Quantification of volumes, diffusion barriers and measuring dimensions of giant ECVs

To analyse volumes of villous components and the potential cellular barriers to diffusion in terminal villi, a stereological approach was adopted for SBFSEM stacks as described in Chapter 2.7 (Mayhew, 2006). All the stereological analysis was performed by myself. It is important to note that these measurements are specifically for terminal villi, which are believed to be the primary exchange area within the villi and not the villi as a whole. Terminal villi were distinguished from the intermediate and stem villi by the presence of vasculosyncytial membranes, dilated sinusoidal capillaries and less stromal volume compared to intermediate and stem villi (Haeussner et al., 2015). In total 4944 points were categorised on 309 slices. This included 3136 points falling on villous components and 1808 on intervillous space.

To calculate proportional volumes of villous features the number of points where the lines intersected falling in each cell type or area of interest (syncytiotrophoblast, cytotrophoblast, stroma, fibroblast-like stellate cells, macrophages, pericytes, endothelial cells, endothelial lumen and intervillous space) were counted and expressed as the proportion of the total number of points falling on villous tissue (but not intervillous space). Tissue volume was determined from the number of points falling on the tissue as a proportion of total points falling on the image times the volume of the region analysed.

To assess how cell types within and around the stroma may act as diffusion barriers between the syncytiotrophoblast and endothelium we calculated:

A. the proportion of syncytiotrophoblast covered by cytotrophoblast

B. the proportion of fetal capillary endothelium covered by pericytes

C. the proportion of the stroma between the trophoblast and endothelium which contain fibroblast-like stellate cells.

86

For these measurements the randomly selected slices and the randomly offset grids described in Chapter 2.7 were used counting intersections on the vertical lines. To determine the proportion of syncytiotrophoblast basal membrane covered in cytotrophoblast in the terminal villi, the number of intersections with syncytiotrophoblast basal membrane in direct contact with cytotrophoblast was divided by intersections with syncytiotrophoblast basal membrane. To determine the proportion of the capillary covered by pericytes in terminal villi, intersections with endothelial basal membrane in direct contact with pericytes were divided by the total intersections with endothelial basal membrane. To determine the proportion of pathways across the villous stroma that are blocked by fibroblast-like stellate cells the number of times that a horizontal grid line between syncytiotrophoblast basal membrane and endothelial basal membrane intersected a fibroblast-like stellate cell was divided by the total number of times the lines intersected both syncytiotrophoblast basal membrane and endothelial basal membrane.

To determine the length and width of the giant ECVs identified by the stereological approach, their locations were identified within the SBFSEM stacks and all the slices in which each vesicle appeared were inspected. The longest distance in the x, y and z axis (as determined by block orientation) were measured. The longest axis was taken to be the length and the average of the two shorter axes was taken to be the width.

4.2.7 Quantification of standard stromal vesicles

The volume of standard stromal vesicles of the typical sizes seen in other tissues was too low to allow identification of many of these by the systematic point counting approach. So in order to estimate the size of these vesicles 2 - 3 vesicles per placenta were identified by eye and the length and width were measured in the same way as in the giant ECVs.

4.2.8 Data analysis

For stereological analysis, running means were plotted to assess the adequacy of the sample size. Data are presented as mean and SEM or median and range as appropriate. Statistical comparisons were performed using a Student's t test or a Mann Whitney t test when the values are considered not normally distributed. $P \leq 0.05$ was taken as significant.

4.3 Results

4.3.1 Composition of the villi and villous stroma

The composition of the terminal villi was assessed in 27 SBFSEM stacks from eight different placentas. The relative volumes of the villous trophoblast, stroma and vascular compartments and the different cell types therein are reported in **Table 4.1**. Hofbauer cells have not been measured due to the fact that the regions examined in stacks were between trophoblast layer and fetal capillaries, near the outside of the terminal villi, rather than the centre of the terminal villi where Hofbauer cells are more likely to be present.

Table 4.1: Volume percentages of the components of terminal villi

	% of villous volume Mean ± SEM (n = 8 placentas)
Trophoblast compartment	47.0 ± 3.0%
Syncytiotrophoblast	41.4 ± 3.1%
Cytotrophoblast	5.6 ± 1.8%
Stromal compartment	19.2 ± 3.3%
Extracellular matrix	13.0 ± 2.1%
All Extracellular vesicles	0.7 ± 0.2%
Fibroblasts	5.4 ± 1.3%
Vascular compartment	33.8 ± 4.7%
Pericytes	2.3 ± 0.5%
Endothelial cells	8.3 ± 0.8%
Endothelial lumen	23.2 ± 4.6%

4.3.2 Extracellular vesicles

Within the villous stroma, ECVs constitute 3.9% of stromal volume (**Table 4.2**). Stromal vesicles are typically 200 nm in diameter but the majority of those observed in the placenta were much larger. This non-systematically selected sample of 19 ECVs from eight placentas had an average length of 0.35 ± 0.02 µm (range 0.18 - 0.55 µm), average width 0.20 ± 0.01 µm (range 0.12 - 0.28 µm) and width to length ratio 0.59 ± 0.04 (range 0.25 - 0.82) (**Table 4.3**). The length of the giant stromal vesicles spanned a wide range and were not normally distributed, compared to the typical size stromal vesicles which showed normal size distribution (**Figure 4.1**).

Table 4.2: **Volume percentages of the stromal components**

	% of stromal volume
	Mean ± SEM (n = 8 placentas)
All stromal vesicles	3.9 ± 1.3%
Giant stromal vesicles (> 600 nm)	3.8 ± 1.2%
Fibroblasts	25.1 ± 4.6%
Extracellular matrix	71.0 ± 4.7%

Table 4.3: **Giant and small extracellular vesicle dimensions**

	Giant vesicles Mean ± SEM (n = 27 vesicles, 8 placentas)	Typical stromal vesicles Mean ± SEM (n = 19 vesicles, 8 placentas)
Longest axis (µm)	3.04 ± 0.39	0.35 ± 0.02
Width (µm)	2.00 ± 0.29	0.20 ± 0.01
Width to length ratio	0.66 ± 0.03	0.60 ± 0.04
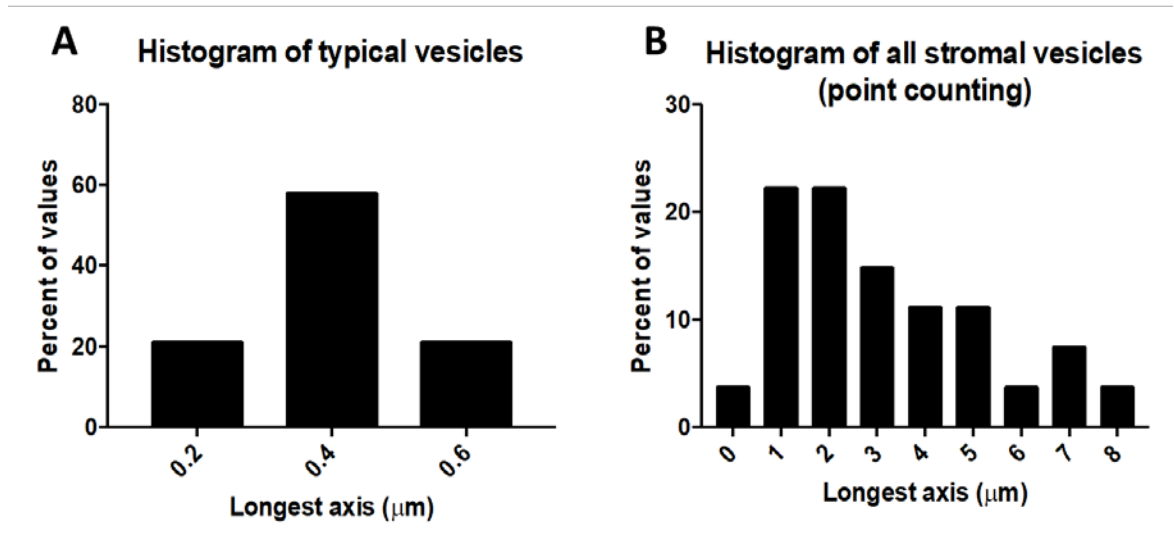
Figure 4.1: ***Histograms of the ECVs***. ***A***. *Histogram showing the distributions of typical size vesicles selected in a non-systematic manner and* ***B***. *Histogram showing the distribution of all stromal vesicles identified systematically by point counting.*

The standard stromal vesicles constituted a very small proportion of stromal volume, in the order of 0.1%. As only one point fell on a standard vesicle this value must be regarded as an estimate and we were not able to estimate the size of these vesicles using our systematic approach. The standard sized stromal vesicles did not interact with the stellate cells nor did they have visible contents. The identification of vesicles was confirmed by scrolling through the SBFSEM stack. Not all features that appeared to be vesicles in 2D slices were in fact vesicles when viewed in multiple slices. Within the villous stroma, the processes of fibroblast-like stellate cells often appeared to be standard stromal vesicles in single slices (**Figure 4.2**).

The giant ECVs were in contact with a stellate fibroblast-like cell at some point on their surface in 63% of cases. Vesicles in contact with fibroblasts tended to be larger than those without contact with fibroblast-like stellate cells (3.25 ± 0.47 µm range of 0.70 - 7.73 vs. 1.53 ± 0.58 µm, range of 0.35 - 5.57, $P = 0.03$)**.**
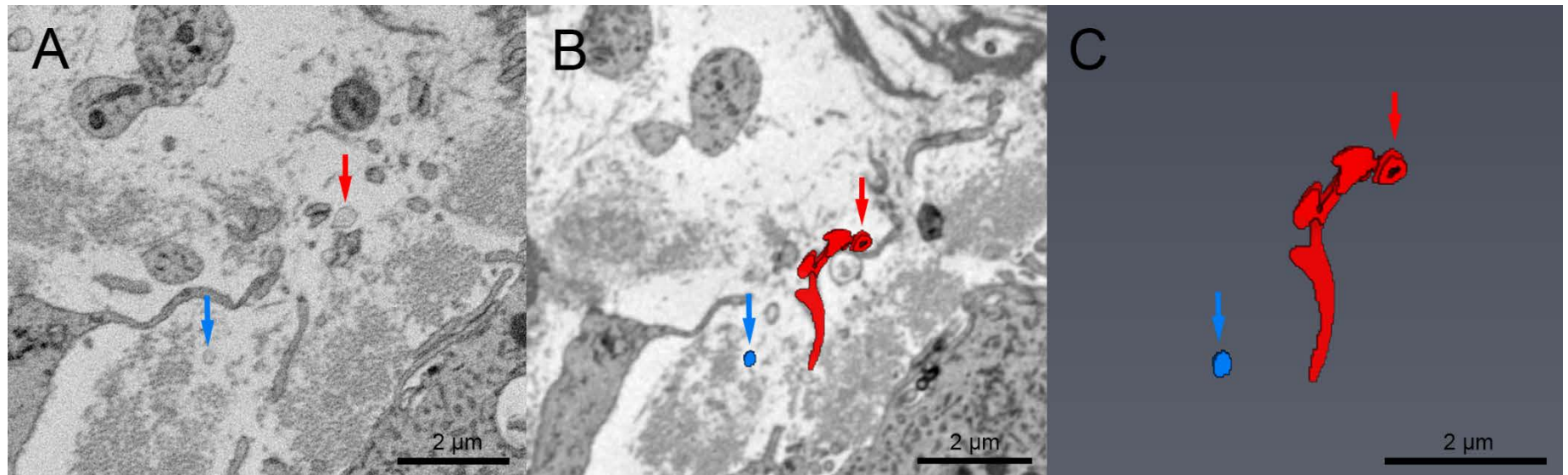
Figure 4.2: ***SBFSEM imaging of ECVs in the stroma.*** ***A.*** *A small stromal vesicle in the villous stroma (blue arrow). The red arrow points to a stromal component which looks like a typical extracellular vesicle.* ***B.*** *Segmentation and reconstruction shows that the apparent typical extracellular vesicle indicated by a red arrow is in fact part of a stellate cell process shown in red.* ***C.*** *3D image of the blue small stromal vesicle which is not attached to anything and the red one which is part of the stellate process.*

Nearly 22% of the big vesicles (3 µm in size) seem to be in touch with fibroblast processes, while almost 35% of the typical stromal vesicles (ranging from 1 to 2 µm in size) are not in touch with the fibroblast processes (**Figure 4.3**). TEM showed that the membrane of one extracellular vesicle was closely adjacent to the membrane of the stellate cell process but the two structures maintain discrete membranes and no points of fusion were observed (**Figure 4.4 B and C**). In a limited number of samples, TEM imaging of the giant extracellular vesicle membranes demonstrated the leaflets of the lipid bilayer (**Figure 4.4 C**).

Histogram of vesicles touching and not touching fibroblasts
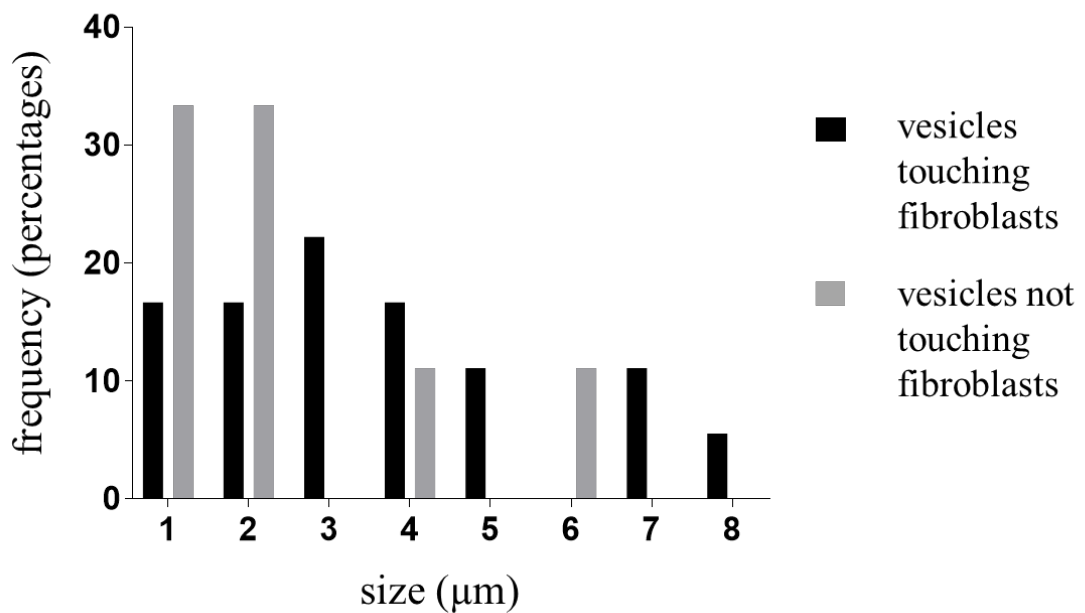
Figure 4.3: Histogram showing the distributions of the vesicles touching and not touching the fibroblast processes. The graph shows that those vesicles touching fibroblast processes tend to be bigger in size than the typical stromal vesicles and the typical stromal vesicles are not likely to interact with fibroblast processes.

While the ECVs were largely devoid of electron dense contents they did often contain membranous strands or vesicles which in one case was demonstrated to be a lipid bilayer by TEM (**Figure 4.5**). However, the vesicles rarely contained more than one or two of these membranous structures and there was nothing resembling organelles or apoptotic bodies.
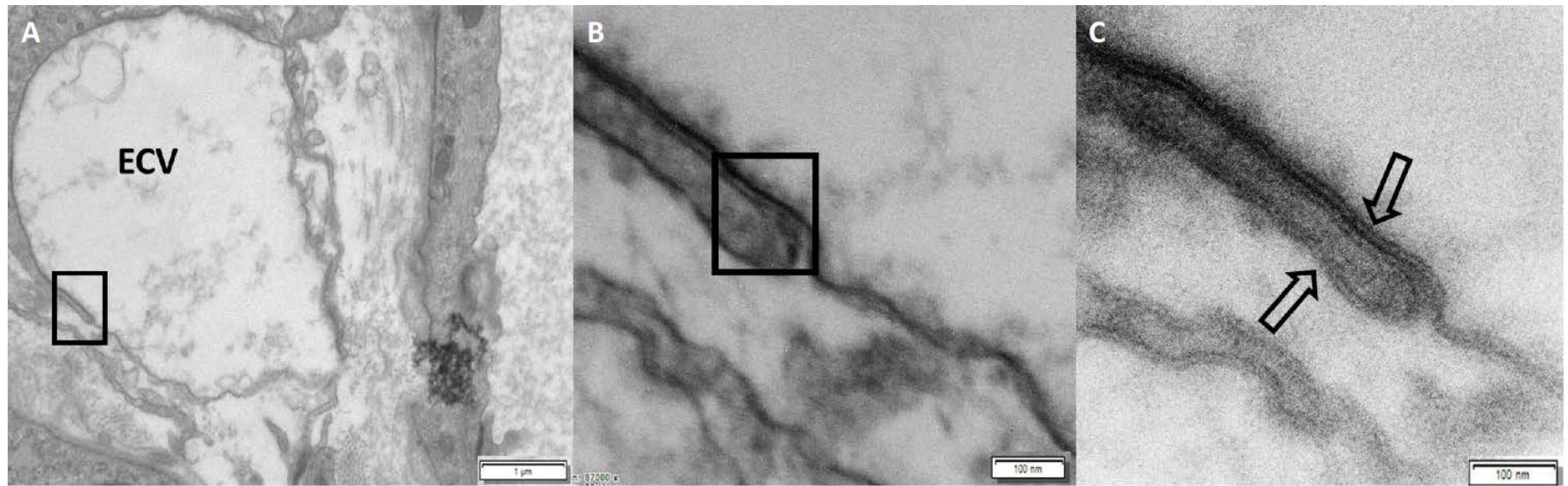
Figure 4.4: ***TEM of stellate cell-stromal vesicle connections showing that both have separate membranes. A.*** *extracellular vesicle surrounded by a fibroblast-like stellate cell process. The black box shows the area of interest.* ***B.*** *TEM image showing the membrane of the extracellular vesicle adjacent to the membrane of the fibroblast process as shown by the black box.* ***C.*** *higher magnification image showing the lipid bilayer of the extracellular vesicle and adjacent fibroblast process (black arrows).*
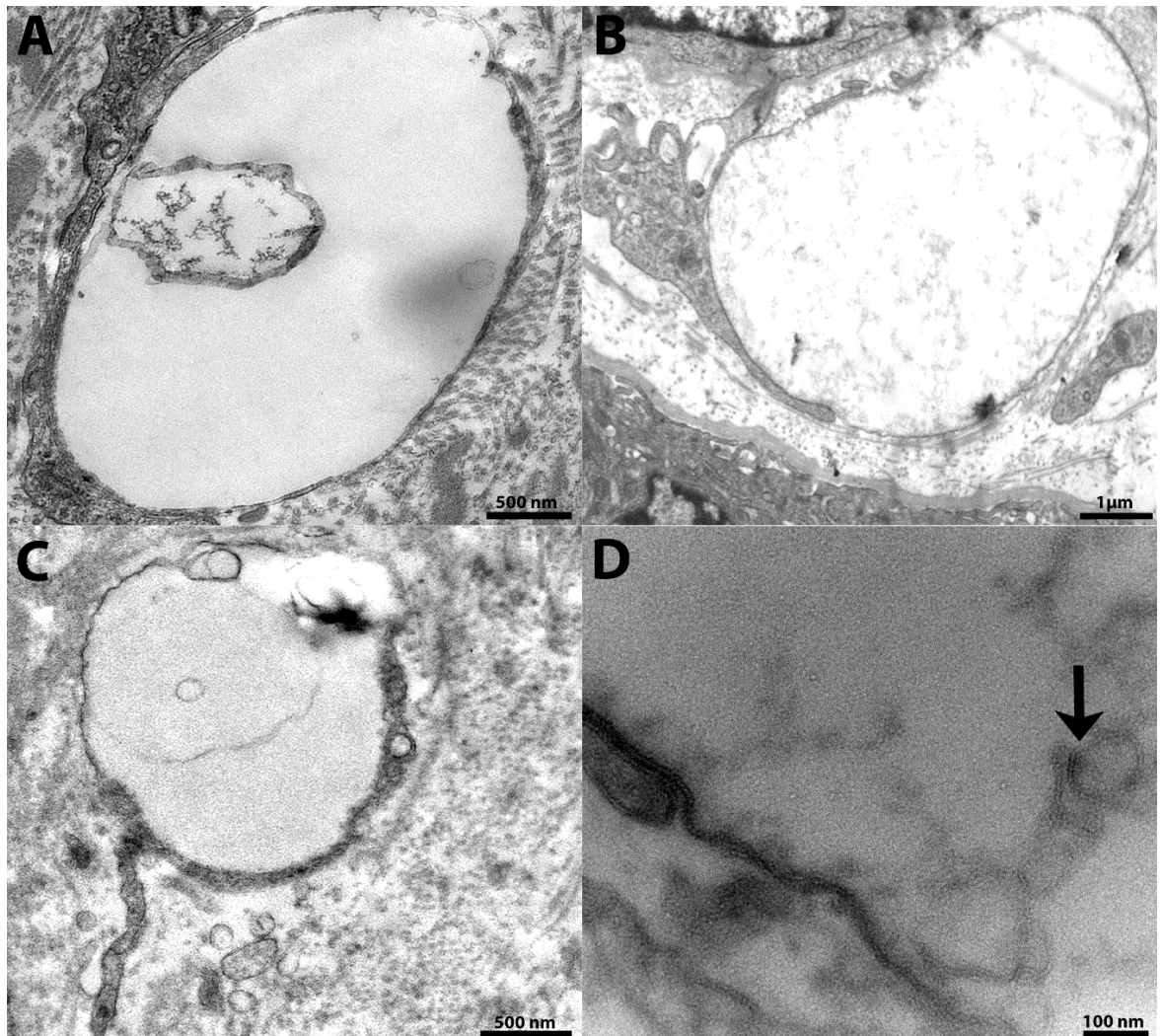
Figure 4.5: TEM images of giant stromal ECVs including those with internal material. *A. stromal extracellular vesicle containing a membranous component inside its cavity. **B.** extracellular vesicle that contains strands inside its cavity. **C.** Another extracellular vesicle containing a different membranous component. **D.** Higher magnification image showing the lipid bilayer in one of the membranous components (white arrow) inside the cavity of a giant extracellular vesicle.*

4.3.3 Fibroblast-like stellate cells

Within the 3D SBFSEM stacks the fibroblast-like stellate cells could be seen throughout the terminal villi, with many apparent cell-cell connections. Segmentation and 3D reconstruction of a stromal stellate cell demonstrated a cell with limited perinuclear cytoplasm and multiple long thin processes extending out into the extracellular matrix (**Figure 4.6 A, B, C and D**). Stellate processes were also in contact with giant ECVs (**Fig 4.6 E and F**). The processes from the fibroblast like stellate cells formed a thin sheet, or sail, which were observed closely aligned with the underlying capillaries (**Fig 4.6 E**).

95

A population of cells in the stroma with a stellate appearance were shown to bind an antibody to SCL22A11 (**Figure 4.7**). The stellate cells did not co-localise with the macrophage marker CD163 or AAL lectin which bound to endothelial cells around capillaries. Some SLC22A11 staining was also observed on discrete regions of endothelium but this was easily distinguishable from stromal staining in a 3D stack based on capillary markers. Confocal imaging showed that vimentin a recognized fibroblast marker was observed to bind to fibroblasts-like stellate cells making connections with a number of fibroblast-like stellate cells in the villous stroma the same way as the SLC22A11 (**Figure 4.8**).

Analysis of fibroblast-like stellate cell networks in confocal stacks from three placentas suggested that the average number of fibroblast nuclei per network was 3.3 ± 0.3. The 3D reconstruction of a placental fibroblast-like stellate cell from a SBFSEM stack was used to demonstrate fibroblast-like stellate cells in close contact with each other. The 3D fibroblast-like stellate cell structure showed that they were different fibroblast-like stellate cells and not regions of the same cell, something that cannot be demonstrated from a 2D image (**Figure 4.9 A and B**).
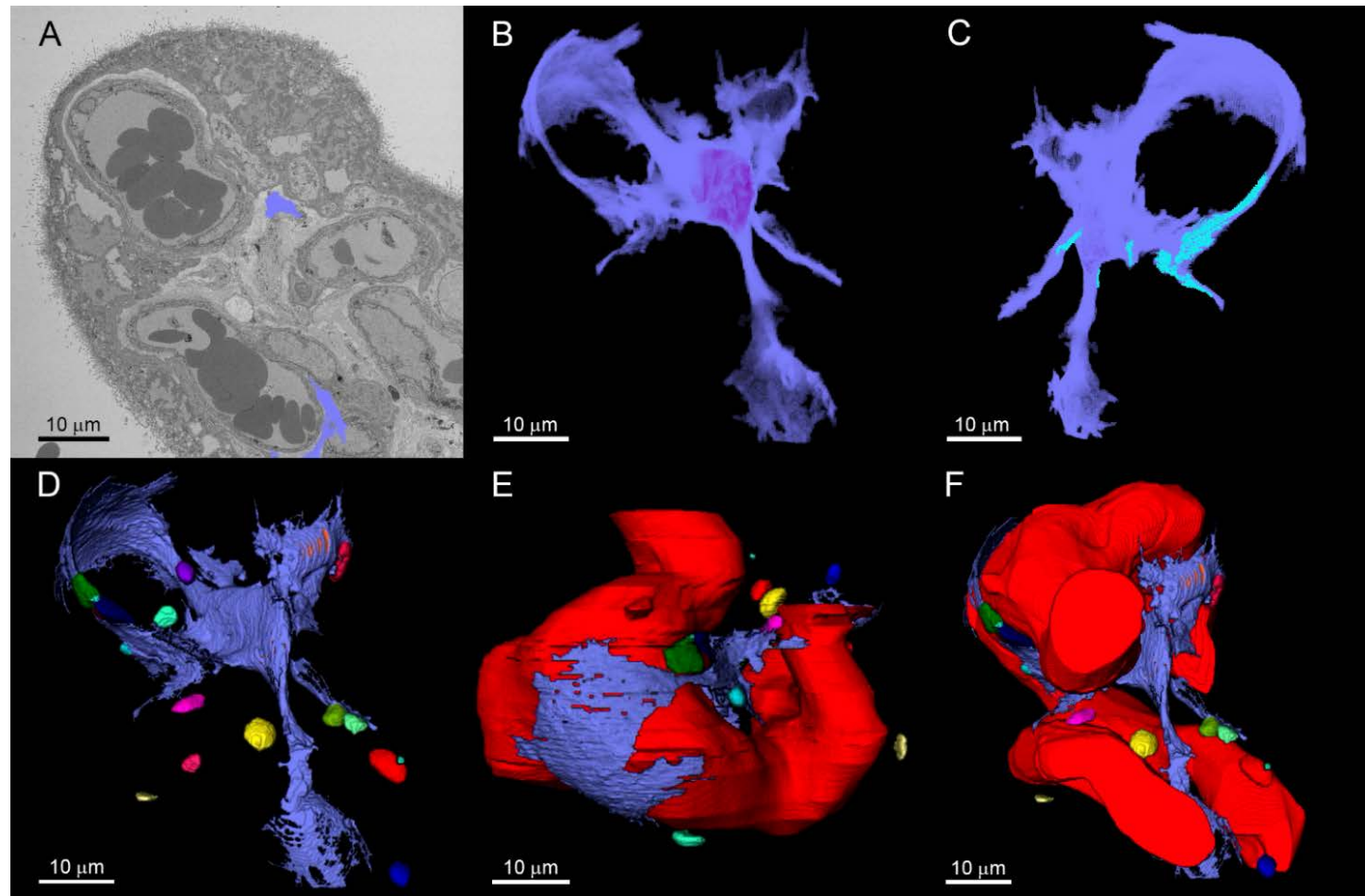
Figure 4.6: **3D reconstruction of a fibroblast-like stellate cell and its relationship with capillaries and giant stromal ECVs in the stroma. A.** *SBFSEM of a placental stromal fibroblast.* **B.** *segmented 3D fibroblast structure.* **C.** *Regions on the stellate cell where there were interactions with other stellate cells are shown in light blue.* **D.** *Fibroblast interactions with ECVs in the villous stroma.* **E.** *The relationship between the fetal capillary and the fibroblast.* **F.** *The stellate cell's association with the fetal capillary and the ECVs.*

97
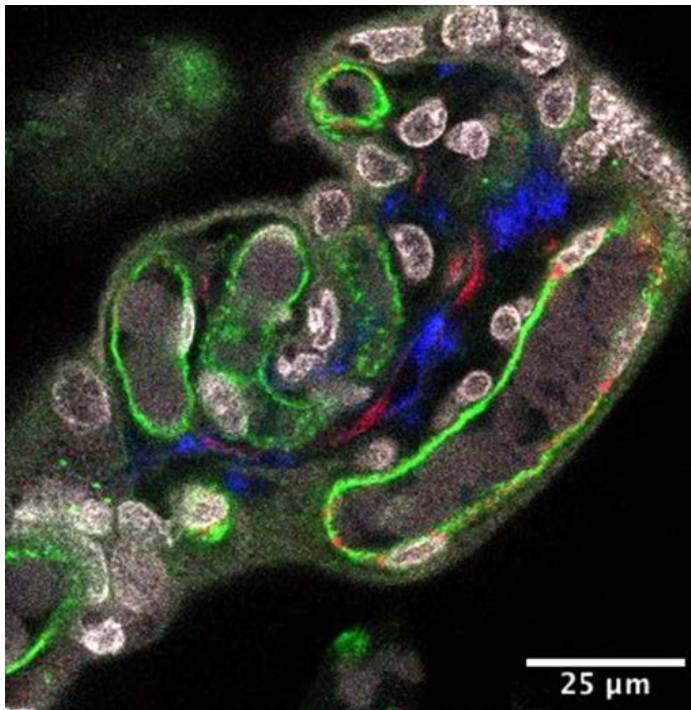
Figure 4.7: *SLC22A11 staining.* *Confocal image of term placental villi showing that SLC22A11 bind stellate like fibroblast cells and not macrophages. SLC22A11 in red, CD163 in blue, AAL in green, DAPI in white. Figure produced by Professor Lewis.*
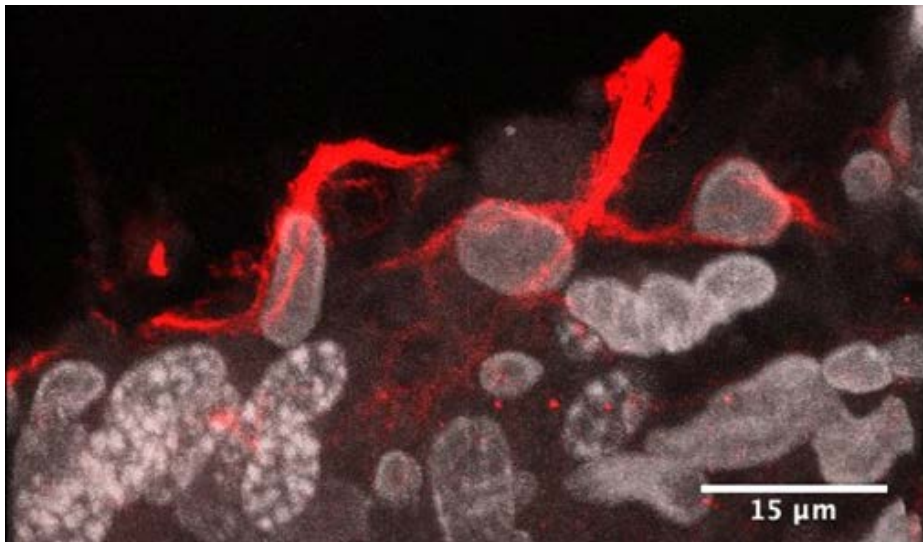
Figure 4.8: **Fibroblast-like stellate cells staining with vimentin**. Projection of a confocal stack showing the fibroblast like stellate cells stained with vimentin, which is a recognised fibroblast marker. The two cells on the right appear joined by their processes as seen with SCL22A11 and in the SBFSEM stacks. Figure produced by Jenny Pearson Farr.
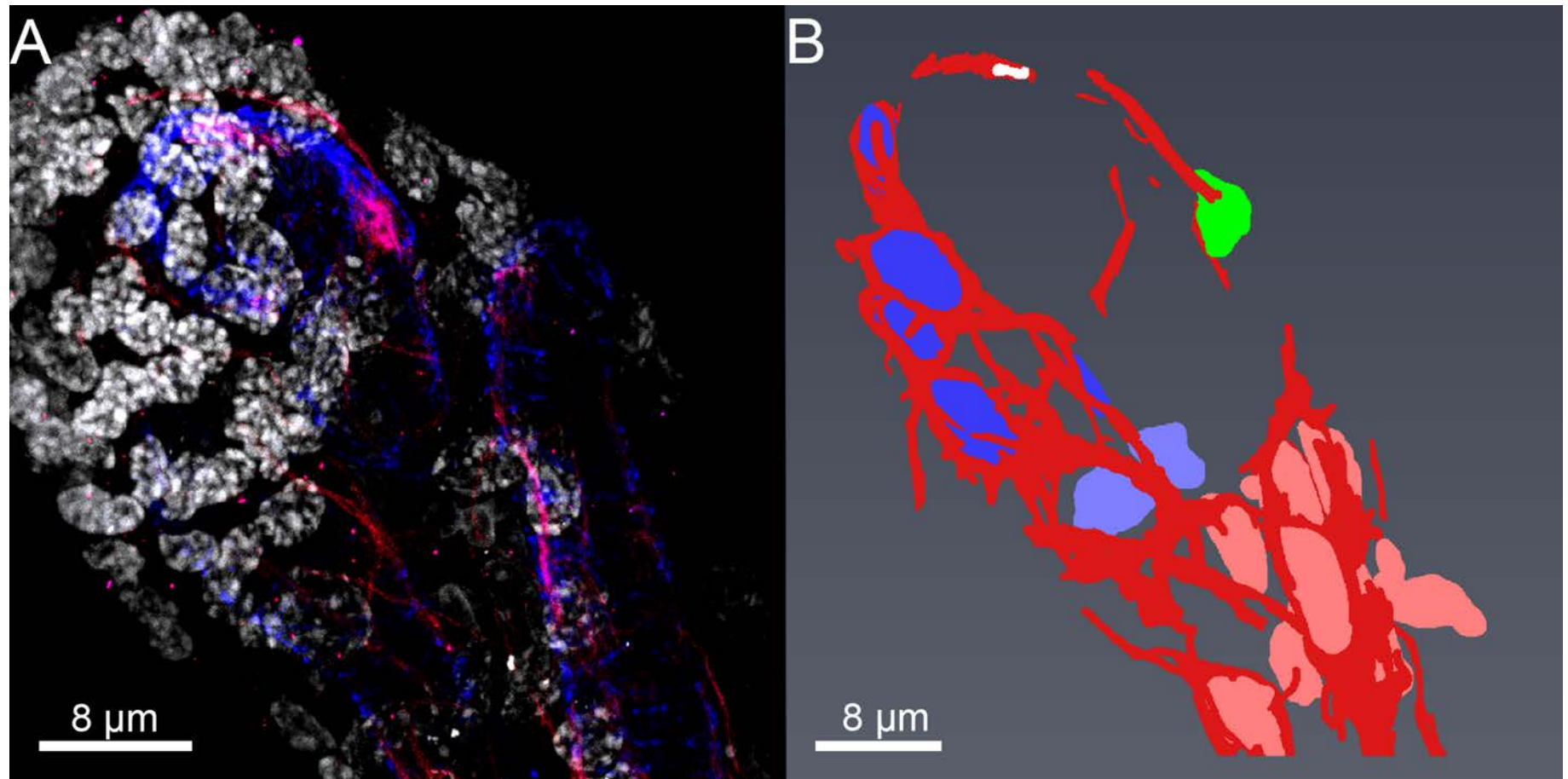
Figure 4.9: ***Wholemount confocal of networks of fibroblast-like stellate cells.*** *A Fibroblast networks stained with SLC22A11 (red), pericytes surrounding fetal capillaries stained with α-SMA (blue) and the nuclei stained with DAPI (white).* ***B****. Segmentation of the fibroblast like stellate cell networks. The fibroblast like stellate cell processes are shown in red and their nuclei are shown in four different colours (blue, light blue, green (isolated cell) and pink) demonstrating three different networks.*

Evidence from TEM and SBFSEM images showed that adjacent stellate cells or their processes were connected by desmosome-like junctions (**Figure 4.10 A and B**). These desmosome-like junctions were not clearly identifiable on SBFSEM stacks, so it was not possible to accurately estimate their numbers or density.

TEM imaging of a stellate fibroblast process demonstrated that regions away from the cell body contain mitochondria and rough endoplasmic reticulum (**Figure 4.10 C**).

4.3.4 Diffusive barriers

Within the stroma, fibroblast-like stellate cells were shown to lie between the trophoblast basal membrane and fetal capillaries shielding 32% of the fetal capillaries. Pericytes were shown to cover around 15% of the endothelium and the cytotrophoblast cover around 24% of the syncytiotrophoblast basal membrane as shown in **Table 4.4**.

Table 4.4: Stellate cells, pericytes and cytotrophoblast as diffusive barrier in the stroma

	Mean ± SEM N = 8 placentas
Stellate cell between syncytiotrophoblast and endothelial basal membrane	32.3 ± 7.8%
Cytotrophoblast on syncytiotrophoblast basal membrane	23.9 ± 10.4%
Pericytes on endothelial basal membrane	15.3 ± 3.8%
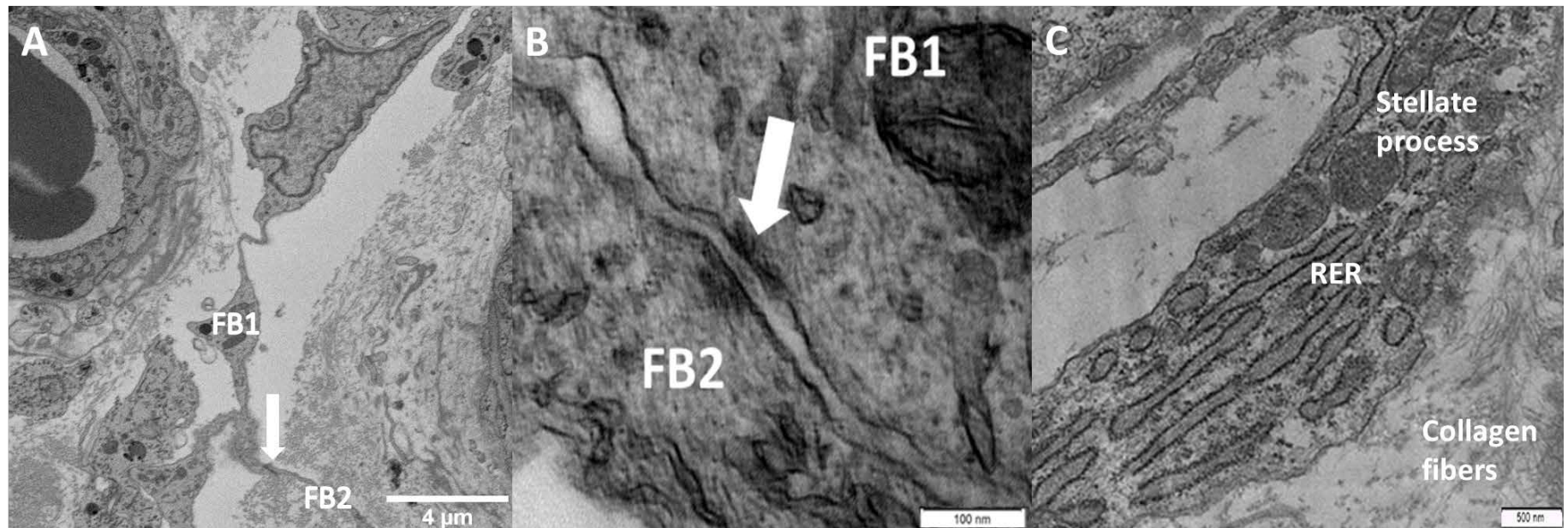
Figure 4.10: ***TEM images of placental stromal stellate cells. A.*** *shows the networks of stellate processes within the stroma with the white arrow indicating the junction between two stellate cells (FB = fibroblast-like stellate cell).* ***B.*** *TEM image of two adjacent stellate cells connected with a desmosome-like junction. The desmosome-like junction is marked with a white arrow and the two stellate cells are marked FB1 and FB2.* ***C.*** *TEM image of a fibroblast processes containing cellular machinery. RER = rough endoplasmic reticulum.*

4.4 Discussion

This study demonstrates the presence of ECVs within the villous stoma including a population of stromal vesicles much larger than previously observed in tissue or plasma. These giant stromal ECVs were typically found in close association with fibroblast-like stellate cells, which were shown to form local networks, suggesting a higher level of organisation within the stroma. These findings demonstrate how a multiscale 3D imaging approach can provide novel biological insight into features that are visible but not easily interpreted in 2D slices, and demonstrate the complex interactions between different cell types or cellular compartments.

In other tissues, stromal ECVs play important roles but these have volumes hundreds of times smaller than the giant ECVs we report here (Rilla et al., 2019, Stik et al., 2017). These giant vesicles were surrounded by a lipid bilayer, contained little or no electron dense material, were typically ovoid in shape and were almost always in contact with a fibroblast-like stellate cell at some point or covering their entire surface. While these giant ECVs are easy to visualise on TEM sections, without the 3D information provided by SBFSEM they are difficult to interpret. There is only one paper which has reported these structures in the human placental villi on the TEM, suggesting that these big extracellular vesicles may originate from apoptosis of pericytes (Jones and Desoye, 2011). The size and abundance of these vesicles was greater than expected and identifying their function is of significant interest.

While the giant ECVs were the predominant species by volume, vesicles within the more typical size range for stromal vesicles (200 - 600 nm) could also be observed. An important question is whether the stromal vesicles represent one continuous population or whether they are distinct populations with distinct origins and biological roles. The standard stromal vesicles were not associated with fibroblast-like stellate cells, there were not any contents easily visible by electron microscopy and their size distribution suggest that they

may be a distinct population from the giant vesicles. The fact that standard ECVs are not in touch with fibroblast processes may just suggest that due to their small size, they are not big enough to be in contact with the fibroblast processes. The giant ECVs however, may cover more surface area in the stroma and so it is more likely to be in touch with the processes. Even though the frequency distributions showed a significant trend of the big vesicles touching the fibroblast processes, a conclusion cannot be drawn. The difficulty in observing the typical stromal ECVs and the difficulty in systematically selecting small stromal vesicles in the 27 stacks of eight different placentas means the sampling has the potential to be biased, and further work is required to quantify them in other placentas, assess their size in comparison to the giant ECVs, and find the correlation between the size of the vesicles and contact with fibroblast processes.

While giant ECVs were in close contact with stellate fibroblast-like cells there was no evidence that the giant ECVs were in any way joined to them and both appeared to have discrete membranes with a lipid bilayer. If the giant vesicles have similar roles to standard stromal vesicles they may be acting as signposts within the stoma and stellate fibroblast-like cells may be touching them to receive some form of chemical message or may induce the proliferation and migration of fibroblasts (Ferreira et al., 2017). Alternatively, the fibroblast-like stellate cells may be secreting substances into the vesicles or even guiding them through the stroma.

The origin of the giant stromal vesicles is not clear as they are not typical ECVs and their size suggest there may be a novel mechanism of formation. It is unlikely that they form like exosomes within the cell or by membrane budding like microvesicles. They are closely associated with fibroblast-like stellate cells, but there was no evidence of them being joined to or coming from these cells. No clear associations were observed with other cell types. While they contain occasional membranous structures or strands of material, they do not

contain organelle like structures that would suggest that they were apoptotic bodies. Their size raises the question whether they were once cells, but their limited contents argue against this. Another possibility is that they are derived from organelles extruded from a cell but again their size may argue against this (Nakajima et al., 2008). As no evidence of their formation was observed it is also possible that they have formed at an earlier point in gestation, or being part of the stroma channels. However, since these stroma channels are replaced by dilated capillaries forming loops in the terminal villi, it suggests that these giant ECVs cannot be remnants of the stroma channels (Kaufmann et al., 1977).

What the giant stromal vesicles contain is not clear but answering this question is key to determining their function. If the giant stromal vesicles are like standard stromal vesicles they may contain hormones and other signals such as microRNA. Alternatively, they may be storage or transport vesicles. Their low electron density would be consistent with fluid filled vesicles or possibly lipid droplets. As the giant stromal vesicles have a lipid bilayer this argues against them containing lipids, because lipid droplets have a phospholipid monolayer, and because lipid is usually electron dense when stained with osmium but the vesicle contents were clear (Vanni, 2017). Glycogen typically has a dark appearance on the electron microscope so it is not likely to be the content of the vesicles (Revel et al., 1960). They could contain fluid, but it is not clear what role fluid filled vesicles would perform within a fluid filled medium, although they could play a mechanical cushioning role within the villi.

Purifying stromal vesicles from homogenised placental tissue will require specific markers as it would not be possible to distinguish them from vesicles formed from cell contents formed during the isolation process. Specific protein markers could be identified utilizing immunogold on TEM sections. This would allow flow cytometry of placental homogenates in order to identify and purify these vesicles (Welsh et al., 2018). Raman spectroscopy

would be an in situ way of identifying whether the vesicles contain lipid (Devitt et al., 2018). Mass spectroscopy based microscopy may be another approach but it does not currently have the required resolution (Norris and Caprioli, 2013).

The stellate fibroblast-like cells formed small local networks which may allow cell-cell communication and potentially regional coordination of their activities. The observation of desmosome-like junctions between stellate cells suggests that these connections are more than transient contacts. The average fibroblast-like stellate cell network as observed by confocal was just 3 cells. However, using the confocal may underestimate the true size of the networks as the thin stellate processes of the fibroblasts may not always be clearly visible within the confocal stacks especially where the Z axis (typically 2 µm) was considerably thicker than the processes, some of which were just 0.2 µm thick.

The structure of the stromal stellate fibroblast-like cells observed by SBFSEM was complicated with processes extending throughout the stoma and forming contacts with many other stromal features. As can be seen from the 3D reconstruction, fibroblast-like stellate cell structure was intimately connected to the surrounding structures including the capillary, the stromal ECVs and the collagen forming the extracellular matrix.

An unexpected observation was the extent to which the stellate fibroblast-like cells formed a diffusive barrier between the trophoblast basal membrane and the fetal capillaries. Solutes such as glucose and amino acids are assumed to diffuse freely across the stoma (Cleal et al., 2018b). However, in terminal villi and more specifically near the vasculosyncytial membranes, the primary exchange area, over a quarter of the capillary is blocked by fibroblast-like stellate cell processes. The 3D structure of placental fibroblast-like stellate cells demonstrates that it forms a large sail-like structure shielding the capillary. These structures have been inferred from 2D imaging (Castellucci et al., 1990a) but it is a marker of how little

we understand the role of these cells or the villous stroma that we do not understand what the function of such structures are.

Pericytes also constitute a diffusive barrier as this study revealed that 15.3% of the pericytes cover the endothelial basal membrane, which has not been observed before in the human placenta. Little is known on the pericytes coverage in the placental villi volume, but a study in mouse placenta revealed that placentas with platelet derived growth factor (PDGFB) deficiency demonstrate pericyte and trophoblast loss and fetal blood dilation (Ohlsson et al., 1999). The same study also showed that pericytes are positioned between labyrinth capillary loops. Therefore, the pericyte coverage in the human placenta may suggest the importance of the pericytes in the fetal capillary dilation and in the attachment of the capillary loops to each other. Stereology data in this study also showed that pericytes constitute 2.3% of the placental villi volume, while the endothelial cells constitute 8.3% of the total placental villi volume, suggesting that the volume ratio between endothelial cells and pericytes is 1:4 in the terminal villi of normal human term placenta. There is limited if any research on the volume ratio between pericytes and endothelial cells in other human and animal tissues, but a study has shown that the cell ratio between endothelial cells and pericytes in normal human tissues varies between 1:1 - 10:1 and the pericyte coverage between 70% and 10% respectively (Sims, 1986). In a more recent study on the human central nervous system (CNS) the endothelial cell-to pericyte ratio was found 1:1 - 3:1 and the pericyte coverage reached 80% (Mathiisen et al., 2010). In another study it has been reported that diseased human skeletal muscle can have a 100:1 cell ratio between endothelial cells and pericytes (Diaz-Flores et al., 2009), while a study in rats showed that the coverage of pericytes in cardiac muscle is 11% and in retina 41% (Hall, 2006). Since the pericyte coverage in the fetal capillaries in the terminal villi of normal term human placentas was found 15%, this may suggest that placental fetal capillaries may be more similar to the capillaries in

muscle with low pericyte coverage and density, than the ones in CNS which are considered to have the highest density and coverage of pericytes than other tissues (Armulik et al., 2011).

This study also revealed that cytotrophoblasts cover around 24% of the syncytio-trophoblast basal membrane. This number contradicts the results of two previous studies, one showing that cytotrophoblast can cover 80% of the trophoblast basal lamina (Mori et al., 2007b) and the other more recent study showing that cytotrophoblast can cover 44% of the trophoblast basal lamina (Jones et al., 2008). Due to the fact that stereology approach was applied to SBFSEM stacks and not high resolution TEM images, there is a possibility that very small and thin cytotrophoblastic processes could not be easily observed and there-fore quantified, as in the previous study (Jones et al., 2008). However, the results of this study showing that cytotrophoblasts in terminal villi cover around 24% of the trophoblast basal membrane are the same as stated in an old study showing that term cytotrophoblasts do not cover more than 24% of the trophoblast basal lamina (Sen et al., 1979).

A recent study has demonstrated that is possible to grow placental organoids in the lab (Turco et al., 2018). These placental organoids may suggest an alternative way of isolat-ing the giant ECVs and study their role in healthy placentas. Understanding the role of the giant ECVs in healthy placentas will enhance our knowledge in understanding the changes that occur in the structure and function of the vesicles in the diseased placentas. Lab-grown placental organoids could also suggest a potential system for growing fibroblast networks (Turco et al., 2018). This will provide a better understanding of the amount of fibroblast networks in a healthy term placenta and determine whether these networks are local or larger networks consisting of more fibroblast nuclei. Understanding the quantity and role of fibro-blast networks is essential in order to understand whether these networks play a crucial role in the diseased placentas.

The 3D ultrastructural characterisation of the villous stroma in healthy pregnancy presented here demonstrates how these approaches can enhance our understanding in the placental structure. These techniques can now be used to understand whether these structures change in disease and whether they contribute to pregnancy pathology. The structure of the villous stroma may play an important role, perhaps more important than the number of transporters in the syncytiotrophoblast, in facilitating placental function and therefore fetal growth. Fetal development builds the foundation for lifelong health and the role of the stroma in this remains to be fully determined.

To conclude, this study demonstrates for the first time the 3D complicated structure of placental fibroblast processes and the interactions of the fibroblast processes with other fibroblasts and with giant stromal ECVs. Stereological analysis enhanced the results of this study showing the existence of fibroblast networks and the giant vesicles. These findings demonstrate the complex structure of the villous stroma and a high order of organisation, which could suggest a potential barrier to diffusion of nutrients across the stroma and so further investigation of the role of the stroma is required.

Chapter 5: 3D imaging of novel interendothelial protrusions inside endothelial cells

5.1 Introduction

The structure and arrangement of endothelial cells lining blood vessels varies between tissues and different vascular systems depending on their function (Aird, 2012). For instance, in capillaries where nutrient exchange takes place the arrangement of cells and the permeability of the junctions will be different to that in arteries. In term human placenta, there is limited information about endothelial architecture in different regions of the villous tree. The dilated capillaries in terminal villi where nutrient transport is believed to occur, represent specialized regions not seen in other tissues (Kaufmann et al., 1979). This study will seek to investigate the structure of villous capillaries and determine if there are structural adaptations that may relate to their function.

Endothelial cells communicate with neighbouring cells across the endothelial interface between adjacent endothelial cells (Lampugnani, 2012). Two of the three types of junctional complexes that have been identified between endothelial cells in vessels are the tight and adherens junctions and the third type is gap junctions (Bazzoni and Dejana, 2004). The tight junctions are responsible for maintaining cell polarity between the apical and basal side and determine the paracellular pathway regulating the selective permeability of solutes in size, ion charge and electrical resistance. Tight junctions restrict the leakage of transported solutes and water and allow the passage of small ions (Bazzoni and Dejana, 2004). The adherens junctions serve as a bridge by connecting the actin cytoskeleton between two neighbouring endothelial cells contributing to the tube formation and are involved in cell growth and apoptosis. In general junctions play a crucial role in the formation and maintenance of a semipermeable in size (less than 3 nm in diameter) and ion-specific endothelial barrier (Irie et al., 2004).

Placental capillary endothelial interface between adjacent endothelial cells comprise of tight and adherens junctions which are responsible for regulating the tightness of endothelial interface between adjacent endothelial cells and therefore the rate of paracellular diffusion of nutrients, wastes and other components (Burton et al., 2009). Placental capillaries in terminal villi in term human placenta are more permeable to macromolecules and the diffusion of small molecules resembling more to continuous non-brain capillaries (Leach and Firth, 1992). Human placental capillaries resemble less tight continuous capillaries as seen in skeletal muscle, in which there are discontinuous tight junctional strands creating small pores to increase the paracellular permeability of water, small molecules and ions (Eaton et al., 1993). The number of junctional complexes determines the permeability of the endothelial interfaces between adjacent endothelial cells in the placental capillaries and inhibits or increases the cell proliferation. The tight junctions in the fetal capillary endothelium tightly link the adjacent endothelial cells and also determine the permeability of the paracellular route for the diffusion of nutrients and passage of water and hydrophilic solutes that can cross the endothelium. In the placental endothelium tight junctions are interspersed in the paracellular cleft and not in the luminal or abluminal surface and as mentioned above have the structural characteristic of small pores, 4nm separation between the two membranes of the neighbouring endothelial cells. Tight junctions in the placenta have the junctional integral molecule occludin which has different frequency across the placental vascular tree, with absence of occludin in tight junctions in the terminal villi vessels. Occludin may play an important role in the stability of the junctions between adherent endothelial cells. Therefore, absence of occludin in the tight junctions in the terminal villi vessels may suggest that these vessels demonstrate higher permeability in solute exchange, which is expected since the terminal villi vessels are the main sites of nutrients exchange between the mother and the fetus (Leach et al.,

2000). Increased permeability in the capillary endothelium is also due to the lack of plako-globin in adherens junctions (Lampugnani et al., 1995). Both plakoglobin and occludin reduce the permeability of endothelial interfaces between adjacent endothelial cells to macro-molecules. Placental endothelial interfaces also have adherens junctions that contain VE-cadherin and other catenins that are involved in cell proliferation and angiogenesis (Leach et al., 2000). Therefore, endothelial interfaces in placental capillaries may play a role in the remodelling and angiogenesis of the vascular bed (Leach, 2002).

Work in the placental laboratory in Southampton has produced 3D images of a feto-placental arteriole and venule based on segmentation of a SBFSEM stack (**Figure 5.1**). In this image, the size and shape of endothelial cells are different in arteriole compared to venule as shown in **Figure 5.1**. The longer and less wide (in the direction perpendicular to flow) cells around the arteriole, compared to the venule cells, are consistent with the higher shear stress that would be expected in a smaller vessel transporting the same volume of blood. This finding is in accordance with studies showing that human cardiac arterioles bear the highest blood pressures and are smaller vessels with a lumen diameter around 30 µm, compared to the venules with a bigger lumen diameter ranging between 7 and 100 µm (Kaufmann A., 2019, Martinez-Lemus, 2012).
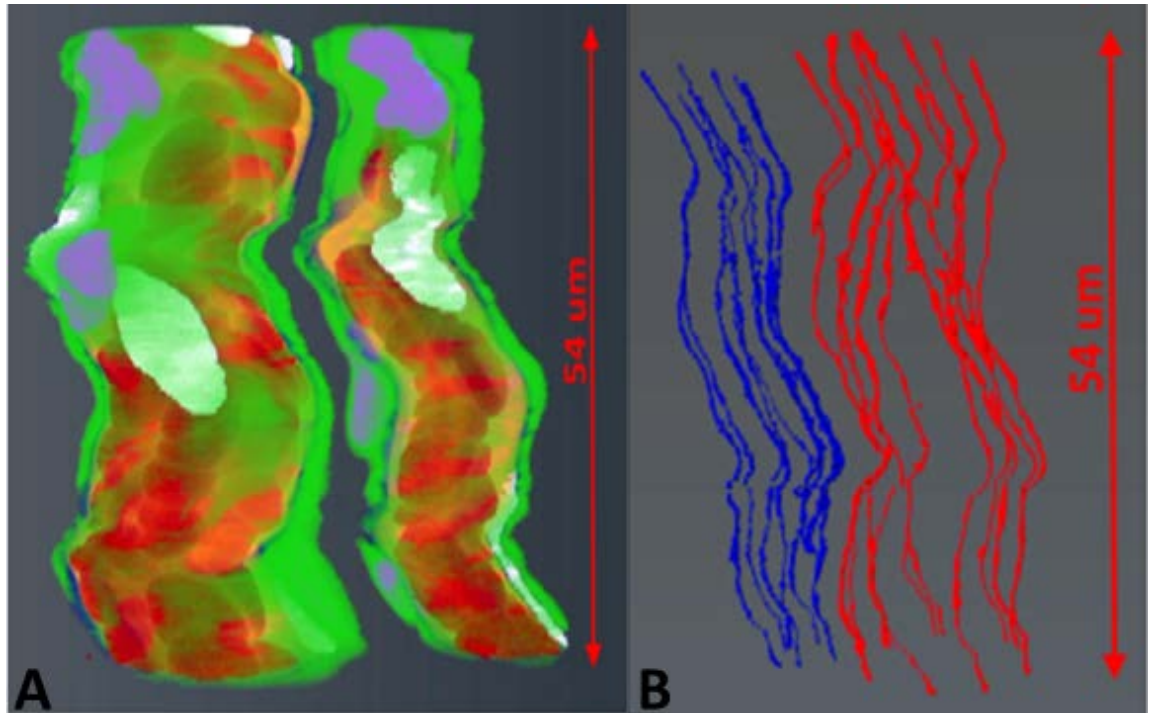
*Figure 5.1: 3D reconstruction of arteriole and venule. A: venule on the left and arteriole on the right. Green: pericytes, purple: nuclei of pericytes, white: nuclei of endothelial cells, red: endothelial lumen, blue: endothelial cells. **B**: endothelial interfaces between adjacent endothelial cells in the arteriole (blue) and the venule (red). Segmentation performed by Wendy Chiu and Rodolfo De Souz).*

The number of endothelial cells in a vessel determines the number of endothelial interfaces. Both the permeability and the number of endothelial interfaces in a vessel will determine its permeability. An interesting question is whether there would be more endothelial interfaces between adjacent endothelial cells in dilated terminal capillaries where most nutrient transport is thought to occur than in other placental capillaries or capillaries in other tissues.

In the literature there are few systematic studies of the number of endothelial cells in a capillary cross section, which may reflect the difficulty of determining this in 2D images. There is limited research on the number of endothelial cells per lumen surface area in the capillary (Glyn and Ward, 2000). Based on a few TEM images in the literature, the number of endothelial interfaces around a capillary lumen is typically low compared to the number of endothelial interfaces that this study demonstrates. In human muscle continuous capillary

for example, there are two endothelial interfaces (**Figure 5.2 A).** Other studies show three

endothelial interfaces around a rat myocardium capillary (Firth, 2002), three to four endothe-

lial interfaces around human cardiac capillaries (Glyn and Ward, 2000) and two to three

around a human muscle capillary (Wolburg et al., 2009). In a human pancreatic capillary

there are four endothelial interfaces (**Figure 5.2 B**), and in a kidney glomerular capillary

there are around three interfaces (**Figure 5.2 C**) (Joseph, 2017).
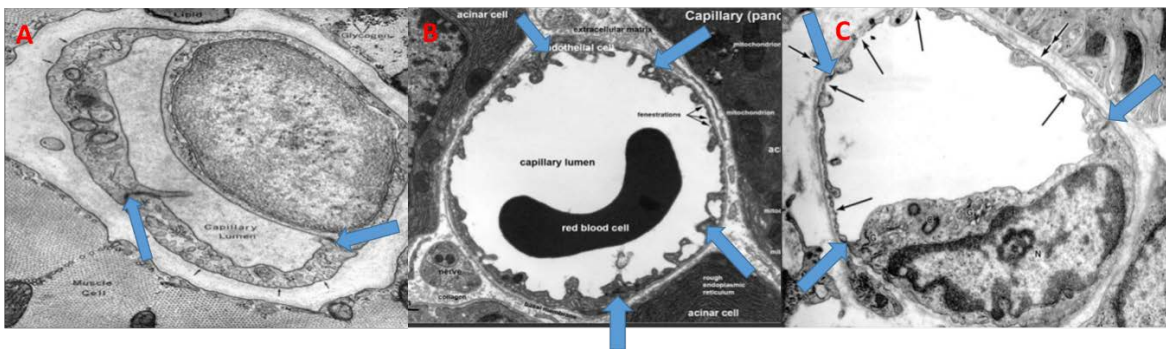
*Figure 5.2: **TEM images of cross sections of the capillary endothelial lumen from different tissues. A**. Endo-
thelial lumen of a human muscle continuous capillary. The blue arrows point to the endothelial interface be-
tween adjacent endothelial cells. **B**. The endothelial lumen of a capillary in pancreas. The blue arrows point to
endothelial interfaces and the three little black arrows at the top right of the image point to fenestrations. **C**.
The endothelial lumen of a kidney glomerular capillary. Blue arrows show the endothelial interfaces, while the
black arrows point to fenestrations. Figures modified from (Joseph, 2017).*

Recent advances allowing 3D imaging at the ultrastructural level may allow identifi-

cation of specialized structures important for endothelial function. As illustrated in Chapter

4, 3D imaging can highlight structures that are not apparent in 2D.

In initial studies I observed a novel type of cell connection between adjacent endo-

thelial cells that I have termed interendothelial protrusions (IEPs). This study aims to inves-

tigate more in depth the IEPs in feto-placental capillaries.

Specific aims of this study are:

- Characterize and quantify the number of novel ultrastructural features in a
  fetal capillary

- Study the structure of the villous feto-placental capillary in 3D

- Quantify the number of endothelial interfaces in a villous capillary as this will contribute to the permeability of the feto-placental capillary

5.2 Methods

Samples from term human placenta were observed under SBFSEM and TEM microscopy as described in Chapter 2.1.

5.2.1 Preparing samples for SBFSEM

Tissue was collected as described in Chapter 2.1 and processed for SBFSEM as described in Chapter 2.2.3.

Placental tissue was imaged using a Gatan 3View inside an FEI Quanta 250 FEGSEM at 3.0 KV accelerating voltage, spot size 3 and with a vacuum level of 40 Pa. I generated 33 stacks from eight normal term placentas. From the 33 stacks, the 27 stacks containing images of terminal villi were selected to perform the stereology based analysis of tissue volumes as well as quantification of the numbers of endothelial interfaces, complex endothelial interfaces between adjacent endothelial cells and IEPs. The segmentation of the IEPs was performed in Amira (version 6.0, UK). The slices showing the IEPs were between 20 and 80 selected from two different stacks. The 3D visualising of a fetal capillary was achieved by segmentation of a stack consisting of 467 slices. The voxel size of each slice was 4.2 x 4.2 x 50 nm, while the total image size was 3000 x 3000 pixels.

5.2.2 Processing stacks in Amira

Images were processed in Fiji (version 2.0.0 - rc - 43) (Schindelin et al., 2012) using Gaussian blur (sigma radius 2%) and enhanced contrast (0.4%-saturated pixels). The whole stack that was used for segmenting the fetal capillary was imported into Amira (version 6.0, UK) and processed as described in Chapter 2.3. On every image each endothelial cell was manually segmented.

The stacks used to segment the different types of endothelial interfaces between adjacent endothelial cells were downsized to 3000 x 3000 pixels in FIJI.

5.2.3 Segmentation of IEPs

Selected regions that showed the IEPs were isolated from the stacks 15 (placenta number 5) and 27 (placenta number 8), and to improve clarity, enhance contrast 0.4% saturated pixels was applied to the selected slices.

5.2.4 TEM processing and imaging

To image IEPs, complex endothelial interfaces between adjacent endothelial cells and endothelial interfaces, placental villous tissue was collected as described in Chapter 2.1 and processed for TEM as described in 2.2.2.3. Placental tissue was fixed with osmium tetroxide, aqueous uranyl acetate, infiltrated into resin and cut into ultrathin sections (ranging between 90 - 100 nm thickness) slices using an ultramicrotome (Ultracut Reichert-Jung, UK). Slices were imaged under the TEM (Tecnai T12, UK). The images produced by the microscope were captured by a digital camera (Ruska, 1980) and saved as Tiff images.

5.2.5 Measuring the number of IEPs appeared in the seven segmented endothelial cells

The 3D reconstruction of a feto/placental capillary in Amira, was followed by manually measuring the number of IEPs appeared in each of the seven segmented endothelial cells. The values are presented as mean and STD of the total seven endothelial cells.

5.2.6 Quantifying the number of IEPs and complex endothelial interfaces in eight different placentas

Further quantification analysis of IEPs and complex endothelial interfaces was performed in eight different placentas from 27 stacks. A stereological approach was not attempted because the IEPs and complex endothelial interfaces do not appear in many slices and take up very low volume which would mean that even with many points per slice it would be very rare for a point to fall on one of these features. The number of points that would need to have been counted made this approach infeasible. Instead, I inspected every slice by eye and marked all the IEPs that were observed using a region of interest (ROI) marker in Fiji to identify them for the future and prevent double counting. The length of the processes/junctions was assessed as the distance between the base which was considered the endothelial interfaces and the tip (one slice before the process disappears from the stack). The width was calculated as the diameter of the widest point of the process/junction.

5.2.7 Quantifying the number of endothelial interfaces between adjacent endothelial cells in eight different placentas

The number of endothelial interfaces was manually counted on every 50th slice (with a randomly selected first slice as described in section 2.7) in each of the 27 stacks in total from eight different placentas. To achieve accuracy in the quantification of endothelial interfaces, some criteria were set out. 1) The number of endothelial interfaces were counted only where there was a full capillary cross section and 2) where the complete circumference of the capillary was visible (**Figure 5.3**). 3) To ensure that there were no apparent cross sections (for instance a section through a bend in the capillary that did not fully bisect the capillary) the regions to either side of the selected slice were inspected within this stack.

5.2.8 Stereological analysis of the endothelial cell volume in eight different placentas

The endothelial cell volume was measured in the same every 50 slices in which stereology was applied for the volumes and surface areas of the different cell types as mentioned in Chapter 4.2.6. The capillary diameter was measured only in the capillaries that endothelial interfaces between adjacent endothelial cells were quantified as mentioned above. The diameter was measured as the widest point of the capillary cross section on the same every 50 slices where the number of junctions was counted.

5.2.9 Measuring the capillary diameter in all the stacks of eight different placentas

In order to relate the number of endothelial interfaces between adjacent endothelial cells per capillary diameter, the diameter of the capillaries was measured in all the stacks in eight different placentas. To maintain the consistency in the study, the capillary diameter was measured in the same every 50 slices and in the same capillaries in which the number of endothelial interfaces was counted as described in section 5.2.7.

5.2.10 Statistics

The sample size used for this study was eight different placentas from which 27 stacks were generated in total. The graphs were produced in Excel and GraphPad Prism (GraphPad Prism, version 7.0, UK). To identify the different populations of the IEPs and the complex endothelial interfaces a Mann-Whitney test when the data was not normally distributed was performed in GraphPad Prism. Pearson linear correlations were performed using the GraphPad Prism to determine the association between the number of IEPs or endothelial interfaces in different capillary diameters. Data are reported as mean and standard error of mean (SEM).

Cross-section

3D image of a fetal capillary
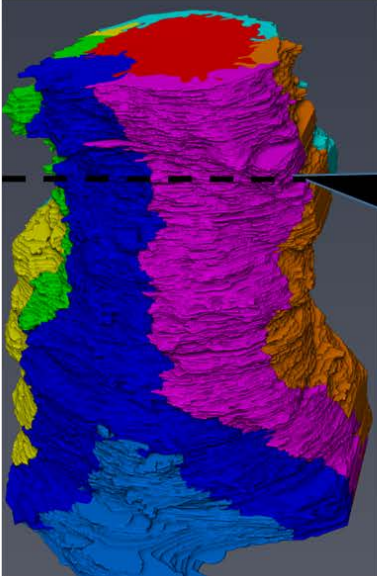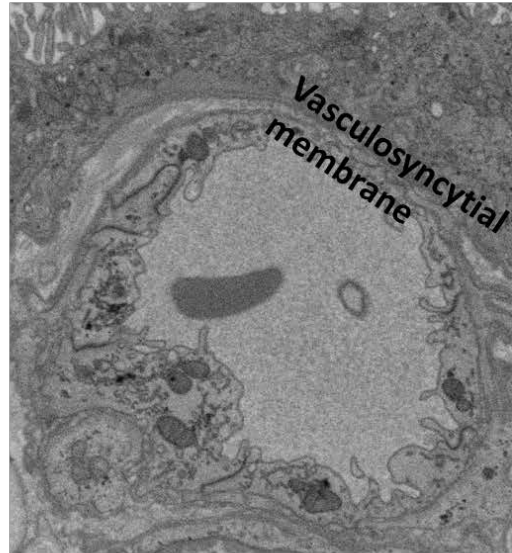
EM image

Vertical section

3D image of a fetal capillary
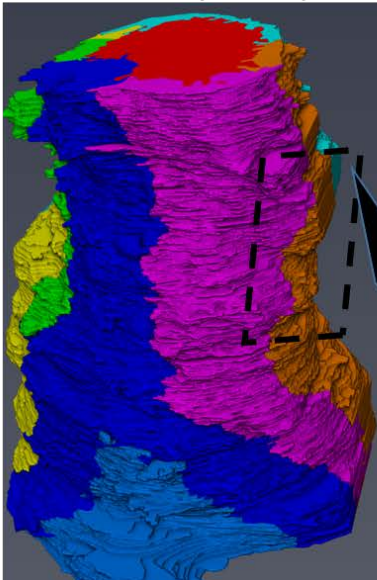
EM image
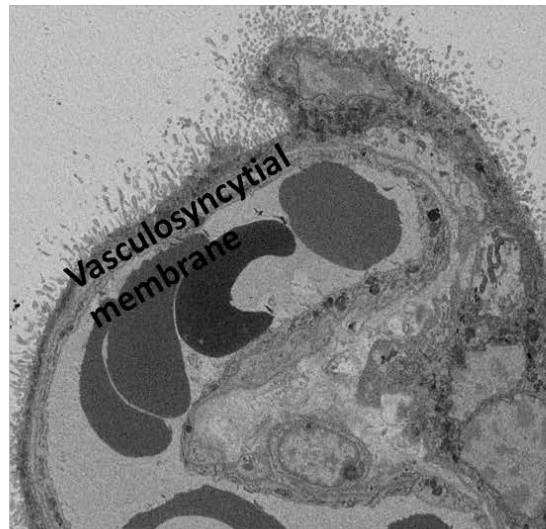
<u>Figure 5.3:</u> *Cross section and horizontal section of a fetal capillary*. *The figure shows cross-sectional and vertical slices of a 3D image of a fetal capillary produced in this study and how these sections are visualized under the electron microscope. The electron microscopy images are representative images of the 27 SBFSEM stacks generated in this study. Only full cross sections were used for counting endothelial interfaces between adjacent endothelial cells.*

5.3 Results

5.3.1 SBFSEM of fetal capillary endothelial cells

To investigate in depth the 3D structure of a fetal capillary in the placental terminal villus, a stack consisting of 467 slices was generated in the SBFSEM. **Figure 5.4** shows a representative 3D image showing the endothelial cells and the IEPs with yellow arrows. A movie of the whole stack is available online DOI:10.5258/SOTON/D0849 (https://doi.org/10.5258/SOTON/D0849). This segmented region of capillary depicts that the capillary is located in terminal villus and moving from a non-dilated to a dilated region of the capillary. The segmented region of this capillary contains seven partial endothelial cells (**Figure 5.4**).

5.3.2 Initial observation of IEPs

An interesting feature of the segmented region of capillary was that there were long IEPs extending from these cells inside their neighbours (**Figure 5.5**). The IEPs grow from the donor cell at the endothelial interface and extend within recipient cell with both cells maintaining the integrity of their plasma membranes (**Figure 5.5** and **5.6**).

5.3.3 TEM imaging and 3D projections of IEPs

Following the observation in the SBFSEM stacks TEM images, which have a higher resolution than SBFSEM images, were studied to identify profiles of the IEPs. Profiles consistent with IEPs and complex endothelial interfaces between adjacent endothelial cells were observed in four different normal human term placentas under TEM as shown in **Figure 5.6 A, B, C and D**. TEM images showed that the IEPs can contain tight junctions (**Figure 5.6 A, B, and D**).

The IEPs appear to be distinct from regions of complex or interdigitated endothelial interfaces between adjacent endothelial cells, which are observed in placenta and other tissues as shown in **Figure 5.7**. 3D projections of different types of complex endothelial interfaces and IEPs are shown in **Figure 5.8**. Segmentation of the three SBFSEM stacks revealed that the complex endothelial interfaces (**Figure 5.8 Ai, Aii**) do not penetrate as far into the adjacent endothelial cell as the IEPs (**Figures 5.8 Bi, Bii, Ci, Cii,**). Complex endothelial interfaces between adjacent endothelial cells do not penetrate further than 1 µm in length in the adjacent endothelial cell, while the IEPs can be as long as 7 µm as shown in **Figure 5.8 Ci, Cii**. Complex endothelial interfaces are wider and shorter in length than the IEPs which are longer and narrower.

5.3.4 Counting the number of IEPs

For the protrusions observed in the segmented region of the fetal capillary, the density of protrusions per endothelial volume and surface area in this one segmented region are presented in **Table 5.1**. The endothelial surface area and volume of the seven segmented endothelial cells are given by Amira. The results shown in **Table 5.1** cannot be considered as indicative rather than representative, as they are based on only one segmented region of a part of a fetal capillary.

Segmentation of larger regions of fetal capillaries was not a feasible approach to obtain a more representative quantitative assessment of the number of protrusions due to the large amount of time involved. For this reason, a different approach was adopted. The IEPs were manually counted in every slice in all the 27 stacks in the terminal villi of eight different normal term placentas.

The total number of complex endothelial interfaces observed was 132, while the number of IEPs was 89. The average length of these protrusions was 2.00 µm (SEM 0.24),

while the average length to width ratio was 9.69 (SEM 1.71). The average length of the complex endothelial interfaces between adjacent endothelial cells was 0.50 µm (SEM 0.03), while the average length to width ratio was 2.95 (SEM 0.37). Analysis also revealed that there are more IEPs found as the endothelial cell volume increases per stack (P <0.001) (**Figure 5.9**).

Based on literature values for the percentage of placental volume taken up by inter-villous space (35%) and villi (65%) (Mayhew, 2009) I calculated the number of IEPs per cm^3 of placental tissue based on my measurement of endothelial cell volume (cm^3) and per villus and placenta (cm^3) based on endothelial cell volume (**Table 5.2**).

Analysis of the complex endothelial interfaces between adjacent endothelial cells and the IEPs in eight different placentas showed that the endothelial interfaces and the protru-sions are different types of complex endothelial interfaces between adjacent endothelial cells as shown in **Figure 5.10.** The IEPs have a higher length to width ratio between 5 and 10 (**Figure 5.10 A**) compared to the length to width ratio of the complex endothelial interfaces which was found to be between 2 and 3 (**Figure 5.10 B**). This suggests that the majority of IEPs tend to be longer compared to the complex endothelial interfaces. When the two histo-grams are combined together, it is observed that some of the IEPs can be as small as complex endothelial interfaces between adjacent endothelial cells (**Figure 5.10 C**). There is a clear separation between complex junctions and IEPs concerning the length to width ratio showing that IEPs are significantly different from complex endothelial interfaces (P = 0.0002), how-ever there is an overlap between complex endothelial interfaces and IEPs when this ratio is below 4.

5.3.5 Counting the number of endothelial interfaces between adjacent endothelial cells per fetal capillary

To maintain consistency in this project, stereological analysis was used at the same way as described in Chapter 4. The number of the endothelial interfaces between adjacent endothelial cells was counted in every 50 slices of each of the 27 stacks using the 4 x 4 grid. The diameter of the capillary was also counted in the same slices as the endothelial interfaces. **Figure 5.11** shows the relationship between endothelial interfaces and capillary diameter as measured in 27 stacks. The mean number of junctions was 4 ± 0.25, found in 13 different capillary profiles from terminal villi of eight normal term placentas. The number of junctions/capillary profile in every 50 slices of the 27 stacks was positively related to the cross sectional capillary diameter ($r = 0.37$, $P = 0.0007$, $n = 76$) as shown in **Figure 5.11**. Capillaries with an average lumen diameter between 5 and 10 µm are considered non-dilated, while those with a diameter above 11 µm are dilated (Kaufmann A., 2019). In dilated capillaries the mean number of junctions was found 5 ± 0.33, $n = 19$, while in non-dilated the mean number of junctions was 4 ± 0.22, $n = 56$.

Table 5.1: **Volume, surface area, total number of IEPs and number of protrusions per volume and surface area in the seven segmented endothelial cells.**

	Count
Number of partial endothelial cells in the segmented region	7
Total number of protrusions in the segmented region	18
Total endothelial cell volume (μm^3)	275.6
Total endothelial cell surface area (μm^2)	1594
Protrusions/endothelial surface area (μm^2)	0.01
Protrusions/endothelial volume (μm^3)	0.07

Table 5.2: Number of IEPs per endothelial cell volume, villi and per placenta based on endothelial cell volume.

	Number of IEPs
Number of IEPs in total tissue volume in all stacks (cm^3)	89
Number of IEPs per endothelial cell volume (cm^3)	1,619,669,715
Number of IEPs per villi (cm^3) based on endothelial cell volume	134,432,586
Number of IEPs per placenta (cm^3) based on endothelial cell volume	87,522,133
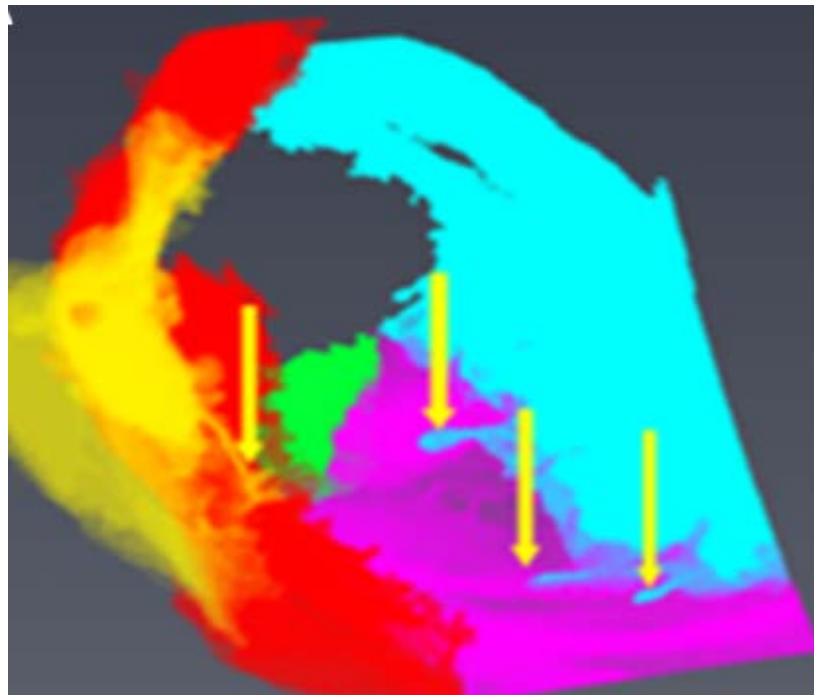
Figure 5.4: Identification of IEPs in adjacent endothelial cells in capillaries from terminal villi. *Partial segmentation of the fetal capillary showing five out of seven in total endothelial cells (each cell in a different colour) showing the IEPs into adjacent cells which are identified by arrows. The IEPs are drawn the same colour with the endothelial cell they belong to. Note that these are not interdigitations but protrusions within the neighbouring cell.*
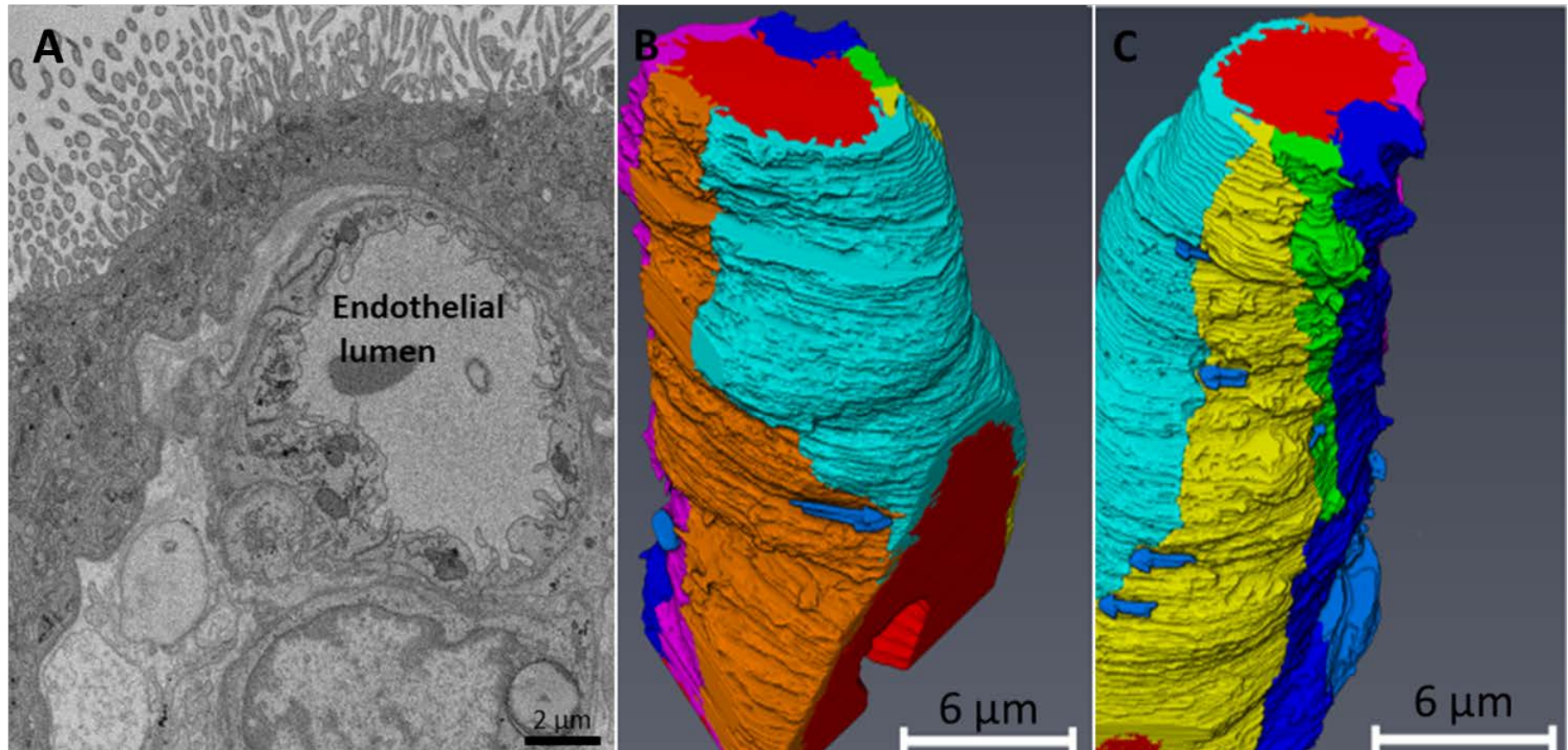
Figure 5.5: ***3D imaging of the fetal capillary.*** *A Image showing a representative slice of the 467 slices stack showing the endothelial lumen and the endothelial cells. **B and** **C***: *The 3D structure of the segmented fetal capillary showing IEPs. The processes are shown with blue arrows between different endothelial cells. The arrowhead points the cell where the IEPs belongs to, while the rest of the arrow shows where the endothelial IEPs is found.*
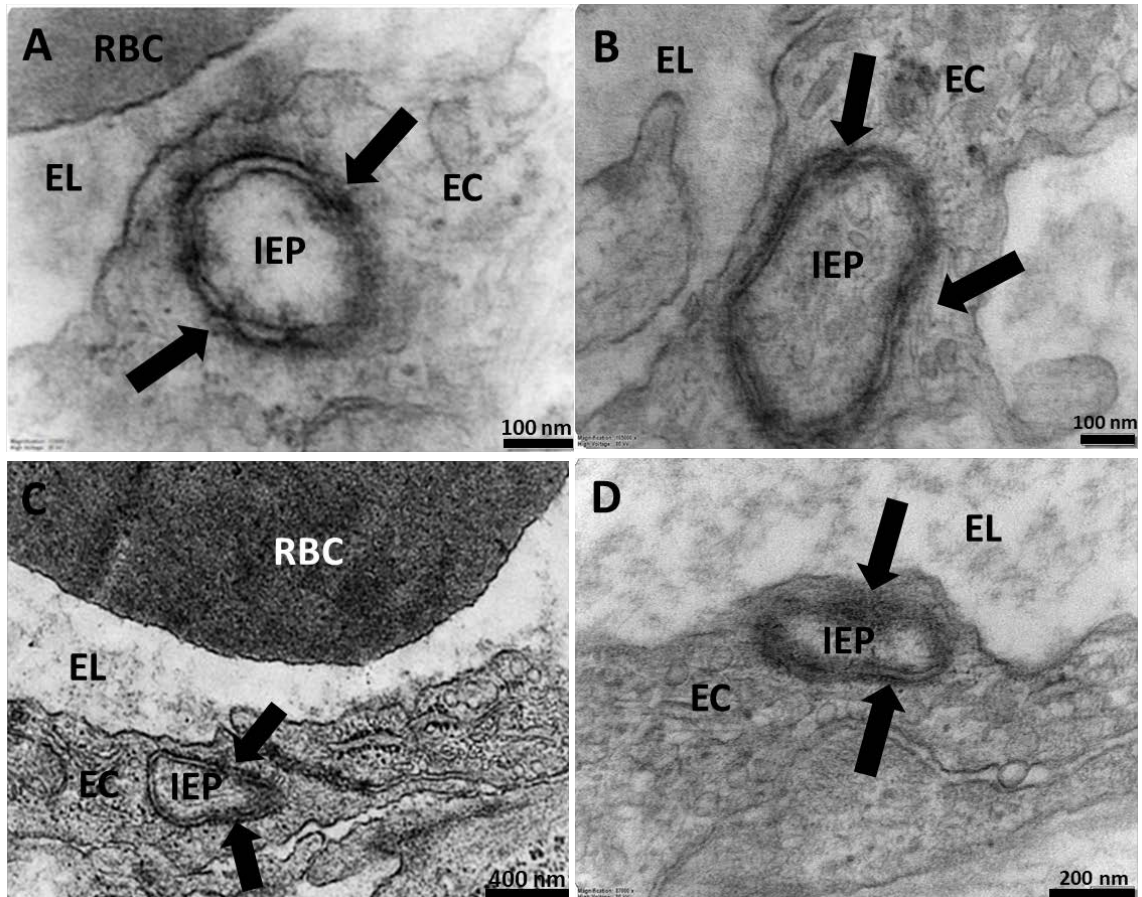
Figure 5.6: ***High-resolution TEM images showing IEPs in different cells in 4 different placentas. A and B.*** *There appear to be tight junctions (black arrows) within the IEPs. **C.** A high-resolution TEM image showing tight junctions (black arrows) of a complex endothelial interface between adjacent endothelial cells. **D.** High-resolution TEM image showing another IEP and the tight junctions (black arrows). **EL**: endothelial lumen, **EC**: endothelial cell, **IEP**: IEPs, **RBC**: red blood cell*
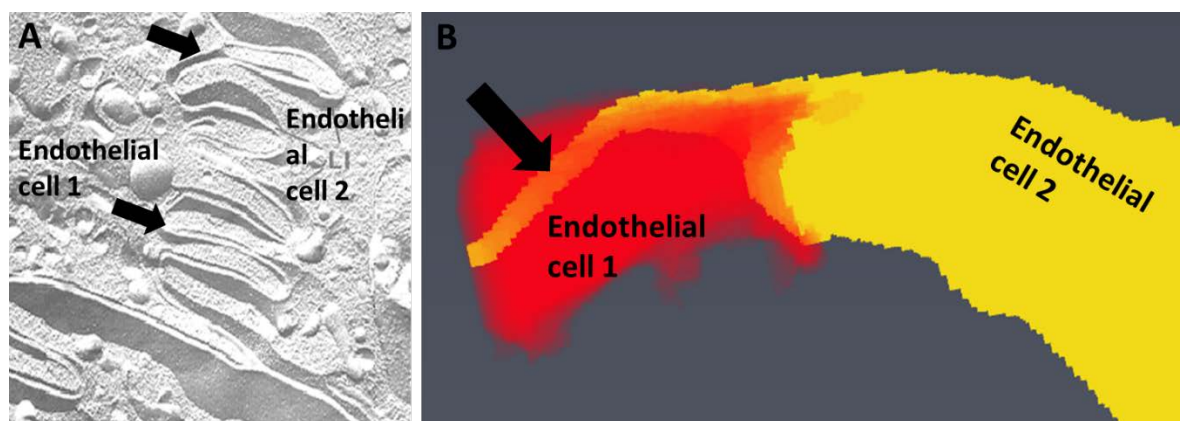
Figure 5.7: ***Interdigitations and IEPs have distinct morphologies. A***. *Freeze-fracture electron microscopy image showing interdigitations (black arrows) between two adjacent endothelial cells. Figure reproduced from https://www1.udel.edu/biology/Wags/histopage/empage/ecu/ecu.htm. **B.** Reconstruction of IEPs in 3D of endothelial cell 2 inside endothelial cell 1. The IEPs that penetrates the adjacent cell is shown in black arrow.*
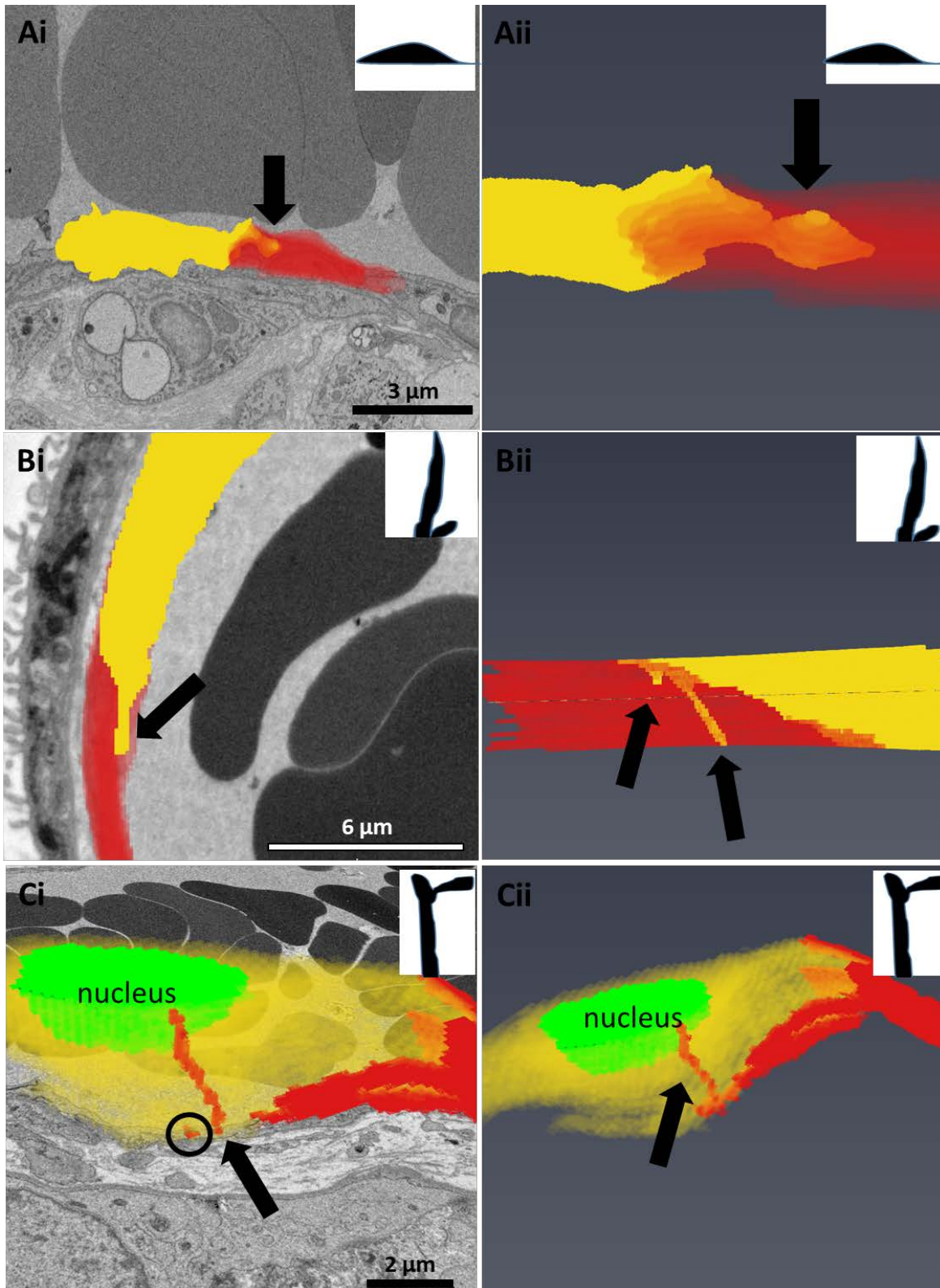
Figure 5.8: ***3D images of complex endothelial interfaces between adjacent endothelial cells and IEPs. Ai)*** *complex endothelial interface between adjacent endothelial cells (shown with black arrow) between the endothelial cell that the junction belongs to (in yellow) and its adjacent cell (in red).* ***Aii):*** *3D projection of the complex endothelial interface between adjacent endothelial cells.* ***Bi):*** *IEPs shown in black arrow.* ***Bii):*** *3D projection of the IEPs.* ***Ci):*** *IEPs that splits into 2 (the second one is in the black circle).* ***Cii):*** *3D projection of the protrusion that splits into two. Green is the nucleus of the yellow cell.*

130
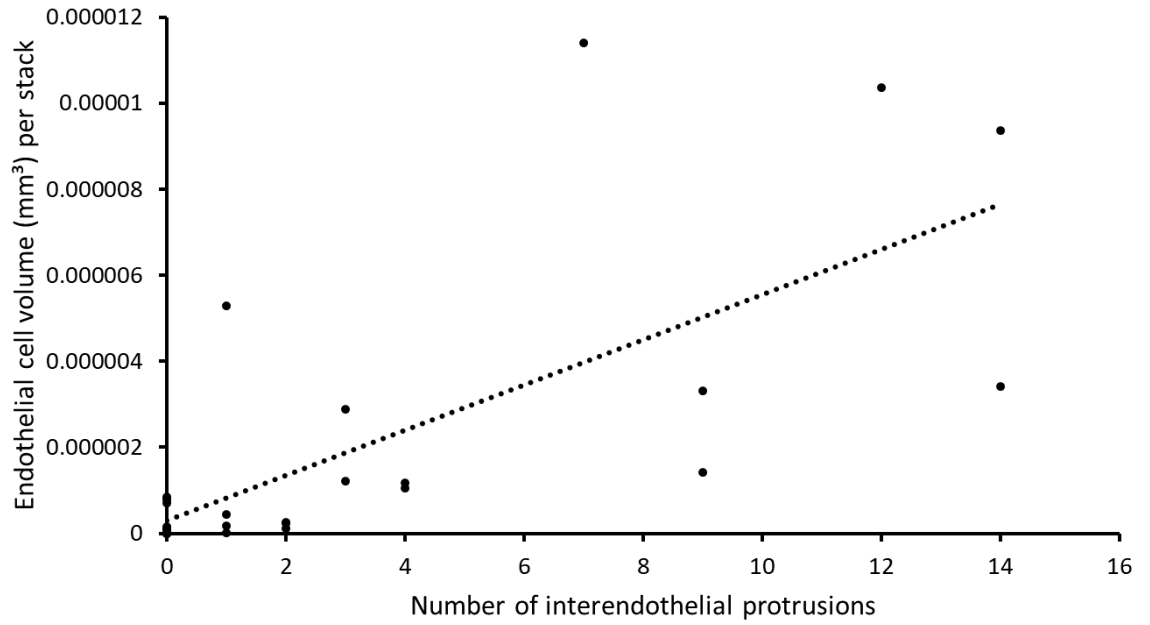
Figure 5.9: **_The number of IEPs per endothelial cell volume per stack._** *The number of the protrusions increases proportionally with the endothelial cell volume of each stack. P < 0.0001, r² = 0.51, n = 27 IEPs. The number of IEPs represents the total number of IEPs per stack.*

Figure 5.10: IEPs and complex endothelial interfaces between adjacent endothelial cells' distributions. *A. Graph showing that most IEPs have length to width (L/W) ratio 10. B. Histogram shows that most complex interfaces have a length to width ratio of 2, much smaller compared to the IEPs. C. Histogram showing that there is an overlap between IEPs and complex junctions regarding the length to width ratio but it is clear that when the length to width ratio is above 5 then it is definitely an IEP. D. Graph showing the different length to width ratios (mean ± SEM) of IEPs (9.69 ± 1.71) and complex junctions (2.64 ± 0.23), * p =0.0002 the L/W ratio of complex endothelial interfaces between adjacent endothelial cells significantly different to the L/W ratio of IEPs.*
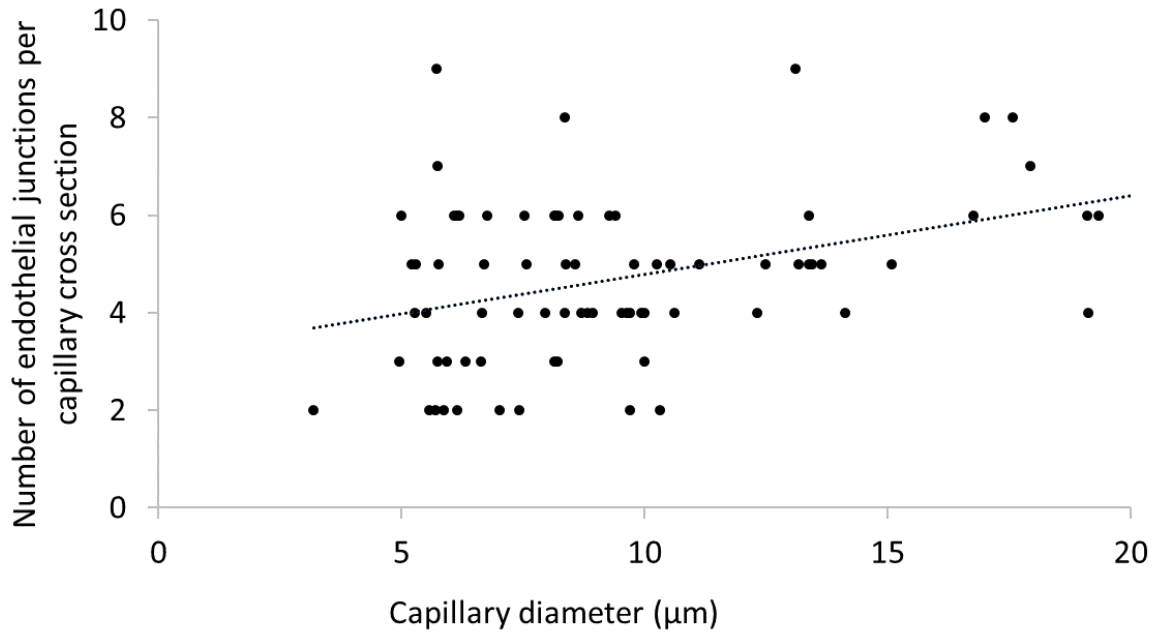
Figure 5.11: _There is a correlation between the number of endothelial interfaces between adjacent endothelial cells and the capillary cross section diameter._ *This graph shows that as the capillary diameter increases the number of endothelial interfaces increases as well. The number of interfaces was studied in 13 capillaries in total from eight different placentas. P = 0.0007, r^2 = 0.15, n = 76 endothelial interfaces between adjacent endothelial cells.*

5.4 Discussion

This chapter demonstrated the existence of novel IEPs, which have not been observed before in placenta or in any tissue to my knowledge. In addition, this study also revealed that the number of endothelial interfaces between adjacent endothelial cells connecting endothelial cells in the feto-placental capillaries appears to be higher than in other tissues. 3D images were combined with quantification and statistical analysis to show that these protrusions are not that scarce in the feto-placental capillaries and are different from the known endothelial interfaces.

5.4.1 3D images of IEPs and complex endothelial interfaces between adjacent endothelial cells

Novel 3D demonstrations of IEPs and complex endothelial interfaces between adjacent endothelial cells identified novel structures originating from the endothelial interfaces, which have not been observed before in the placental tissue.

3D reconstruction of a feto/placental capillary allowed the 3D imaging of seven fetal endothelial cells and the identification for the first time of the IEPs between them. This could have not previously been observed utilizing conventional 2D imaging techniques. Conventional 2D imaging would identify the protrusions as small circles inside the endothelial cells but it would have been very difficult to identify their origin and observe how deep the IEPs penetrate inside the adjacent endothelial cell. Even though the 3D reconstruction of the fetal capillary enabled the 3D imaging of the fetal endothelial cells and the IEPs, the 3D imaging was achieved in only a small part of the feto/placental capillary, due to the limitations of the small area that I was able to image. While the 3D reconstruction gives an idea of the structure of the fetal capillary it does not produce representative quantitative data.

To enhance the results of the 3D images of IEPs in the fetal endothelial cells, more 3D images of IEPs were produced showing how far the IEPs penetrate inside the adjacent endothelial cell. This finding could not have been made using conventional 2D imaging techniques, since 2D images could not provide any information about the z dimension and so the protrusions will just look like small vesicles inside endothelial cells as mentioned before. The 3D images of the IEPs clearly demonstrated that IEPs are different to complex endothelial interfaces since IEPs could penetrate inside the adjacent endothelial cell more deeply (7 μm) than the complex endothelial interfaces which they just penetrate as far as to create a small bulge (1 μm) inside the adjacent cell. Analysis also demonstrated that complex endothelial interfaces have a smaller length to width ratio compared to the IEPs, providing more evidence that IEPs are different to complex endothelial interfaces between adjacent endothelial cells.

Electron microscopy images of complex endothelial interfaces also known as interendothelial boundary (Wallez and Huber, 2008) have been generated for other tissues such as human brain (Le Bihan et al., 2015) but there is no research that I am aware of on 3D images on complex endothelial interfaces between adjacent endothelial cells in the human placenta. This study also used high-resolution TEM images of putative IEPs and complex endothelial interfaces from four different placentas to enhance our understanding of the structure of these IEPs. Without 3D images it is difficult to be sure that the TEM profiles are actual IEPs or complex endothelial interfaces between adjacent endothelial cells, hence referring to them as putative IEPs. TEM images showed that these putative IEPs have tight junctions. As mentioned before the tight junctions in the placental endothelial interfaces play an important role in regulating the tightness of the endothelial interfaces and in the paracellular diffusion of nutrients (Burton et al., 2009). However, as mentioned at section 5.4.2 there are around nine IEPs in every endothelial cell and so their small number is highly unlikely to contribute to

the paracellular diffusion. It is more likely that the IEPs contribute more to linking tightly the adjacent endothelial cells. TEM images of these novel called as IEPs also showed that the plasma membrane of the donor cell and recipient cell maintain their integrity and the existence of tight junctions inside the IEPs also suggests that the protrusion is tightly linked to the cell it lies within. The deep penetration of these processes, which can reach 7 μm in length into the adjacent cell may suggest another potential role of IEPs in sensing shear stress which could be passed from one cell's cytoskeleton to the other. This may suggest that the IEPs may play a role in vascular development and homeostasis of the fetal capillary (Tzima et al., 2005).

5.4.2 Quantification and statistical analysis of the IEPs and complex endothelial interfaces between adjacent endothelial cells

Quantifying the number and length of the IEPs and complex endothelial interfaces between adjacent endothelial cells has provided information about the density of the IEPs and complex endothelial interfaces in the placental villi and endothelial cell volume.

These novel IEPs were found to be abundant in the placental tissue. Even though the IEPs are not easily distinguished in the tissue, I was able to count 89 of them in the small total volume of tissue that was imaged which suggests they are not rare. When scaled up to 1 cm^3 of tissue, taking account of the intervillous space this came to approximately 88 million/cm3. Although this number seems high it needs to be placed in the context of the number of endothelial cells in this volume of tissue.

To estimate the number of IEPs per endothelial cell, I needed to estimate the number of endothelial cells in a gram of placental tissue. When endothelial cells are purified from placental tissue recovery rates are reported to be 1 million endothelial cells from 1 g (approx. = 1 cm^3) of fresh placental tissue so there should be at least this number of endothelial cells

(Ugele and Lange, 2001). However recovery is not likely to be 100% efficient and there are literature values suggesting that 10 - 15% efficiency of recovery based on data on endothelial cell recovery from veins, if this was similar for placenta then there could be in the order of 10000000 endothelial cells per cm^3 of placental tissue (Shindo et al., 1987). This figure agrees with another study showing that from human brain it is possible to isolate from 2 to 10 million human brain capillary endothelial cells (Dorovini-Zis et al., 2003). Therefore, it does not seem unreasonable to assume that there could be around 10 million endothelial cells in every cm^3 of human placenta. Given my estimate of approximately 88 million IEPs /cm^3, my ballpark estimate suggests 9 IEPs per human placental endothelial cell. In the segmented region of capillary there were 18 IEPs on 7 partial endothelial cells which suggests that there are > 2 IEPs per endothelial cell. While it is difficult to be definitive, taken together this data suggest that it is likely that placental endothelial cells typically have multiple IEPs.

Since the role of the IEPs is still unknown it is unclear whether the number of these processes may imply a role in sensing shear stress and linking tightly the adjacent placental endothelial cells compared to other tissues. The number of IEPs increased with the endothelial cell volume. The increase in the endothelial cell volume per stack could either mean more endothelial cells in the stack or bigger region of the endothelial cells imaged. Assuming that IEPs are equally distributed in endothelial cells then the number of IEPs should increase proportionally with the endothelial cell volume.

5.4.3 Quantification of endothelial interfaces between adjacent endothelial cells

Analysis of the numbers of endothelial interfaces in capillary cross sections, a proxy indicator for endothelial cell number, revealed that the number of placental endothelial interfaces is greater in dilated capillaries compared to the non-dilated ones. Endothelial interfaces between adjacent endothelial cells contribute to the diffusion of nutrients from the

villous stroma to the fetal bloodstream and so the increased number of endothelial interfaces in dilated capillaries may indicate increased capacity nutrient diffusion in dilated capillaries in the terminal villi and this is consistent (Kolka and Bergman, 2012).

5.4.4 Limitations

This study successfully revealed the existence of novel IEPs and it also demonstrated in 3D these processes, complex endothelial interfaces between adjacent endothelial cells and a feto/placental capillary. However, the techniques that this study utilized had some limitations, which meant that it was not possible to make precise estimates of the frequency of these IEPs in the term human placenta.

One of the techniques that this study utilized is stereological analysis. This is a very time consuming technique which is the main reason that deters many researchers from using stereology to apply morphometric analysis in their samples (Marcos et al., 2015). Due to the large amount of time that stereology needed, there was no time left to calculate the diameter of the capillaries in the regions where the IEPs were counted. Stereology also has the subjective factor as a drawback. Even though this technique is supposed to provide unbiased data, it is mainly based on a person's perception to distinguish the different cell types. In this study the stereological analysis was performed by one individual (myself), however my supervisor double checked some of my analysis to confirm the accuracy of the results. Since the human error is increased in stereology compared to the measurements from Amira, this can explain the overlapping of protrusions and complex junctions for length to width ratio under 4 and may also influence the accuracy of the volume and surface area measurements. Amira on the other hand, can provide more accurate measurements for the volumes and surface areas of each segmented cell but is a much more time consuming and laborious technique compared to the stereology.

SBFSEM is another technique with its own drawbacks. Even though SBFSEM can provide large datasets by generating many stacks consisting of many slices, the stacks may be very different with different regions imaged. Reconstructing SBFSEM stacks can also be very time consuming since it requires manual segmentation of the specific cell type on each slice. Therefore, it does restrict the sample size and so in this study the 3D reconstruction of the feto/placental capillary was achieved in only one fetal capillary from one placental sample, providing no data from another sample in order to acquire a better knowledge in the 3D structure of a fetal capillary. Moreover, this 3D reconstruction was performed in a few hundred slices and so we do not have the whole capillary and the whole endothelial cells to present more representative data of the quantification analysis of the IEPs.

Another drawback of this study is the limited number of high-resolution TEM images of putative IEPs and complex endothelial interfaces between adjacent endothelial cells from four different placentas were presented in this study. This limitation is due to the difficulty finding the IEPs in TEM sections, due to their small size.

Since both stereological analysis and 3D reconstructions required a lot of time, there was no time left to present any functional experiments that could be combined with these structural data to present a more complete image of the function of these novel IEPs and their significance in term human placenta.

5.4.5 Future Work

This study successfully revealed the existence of novel IEPs that have not been observed in human placenta and any other tissues before. These protrusions were also showed to be quite different from the complex endothelial interfaces and the well-known endothelial interfaces between adjacent endothelial cells. Future work will seek to expand this current work investigating the distribution of these IEPs in fetal capillaries identify whether the IEPs

constitute different population to complex endothelial interfaces and combining this structural work with functional experiments.

Seeking for new software to achieve automatic segmentation by using up to date technology will enable 3D reconstruction of more fetal capillaries and IEPs in a quicker and easier way. Automatic segmentation will enable more effective and efficient data collection from all these large SBFSEM stacks by providing more segmented images of IEPs and fetal capillaries. Reconstructing as many fetal capillaries as possible will enable to visualize the distribution of IEPs in the endothelial cells and in different regions of the placental vascular bed. Understanding the distribution of IEPs will enhance our knowledge in the function of these IEPs in the fetal capillaries. If IEPs are found more abundant in the dilated capillaries and due to the presence of tight junctions inside the IEPs as mentioned before, IEPs may have a potential role in the dilated capillaries in sensing the shear stress.

An increased number of 3D reconstructions of IEPs and complex endothelial interfaces between adjacent endothelial cells will also provide more 3D images and enable us to enhance our knowledge in the structure of the IEPs and complex endothelial interfaces and the identification of the base (endothelial interface between adjacent endothelial cells) from which the length of the IEP or complex endothelial interfaces is measured. This will provide more data concerning the length to width ratio of IEPs and junctions and will enable us to set better criteria to distinguish the complex endothelial interfaces between adjacent endothelial cells from the IEPs. These criteria will improve the results from the analysis and will provide more evidence whether the IEPs constitute a different population from the complex endothelial interfaces.

Due to the small size of the protrusions when observed in profile under the electron microscopy, it is difficult to distinguish them and so in the future better methods could be employed to reassess the quantification of the IEPs. One approach could be to repeat the

stereology and analysis with another person. Automatic quantification may be another method but it does require a lot of time and effort spent to use machine learning approach in order to train a software to distinguish the IEPs from the rest of the placental tissue. Trainable WEKA segmentation is a Fiji plugin which utilizes machine learning algorithms using textures and different grey scale values to produce pixel-based segmentation. This approach might be able to distinguish the IEPs and then automatically segment the IEPs. Automatic segmentation of IEPs would then enable the automatic quantification of the IEPs.

The information gained from the high-resolution TEM images that I have made could be enhanced by images generated by the new TEM 3D tomography microscope (Levin et al., 2016). This new TEM microscope will provide high-resolution 3D electron micros-copy images, enhancing the visualization of the structure of the IEPs. To enhance our understanding in the structure of the IEPs, future work could focus on using immunofluores-cence and confocal microscopy to identify the presence of occludin inside the IEPs, the same way as occludin was identified in the stromal and intermediate vessels in the placental villous tree (Leach et al., 2000).

Finally, future work will focus to combine the structure of these novel IEPs with their role in the diffusion of nutrients. It is assumed that nutrients such as glucose and amino acids can diffuse effectively through endothelial interfaces between adjacent endothelial cells (Lewis et al., 2013). The permeability of endothelial interfaces to the diffusion of molecules of different sizes can be estimated using established techniques (Arkill et al., 2011). So far, this sort of analysis has only been done on 2D images but the advent of SBFSEM stacks could allow this to be done using 3D stacks which may provide much more information. I would be interesting to use these SBFSEM stacks to calculate diffusion rates. If it turned out that certain molecules could not effectively diffuse through the endothelial inter-faces then they would need to be transported across the endothelium. Perfusing the placental

vessels with alcian blue staining before SBFSEM imaging would highlight the glycocalyx and this may allow an even more detailed modelling of hydrodynamic ultrafiltration and osmotic flow in these vessels (Arkill et al., 2011).

To conclude this study successfully revealed the existence of IEPs penetrating the adjacent endothelial cell. 3D reconstructions of the IEPs were compared to those of the complex junctions to show the difference between them and quantification analysis followed the 3D reconstructions to provide evidence regarding their frequency in the fetal endothelial cells and in the human placental tissue.

Chapter 6: General Discussion

6.1 Overview

This project successfully used 3D imaging approaches to demonstrate micro and nano scale novel structures and their relationships within term human placenta. Multiscale 3D imaging techniques were utilized to provide a better insight of the structure of a normal term placenta, in order to understand the mechanisms underlying placental dysfunction. The results I have obtained using the 3D imaging approaches have demonstrated the value of the 3D approach compared to 2D approaches. I have identified novel structures which would not have been seen or which could not be easily interpreted in 2D. The 3D imaging approaches allow these structures to be better understood in relation to other cell types or cellular components around them.

6.2 Novel findings that this study revealed

This study used SBFSEM, in combination with confocal microscopy and TEM to identify novel structures, reconstruct cellular structures in 3D and identify cellular interactions using normal term human placentas.

In Chapter 3 SBFSEM revealed a novel structure from a normal placenta showing the syncytiotrophoblast layer stretched and fetal erythrocytes try to protrude through the layer. Even though the underlying stroma was not observed, it was assumed that this novel structure maybe a pathological feature resulting from a possible leakage of a fetal capillary. The 3D reconstruction of trophoblast folds inside the basal membrane along with this novel structure provided evidence that the trophoblast basal membrane may be loosely attached to the trophoblast basement membrane.

In Chapter 4 the SBFSEM demonstrated the 3D reconstruction of a placental fibroblast. This observation enabled the better understanding of the fibroblast structure and re-

vealed the interaction of the fibroblast processes with other fibroblasts creating local networks, and with giant extracellular stromal vesicles. The identification of fibroblast networks raised questions about the coordinating role of the fibroblasts in producing collagen and maintaining the structural integrity of the extracellular matrix. The identification of giant extracellular vesicles, their number (they constitute 4% of the villous stromal volume) and the fact that are in contact with the fibroblast processes raised possibilities about the role of the giant vesicles in communicating with the fibroblasts. The identification of fibroblast networks and the contact with giant extracellular vesicles revealed the high complexity of the villous stroma which has not been studied before.

In Chapter 5 SBFSEM revealed the existence of novel interendothelial protrusions (IEPs) connecting adjacent endothelial cells in the fetal capillaries of terminal villi in term placenta. These IEPs have not been observed before in human placenta and in any other tissue. The 3D reconstruction of the IEPs demonstrated they could protrude 7 μm inside the neighboring endothelial cell, which may suggest a potential role of these IEPs in mechanosensing the stress that the fetal endothelium has to undergo. This is a clear example of a feature that would have been almost impossible to identify using 2D imaging techniques and has not previously been identified.

6.3 How these novel findings contribute to placental function and what functional experiments can we do in vitro to observe any changes of these findings in pathologies?

This study revealed novel findings in the normal placental structure. However, it does not address whether these structures are related to placental function or disease processes. Studying these novel structures in pathologies, such as pre-eclampsia, FGR and diabetic placentas, may provide insight into both their function and the biological basis of disease.

Collecting placentas from complicated pregnancies, fixing the tissue and studying the morphology is one way to study the structural changes. Another way would be to conduct functional experiments mimicking these pathologies and combine the results from the morphology with the functional changes in the placental tissue, such as use placental explants and induce the tissue into hypoxic conditions, culture in vitro placental cell types and impose mechanical forces and perfuse placentas using different pressures.

6.3.1 Syncytiotrophoblast stretch and fetal blood cells pass through the syncytiotrophoblast layer

The first finding of this study, showing the ability of the syncytiotrophoblast to stretch, is a rare observation. The ability of the syncytiotrophoblast to stretch could be associated with the ability of the villi to move in the intervillous space n the normal placentas. In the FGR placentas the villous densities are lower (Vedmedovska et al., 2011) which may imply that the villi cannot move the same way as in the normal placentas, so maybe the syncytiotrophoblast may not stretch the same way as shown in this study. If the syncytiotrophoblast cannot stretch the same way in the FGR placentas, then maybe there is no pathway for fetal cells to pass through the syncytiotrophoblast layer. Even though SBFSEM could be used to observe such structures in other normal and abnormal placentas it is highly unlikely that we would be able to witness such structure in other placentas. It would also be difficult to observe this novel finding with the underlying stroma structure in order to observe whether or not this stretch is caused by a capillary leakage.

6.3.2 Presence of folds inside the trophoblast basal membrane

The presence of folds inside the trophoblast basal membrane has also been observed before but only in 2D images (Jones and Fox, 1991). To understand the importance of folds

we first need to investigate their role. It is known that syncytiotrophoblast basal membrane have transporters such as glucose and amino acids transporters (Simner et al., 2017). Since the folds are inside the trophoblast basal membrane, it would be interesting to observe if there are any glucose and amino acid transporters in the folds. If the folds are found to have glucose and amino acid transporters, then this may suggest a potential role of the folds in the transport of glucose and amino acids from the maternal to the fetal bloodstream. The transport of glucose and amino acids is essential for the normal fetal development and growth. If there are fewer transporters, then the transport of glucose and amino acids could be compromised leading to nutrient deficiency to the baby and increased risk of growth restriction. Deficiency of nutrients is observed in the fetal growth restricted fetuses, so it would be interesting to observe whether there are any changes in the number of folds in the abnormal placentas and whether these changes are associated with reduced number of glucose and amino acids transporters.

The role of folds could be tested using immunocytochemistry to observe the existence of transporters such as the GLUT1 glucose transporter and SLC amino acid transporters in the folds in the normal and abnormal placentas (Simner et al., 2017). The immunocytochemistry can then be combined utilizing immunogold and TEM imaging to count the number of folds in the normal and abnormal placentas. If there are fewer folds and fewer transporters in the FGR placentas where it has been shown that there is nutrient deficiency to the baby, then this may suggest that folds inside the trophoblast basal membrane have a potential role in the supply of nutrients from the maternal to the fetal bloodstream.

Placental explants have been used to study the tissue function (Miller et al., 2005) including proliferation of cell types, uptake of nutrients and hormones under specific in vitro conditions, such as hypoxia, mimicking the preeclamptic conditions (Hung et al., 2001) and

149

the FGR placentas (Thompson et al., 2016). Placental explants from preeclamptic pregnancies demonstrate high levels of syncytiotrophoblast degeneration (Crocker et al., 2004). Therefore, we can use placental explants from preeclamptic pregnancies, culture them in vitro and then fix the tissue for TEM imaging to assess whether there is any change in the number of folds in the preeclamptic placentas. We could also perform immunostaining to observe the existence of glucose and amino acids transporters in preeclamptic placental explants and compare it to the existence of these transporters in normal placentas.

6.3.3 Fibroblast networks in the villous stroma

The existence of fibroblast networks in the placental villous stroma is another important finding of this study that raises questions to their role in the villous stroma. Fibroblast networks in other tissues have been shown to have a coordinating role in the production of collagen but their role in the placenta still remains unknown (Langevin et al., 2004). If fibroblast networks in the villous stroma are found to have the same role in producing collagen, then this may imply that fibroblast networks in the villous stroma are responsible for the maintenance and remodelling of the villous stroma and for the formation and maintenance of the vasculosyncytial membranes. As mentioned previously, vasculosyncytial membranes are regions of terminal villi where there is the highest rate of the diffusion of oxygen and nutrients. If there is a reduction of collagen production or if collagen is produced in wrong places, then this will affect the formation of the vasculosyncytial membranes. If there are fewer vasculosyncytial membranes then this might cause reduction of the oxygen and nutrient diffusion, depriving the fetal bloodstream from the essential amount of nutrient and oxygen supply for the normal fetal growth, leading to fetal growth restricted babies. Therefore, it would be interesting to observe the existence of fibroblast networks in abnormal

placentas, whether there is any change in their number, or whether these networks are local or more widespread.

Immunostaining using specific fibroblast markers such as vimentin could be performed to observe the existence of fibroblast networks in the abnormal placentas, such as preeclamptic, FGR and diabetic placentas and compare it to the normal placentas. Markers for collagen such as collagen type IV could also be used to observe the collagen production in the normal and abnormal placentas. Immunocytochemistry could then be combined with western blot to quantify the number of fibroblast networks in the abnormal placentas and compare it to the normal ones.

Placental explants from normal placentas can be imposed to reduced oxygen, resembling the preeclamptic and FGR placental tissue and then perform immunostaining and western blot as mentioned previously to observe the number of fibroblast networks and the collagen production under hypoxic conditions. SBFSEM and 3D reconstruction of fibroblast networks could also be performed to these placental explants so that to quantify the number of fibroblast networks formed and whether these networks are local or more widespread. We could also grow placental fibroblasts in 3D culture in agarose gel and apply mechanical forces such as shear stress. It has been shown that increased vascular resistance in the FGR fetal capillaries induces shear stress which affects the fetal endothelial cells and other cell types (Vedmedovska et al., 2011). Therefore, it would be worth to observe under the conventional microscope whether fibroblasts can still form fibroblast networks under such conditions.

6.3.4 Giant extracellular vesicles in the villous stroma

The existence of giant extracellular vesicles has been observed in other tissues and in two dimensional slices in the human placenta (Jones and Desoye, 2011), however their

relationship with the fibroblast processes has not been suggested before. If these giant vesicles have similar roles to normal stromal vesicles found in other tissues, then they may contain hormones and other signals such as microRNA which are vital for the remodelling of the stroma and vascular networks or may act as signposts to the cells that are close by. If these giant extracellular vesicles are found to contain fluid, using high resolution TEM imaging, then maybe these giant extracellular vesicles could also have a mechanical cushioning role within the villi, improving the communication between cell types and the distribution of cell types in the stroma. The distribution of the different cell types in the villous stroma is important, since any change in the distribution of the fibroblasts or the Hofbauer cells may constitute another barrier for the oxygen and nutrient diffusion, affecting the nutrient supply from the mother to the baby. Therefore, changes in the number, structure or size of these giant vesicles may suggest changes in the villous stroma function which may have an impact in the normal placental function.

Using immunogold technique with an antibody for vesicles and then visualize under the TEM microscope would potentially be a way to identify the structure, size, number and contents of these vesicles in the diseased placentas and compare to the normal placentas. We could also perform SBFSEM followed by stereology in FGR, preeclamptic and diabetic pregnancies to quantify the number of giant extracellular vesicles and compare it to the normal placentas.

Normal placental explants could also be used to culture placental tissue in vitro under hypoxic conditions, resembling the conditions to most FGR and preeclamptic placentas, and then use immunogold and TEM followed by stereology, to observe any change in the number, structure, size and contents of vesicles. If there is any change in these giant vesicles, then this may explain one of the mechanisms for a dysfunctional stroma leading to a dysfunctional villus in hypoxia.

6.3.5 Existence of novel IEPs inside fetal endothelial cells

The final finding of this thesis was the existence of novel IEPs inside the fetal endothelia cells which have not been observed before in human placenta and any other human tissue. In Chapter 5 3D reconstruction revealed that these IEPs penetrate inside the adjacent endothelial cells, implying that it is highly unlikely that IEPs have a role in the diffusion of nutrients. It is more likely that IEPs participate in the mechanosensing of the hydrostatic pressures on adjacent endothelial cells. In FGR placentas there is reduced blood flow (Vedmedovska et al., 2011) which will affect the pressures within fetal capillaries and on endothelial cells forming the capillary. If IEPs have a role in the mechanosensing then maybe IEPs stretch in response to a decrease in the blood pressure in the fetal capillaries in the FGR placentas. Therefore, it would be worth observing any changes in the number, structure and distribution of these IEPs in the normal and abnormal placentas.

To observe changes in the number and distribution of IEPs in the diseased placentas confocal microscopy using antibody for occludin could be used to visualize the existence of tight junctions inside the endothelial cells, since as mentioned before these IEPs were shown to have tight junctions inside them. To observe changes in their structure SBFSEM stacks can be generated from abnormal placentas and 3D reconstruction could be performed to visualize if there is any stretch in the structure of the IEPs compared to their structure in the normal placentas.

High resolution TEM of the IEPs could also reveal whether there are vesicles inside the IEPs. If there are vesicles inside the IEPs then this might suggest that IEPs could potentially transmit vesicles to the adjacent endothelial cell. If vesicles are present within the IEPs in the normal placentas, we could then use high resolution TEM to identify vesicles if there are any inside the IEPs in the abnormal placentas.

Vascular impoverishment and hypovascularization in the periphery villi (Junaid et al., 2014, Chen et al., 2002) and increased vascular resistance has been observed in the FGR placentas compared to normal placentas (Jones et al., 2015b). To study the effect of reduced blood flow in the number, distribution and structure of the IEPs we could perfuse normal placentas with reduced flow rates, mimicking the FGR placentas, and then fix the tissue for immunostaining using an endothelial cell marker such as CD34 and marker for occludin to observe the distribution of IEPs inside the fetal endothelial cells in the FGR placentas. We could also fix this tissue for SBFSEM and perform 3D reconstruction of the IEPs to see if they stretch as a response to the increased vascular resistance. SBFSEM could then be followed by stereology to quantify the number of IEPs per endothelial cell under increased vascular resistance and compare it to the number of IEPs that this study found, approximately 9 IEPs per endothelial cell, in the normal placentas.

Culturing endothelial monolayers on a distensible surface and subjecting them to different patterns of movement mimicking FGR and preeclampsia placentas, would be another way of determining how mechanical forces could affect IEPs. It is known that endothelial cells are responsible for angiogenesis and mediating shear stress via vasodilation or vasoconstriction of capillaries (Asahara et al., 1997, Yang et al., 2016). We could impose the endothelial monolayers to tension, compression or shear stress as has been studied before in endothelial cells isolated from FGR placentas (Jones et al., 2015b). Then western blot technique using specific antibody for occludin could be used to quantify the number of IEPs in the endothelial cells that undergo stress.

6.4 Future steps towards automatic segmentation

This project has utilized manual segmentation of the SBFSEM stacks of images to demonstrate the 3D structure of placental cell types or structural components. Manual segmentation allows the 3D reconstruction of cells and structures, but this approach is very laborious and time consuming. With the ever-increasing use of 3D imaging techniques to study and reconstruct structures in 3D it is essential to find new automatic methods to segment these large datasets produced by the SBFSEM in an easier and quicker way.

Finding computer software to automatically segment these large datasets generated by the SBFSEM could potentially provide new insights by using this technique to examine more placental samples and so increase the possibility of finding such structures in other placentas. Using SBFSEM to identify such structures in complicated pregnancies, pre-eclamptic and FGR placentas will enable the comparison of the normal placental structure to the abnormal one, which has not been observed before. Potentially, automated segmentation and machine learning approaches may also allow a better quality segmentation of the image.

Currently there are different types of software available such as Amira, Fiji and Scan Ip, which provide the thresholding approach to achieve automatic segmentation. Thresholding approach recognize different grey-scale regions in the image and segment accordingly. In placental tissue though, there are some regions that cannot be distinguished from others because the software is sometimes unable to recognize cell types or structures with only marginal differences in contrast, which would be recognized by the human eye.

Using machine-learning approaches it may be possible to train a computer to recognise the different cell types or cellular components and achieve successful automatic segmentation (Ronneberger et al., 2015). Currently this machine-learning approach has been applied to automatically segment neural networks, glioblastoma-astrocytoma cells recorded

by phase contrast microscopy and HeLa cells on a flat glass recorded by differential inter-ference contrast microscopy (Ronneberger et al., 2015). This approach was successfully tested once in a very small region of placental tissue and more specific a small region of microvilli. To achieve automatic segmentation we collaborated with Dr. Alexander Serov at the Institute Pasteur in Paris. Representative images of the SBFSEM stacks were used to colour differently the different cell types and layers of the human term normal placenta. Dr. Serov managed to write a computer code that identifies the different features/placental cell types/layers according to the different colours. The system managed to segment automati-cally a very small region of microvilli. When this automatic segmentation was compared to the manual one, it was apparent that automatic segmentation was more accurate and valid compared to the manual one and highly successful. So, it would be worth utilizing automatic segmentation to reconstruct in 3D the whole microvillus membrane in order to count the surface area of the microvilli and understand how much the microvillus membrane contrib-ute to the transfer of nutrients, amino acids and glucose. It would also be worth using auto-matic segmentation to reconstruct whole fetal capillaries in 3D in order to visualize the ca-pillary loops in the terminal villi and other cell types such as Hofbauer cells, which have not been observed before in 3D.

Machine-learning approach has its own drawbacks. In order to write a computer code and train the machine to segment automatically a stack of images especially when the dif-ferent cell types and cellular components change their location in each image is a difficult process. The machine-learning approach also needs to be tested in terms of whether the software has segmented correctly the regions and has included the borders of each re-gion/cell or not. The evaluation and assessment of the automated segmentation is still not clear. One approach that could be used is the utilization of a grid, which can be applied to test whether the borders of the automated segmented regions are in the same region with the

lines of the grids. Using a systematic approach like this would avoid bias,but would depend on subjective judgment. Despite the lack of evaluating the automatic segmentation, once the code is written and the computer is trained to segment automatically many different SBF-SEM images then the automatic segmentation still remains the best option to achieve better quality segmentation and in a quicker and easier way compared to the manual segmentation.

In conclusion, hopefully in the near future automatic segmentation of the human term placenta will enable much more rapid and potentially better quality segmentation of structures and cells, which would otherwise take too much time and effort to be segmented. This will enhance our knowledge in structures and cell types in the human placenta and enable us to address more questions that are scientific and investigate the interactions of the different cell types with other cells and/ or cellular components in the human term placenta.

6.5 Conclusion

This project utilized up to date multiscale 3D imaging techniques to reconstruct novel structures in 3D in term normal human placenta. These structures have not been observed before in the placenta and some of them in any other human tissues. The novel structural demonstrations along with the quantification analysis that this study managed to provide with, constitute a significant step towards investigating more in depth the structure of normal placentas.

As mentioned before placenta is a vital organ during pregnancy, which plays an important role in supporting the normal fetal development and growth. Therefore, investigating the structure and function of normal placenta, will enhance our knowledge in understanding the structural and functional changes of placenta in pathological pregnancies.

Even though there is a lot of research investigating the mechanisms underlying placental dysfunction and new therapeutic approaches have been developed in an attempt to reduce complicated pregnancies, there are still a significant number of babies born too small. Further research is essential to enhance our understanding of placental structure and function in order to ensure the normal development and growth of the babies.

Appendices

Appendix 1: List of Abstracts

- **Placental capillary endothelial cells are connected by cytoplasmic processes**
  Eleni Palaiologou, Patricia Goggin, Anton Page, David Chatelet, Jane Cleal, Christopher Torrens, Rohan Lewis (P2.129, IFPA Conference 2017)

- **Extracellular vesicles comprise 5% of the villous stromal volume in terminal villi from term human placenta**
  Helen Palaiologou, Olivia Etter, Patricia Goggin, David S Chatelet, Bram Sengers, Christopher Torrens, Jane K Cleal, Anton Page, Rohan M Lewis (P1.51, IFPA Conference 2018)

- **3 Dimensional Imaging of Placental Endothelial Cells**
  Palaiologou. E, Goggin. T, Chatelet. D, Lewis. R (Post Graduate Medical Conference 2017)

- **Multiscale imaging of placental fibroblasts**
  Palaiologou. E, Goggin. T, Chatelet. D, Lewis. R (Post Graduate Medical Conference 2018)

AWARDS

- Loke New Investigator Travel Award for high quality abstract at IFPA Conference 2018 in Tokyo

- Runner Up for the oral presentation at the Society of Electron Microscope Technology (SEMT) meeting at the National History Museum (December, 2017)

Appendix 2: Publication

Journal of Anatomy

Serial block-face scanning electron microscopy of erythrocytes protruding through the human placental syncytiotrophoblast

Eleni Palaiologou,[1] Patricia Goggin,[2] David S. Chatelet,[2] Emma M. Lofthouse,[1] Christopher Torrens,[1,3] Bram G. Sengers,[3,4] Jane K. Cleal,[1,3] Anton Page[2] and Rohan M. Lewis[1,3]

[1]Faculty of Medicine, University of Southampton, Southampton, UK
[2]Faculty of Medicine, Biomedical Imaging Unit, University of Southampton, Southampton, UK
[3]Institute for life Sciences, University of Southampton, Southampton, UK
[4]Faculty of Engineering and the Environment, University of Southampton, Southampton, UK

Abstract

The syncytiotrophoblast forms a continuous barrier between the maternal and fetal circulations. Here we present a serial block-face scanning electron microscopy (SBFSEM) study, based on a single image stack, showing pooling of fetal blood underneath a region of stretched syncytiotrophoblast that has become detached from the basement membrane. Erythrocytes are protruding from discrete holes in the syncytiotrophoblast suggesting that, under specific circumstances, the syncytiotrophoblast may be permeable to fetal cells. This observation represents a pathological process but it poses questions about the physical properties and permeability of the syncytiotrophoblast and may represent an early stage in the formation of fibrin deposits in areas of syncytial denudation. This study also illustrates how the 3D images generated by SBFSEM allow the interpretation of structures that could not be understood from a single histological section.
Key words: 3D imaging; epithelial barrier; placenta.

Introduction

The human placenta is monochorionic and haemochorial, and its syncytiotrophoblast forms a continuous barrier between the maternal and fetal circulations (Sibley, 2009). Despite the continuous nature of the syncytiotrophoblast, there is functional evidence for a size-selective paracellular route (Sibley, 2009; Bain et al. 1990). The anatomical basis for the paracellular route remains unclear, and although trans-trophoblastic channels have been proposed, they have not been observed to cross the full width of the syncytiotrophoblast. However, partial channels may have been observed under pressure (Kertschanska et al. 1997). Alternatively, evidence exists for regions of syncytial denudation that may allow paracellular diffusion (Brownbill et al. 2000). These regions of syncytial denudation are covered in fibrin deposits whose pathogenesis is not entirely understood. The passive permeability of the placenta decreases

with increasing molecular size and proteins and cells would not be expected to cross the placenta (Bain et al. 1990; Sibley, 2009). Maternal microchimerism demonstrates that non-trophoblastic fetal cells can enter the mother's circulation (Bianchi et al. 1996). In this study, we present evidence that fetal cells could, under specific pathological conditions, cross the syncytiotrophoblast.

Methods

Tissue was collected after vaginal delivery from term placenta from an uncomplicated pregnancy with written informed consent and ethical approval from the Southampton and Southwest Hampshire Local Ethics Committee (11/SC/0529).

Within 30 min of delivery, a villous sample was dissected out and placed directly into 3% glutaraldehyde in 0.1 M cacodylate buffer at pH 7.4 at room temperature (RT) and stored at 4 °C until processing. Samples were treated twice with 0.1 M sodium cacodylate buffer pH 7.4 containing 0.23 M sucrose and 2 mM $CaCl_2$ for 10 min, 4% OsO_4 for 60 min, thiocarbohydrazide for 20 min, 2% OsO_4 for 30 min and finally 2% uranyl acetate for 60 min. Samples were embedded in Spurr's resin, polymerised at 60 °C for 16 h, blocks were trimmed (100 μm²), mounted on an aluminium pin with conductive glue and sputter-coated with gold/palladium (Holcomb et al. 2013). Blocks were imaged using a Gatan 3View inside an FEI Quanta 250 FEGSEM at 3.0 KV accelerating voltage and with a

Correspondence

*Rohan M. Lewis, Faculty of Medicine, MP 887, IDS Building University of Southampton, Southampton General Hospital, Southampton, UK.
E: rohan.lewis@soton.ac.uk*

vacuum level of 40 Pa. The voxel size was 22 × 22 × 50 nm, and the total image size was 3000 × 3000 pixels.

Images were processed in FIJI (version 2.0.0-rc-43) using Gaussian blur (sigma radius 2) and enhance- contrast (0.4% saturated pixels) (Schindelin et al. 2012). To estimate the size of the holes in the syncytiotrophoblast from which erythrocytes were protruding, the maximal diameter on the X Y axis was measured in FIJI along with three to five slices either side to ensure it was the maximum point. The maximal diameter in the Z axis was estimated by counting the number of 50-nm slices in which it appeared. The image stack was segmented in AMIRA (Version 6.1.1; FEI, UK) using thresholding.

The most prominent protruding erythrocyte and the surrounding region of syncytiotrophoblast were manually segmented. The surface area of the syncytiotrophoblast and the cross-sectional area of the first slice were measured using AMIRA. Before calculating the surface area of the syncytiotrophoblast, smoothing was performed to make it comparable to the flat surface of the base.

Results

SBFSEM revealed a region of syncytiotrophoblast detached from the underlying basement membrane. This stack consisted of 426 sequential slices with a Z resolution of 50 nm (Supporting Information Video S1A). The external face of the structure had microvilli, indicating it was the maternal-facing microvillous membrane; the space enclosed by the syncytiotrophoblast contained 78 erythrocytes and one unidentified cell of low electron density (Fig. 1). No endothelium or stroma was apparent on the fetal side of the syncytiotrophoblast nor was there evidence of fibrin deposition. The structure was 19 μm at its deepest point, with an average diameter at the base of 42.9 μm and a circumference of 144.4 μm. Seventeen erythrocytes were observed partially protruding through the syncytiotrophoblast at 25 sites, all located on the side of the structure where the syncytiotrophoblast was thinnest (Fig, 1B & C, Supporting Information Video S1b & S1c). The median diameter of the holes was 0.56 μm (range 0.34–1.41 μm) in the X–Y plane and 0.50 μm (range 0.20–1.85 μm) in the Z plane. In 20 cases the protrusion was covered by syncytiotrophoblast membrane on the maternal side, suggesting that it may have pushed through a relatively weaker area rather than a pre-existing hole. The surface area of the syncytiotrophoblast was 5415 μm^2 compared with the area of the base of the structure of 1628 μm^2, suggesting a 3.3-fold stretch (actual stretch may be less if syncytiotrophoblast is pulled in from adjacent regions).

Fig. 1 Electron microscopy image of the structure and 3D reconstructions of the stack. (A) An image from the SBFSEM showing the syncytiotrophoblast (STB), the erythrocytes (RBC) and the main protruding erythrocyte (arrow). (B) The segmented structure showing the surface of the syncytiotrophoblast and the protruding erythrocytes (arrows) (Supporting Information Video S1b). (C) Segmentation of the largest protruding erythrocyte (red) pushing through the syncytiotrophoblast (blue) in two places (arrows). (Supporting Information Video S1c).
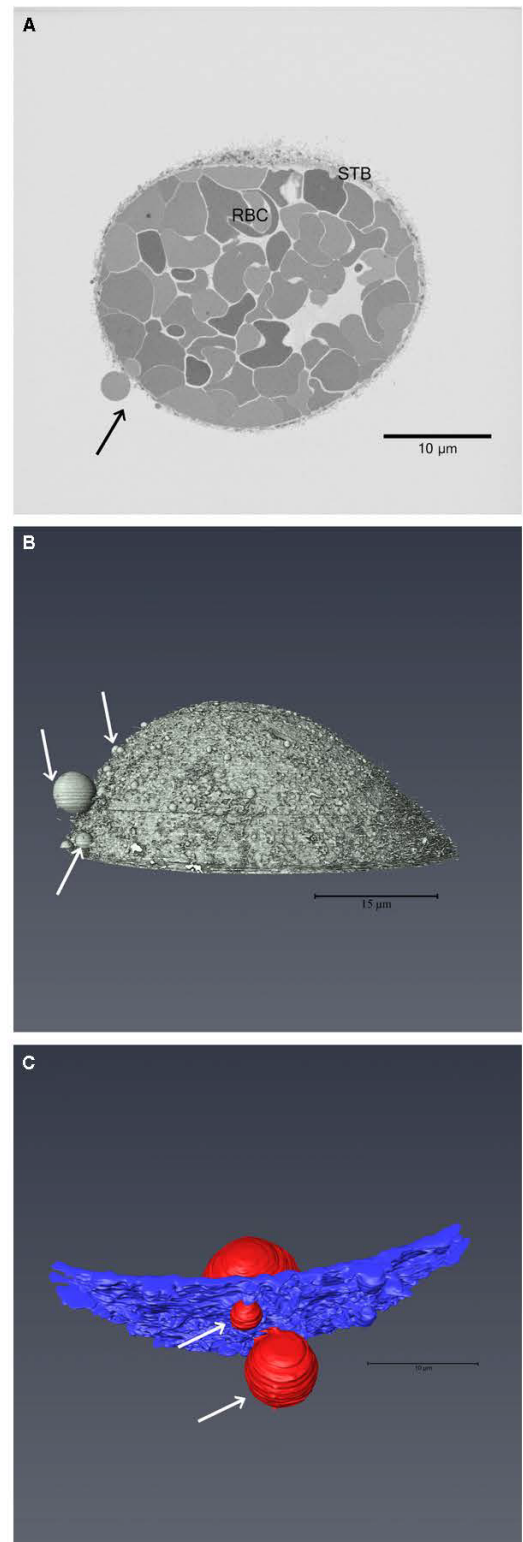
Discussion

This study suggests that the syncytiotrophoblast is distensible and that, under specific pathological conditions, fetal cells can cross the syncytiotrophoblast. We speculate that this structure, which is similar to a blood blister, may represent an early stage in the formation of regions of syncytial denudation. Furthermore, the image stack highlights the value of 3D imaging, as this interesting structure would be difficult to interpret in 2D and may have been overlooked.

We interpret this structure as a pathological feature resulting from leakage from a fetal capillary (not observed) and fetal blood pooling under the syncytiotrophoblast, stretching it away from the basement membrane. Fetal hydrostatic pressure has then pushed erythrocytes through weaker areas in the stretched syncytiotrophoblast.

The structure suggests the association between the syncytiotrophoblast and basement membrane is relatively weak, consistent with observations of denuded regions of villi (Brownbill et al. 2000). It also suggests that the syncytiotrophoblast can stretch, potentially allowing movement of villi. The only holes observed in the syncytiotrophoblast were those with protruding erythrocytes, suggesting that they only open under higher pressures. The holes were smaller than the protruding regions of erythrocyte, indicating that they had sufficient structural integrity to prevent a rip occurring. These holes could represent regions of damage, trans-syncytial channels or a structural feature making the syncytiotrophoblast locally weak.

A limitation of this study is that it is a single observation and that the underlying villus was not observed. This is an inherent limitation of relatively low throughput techniques such as SBFSEM, but the image may help the interpretation of such structures when they are observed in 2D. Another issue is whether shrinkage could have caused the erythrocytes to push through the membrane. However, we do not think this is likely, as shrinkage would primarily occur during dehydration, which occurs after the tissues are hardened due to aldehyde fixation.

Across the villi there are regions of damage in which fibrin deposits replace the trophoblast (Nelson et al. 1990). These could form where the trophoblast is sheared off directly or in regions where blood has pooled below the trophoblast and clotted before the overlying trophoblast died. Although there is no evidence of fibrin deposits in this image, it is possible that this represents an early stage in the evolution of fibrin deposits. Understanding the pathogenesis of these regions is important as they may mediate paracellular diffusion of small solutes (Brownbill et al. 2000).

This observation probably represents a pathological feature, but it does demonstrate a potential route for transfer of fetal cells to the mother through the syncytiotrophoblast. This could explain maternal microchimerism, where fetal lymphoid cells persist in the mother's body (Bianchi et al. 1996). This image raises questions about the strength and permeability of the syncytiotrophoblast and may represent an early stage in the formation of fibrin deposits in areas of syncytial denudation.

Author contributions

RL, BS, JC and CT designed the study and were involved in the provision of financial and maternal resources. EP, EL, PG, CP and AP conducted sample collection, processing and data acquisition. EP and DC performed image analysis. EP, RL, DC and PG composed the initial manuscript. All the authors revised the manuscript and approved the final draft.

References

Bain MD, Copas DK, Taylor A, et al. (1990) Permeability of the human placenta in vivo to four non-metabolized hydrophilic molecules. *J Physiol* **431**, 505 513.

Bianchi DW, Zickwolf GK, Weil GJ, et al. (1996) Male fetal progenitor cells persist in maternal blood for as long as 27 years postpartum. *Proc Natl Acad Sci U S A* **93**, 705 708.

Brownbill P, Mahendran D, Owen D, et al. (2000) Denudations as paracellular routes for alphafetoprotein and creatinine across the human syncytiotrophoblast. *Am J Physiol Regul Integr Comp Physiol* **278**, R677 R683.

Holcomb PS, Hoffpauir BK, Hoyson MC, et al. (2013) Synaptic inputs compete during rapid formation of the calyx of Held: a new model system for neural development. *J Neurosci* **33**, 12954 12969.

Kertschanska S, Kosanke G, Kaufmann P (1997) Pressure dependence of so-called transtrophoblastic channels during fetal perfusion of human placental villi. *Microsc Res Tech* **38**, 52 62.

Nelson DM, Crouch EC, Curran EM, et al. (1990) Trophoblast interaction with fibrin matrix. Epithelialization of perivillous fibrin deposits as a mechanism for villous repair in the human placenta. *Am J Pathol* **136**, 855 865.

Schindelin J, Arganda-Carreras I, Frise E, et al. (2012) Fiji: an open-source platform for biological-image analysis. *Nat Methods* **9**, 676 682.

Sibley CP (2009) Understanding placental nutrient transfer why bother? New biomarkers of fetal growth. *J Physiol* **587**, 3431 3440.

Supporting Information

Additional Supporting Information may be found in the online version of this article:

Video S1a. A movie showing all of the slices in the stack in sequence.

Video S1b. A movie showing a 3D reconstruction of the structure focused on the microvillus surface of the syncytiotrophoblast and the protruding erythrocytes, which can be seen as spheres on the surface.

Video S1c. A movie showing the largest protruding erythrocyte in red and the region of syncytiotrophoblast around it in blue.

Appendix 3: Supplementary material
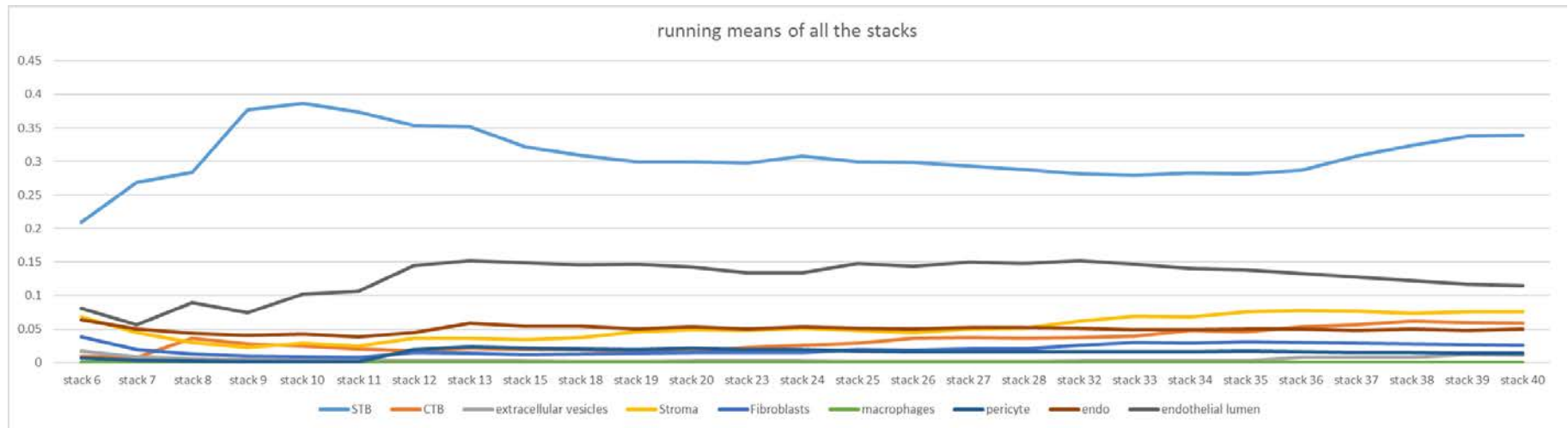
Supplementary Figure 1: Supplementary graph showing the running means of the values as expressed the percentages of the number of points falling on the different cell types and components (tissue only not intervillous space) counted in all the stacks of the eight different placentas.

References

AIRD, W. C. 2012. Endothelial cell heterogeneity. *Cold Spring Harb Perspect Med,* 2**,** a006429.

ARECHAVALETA-VELASCO, F., KOI, H., STRAUSS, J. F., 3RD & PARRY, S. 2002. Viral infection of the trophoblast: time to take a serious look at its role in abnormal implantation and placentation? *J Reprod Immunol,* 55**,** 113-21.

ARKILL, K. P., KNUPP, C., MICHEL, C. C., NEAL, C. R., QVORTRUP, K., ROSTGAARD, J. & SQUIRE, J. M. 2011. Similar endothelial glycocalyx structures in microvessels from a range of mammalian tissues: evidence for a common filtering mechanism? *Biophys J,* 101**,** 1046-56.

ARMULIK, A., GENOVE, G. & BETSHOLTZ, C. 2011. Pericytes: developmental, physiological, and pathological perspectives, problems, and promises. *Dev Cell,* 21**,** 193-215.

ASAHARA, T., MUROHARA, T., SULLIVAN, A., SILVER, M., VAN DER ZEE, R., LI, T., WITZENBICHLER, B., SCHATTEMAN, G. & ISNER, J. M. 1997. Isolation of putative progenitor endothelial cells for angiogenesis. *Science,* 275**,** 964-7.

ATASOY, D., BETLEY, J. N., LI, W. P., SU, H. H., SERTEL, S. M., SCHEFFER, L. K., SIMPSON, J. H., FETTER, R. D. & STERNSON, S. M. 2014. A genetically specified connectomics approach applied to long-range feeding regulatory circuits. *Nat Neurosci,* 17**,** 1830-9.

AUGUSTE, P., JAVERZAT, S. & BIKFALVI, A. 2003. Regulation of vascular development by fibroblast growth factors. *Cell Tissue Res,* 314**,** 157-66.

AVERY, D., GOVINDARAJU, P., JACOB, M., TODD, L., MONSLOW, J. & PURE, E. 2018. Extracellular matrix directs phenotypic heterogeneity of activated fibroblasts. *Matrix Biol,* 67**,** 90-106.

BAIN, M. D., COPAS, D. K., TAYLOR, A., LANDON, M. J. & STACEY, T. E. 1990. Permeability of the human placenta in vivo to four non-metabolized hydrophilic molecules. *J Physiol,* 431**,** 505-13.

BALUK, P., FUXE, J., HASHIZUME, H., ROMANO, T., LASHNITS, E., BUTZ, S., VESTWEBER, D., CORADA, M., MOLENDINI, C., DEJANA, E. & MCDONALD, D. M. 2007. Functionally specialized junctions between endothelial cells of lymphatic vessels. *J Exp Med,* 204**,** 2349-62.

BANERJEE, I., YEKKALA, K., BORG, T. K. & BAUDINO, T. A. 2006. Dynamic interactions between myocytes, fibroblasts, and extracellular matrix. *Ann N Y Acad Sci,* 1080**,** 76-84.

BAPTISTE-ROBERTS, K., SALAFIA, C. M., NICHOLSON, W. K., DUGGAN, A., WANG, N. Y. & BRANCATI, F. L. 2009. Gross placental measures and childhood growth. *J Matern Fetal Neonatal Med,* 22**,** 13-23.

BARKER, D. J., GELOW, J., THORNBURG, K., OSMOND, C., KAJANTIE, E. & ERIKSSON, J. G. 2010. The early origins of chronic heart failure: impaired placental growth and initiation of insulin resistance in childhood. *Eur J Heart Fail,* 12**,** 819-25.

BAZZONI, G. & DEJANA, E. 2004. Endothelial cell-to-cell junctions: molecular organization and role in vascular homeostasis. *Physiol Rev,* 84**,** 869-901.

BELL, A. W. & EHRHARDT, R. A. 2002. Regulation of placental nutrient transport and implications for fetal growth. *Nutr Res Rev,* 15**,** 211-30.

BENIRSCHKE, K. B., G.J, BAERGEN, R.N. 2012. Pathology of the Human Placenta. *New York,* Springer-Verlag.

BERGERS, G. & SONG, S. 2005. The role of pericytes in blood-vessel formation and maintenance. *Neuro Oncol,* 7**,** 452-64.

BIANCHI, D. W., ZICKWOLF, G. K., WEIL, G. J., SYLVESTER, S. & DEMARIA, M. A. 1996. Male fetal progenitor cells persist in maternal blood for as long as 27 years postpartum. *Proc Natl Acad Sci U S A,* 93**,** 705-8.

BIRBRAIR, A., BORGES, I. D. T., GILSON SENA, I. F., ALMEIDA, G. G., DA SILVA MEIRELLES, L., GONCALVES, R., MINTZ, A. & DELBONO, O. 2017. How Plastic Are Pericytes? *Stem Cells Dev,* 26**,** 1013-1019.

BOCK, D. D., LEE, W. C., KERLIN, A. M., ANDERMANN, M. L., HOOD, G., WETZEL, A. W., YURGENSON, S., SOUCY, E. R., KIM, H. S. & REID, R. C. 2011. Network anatomy and in vivo physiology of visual cortical neurons. *Nature,* 471**,** 177-82.

BONNANS, C., CHOU, J. & WERB, Z. 2014. Remodelling the extracellular matrix in development and disease. *Nat Rev Mol Cell Biol,* 15**,** 786-801.

BROWNBILL, P., MAHENDRAN, D., OWEN, D., SWANSON, P., THORNBURG, K. L., NELSON, D. M. & SIBLEY, C. P. 2000. Denudations as paracellular routes for alphafetoprotein and creatinine across the human syncytiotrophoblast. *Am J Physiol Regul Integr Comp Physiol,* 278**,** R677-83.

BURTON, G. J. 2006. Early placental development. *Placenta,* 27**,** A2-A2.

BURTON, G. J., CHARNOCK-JONES, D. S. & JAUNIAUX, E. 2009. Regulation of vascular growth and function in the human placenta. *Reproduction,* 138**,** 895-902.

BURTON, G. J. & FOWDEN, A. L. 2015. The placenta: a multifaceted, transient organ. *Philos Trans R Soc Lond B Biol Sci,* 370**,** 20140066.

BURTON, G. J. & JAUNIAUX, E. 2018. Development of the Human Placenta and Fetal Heart: Synergic or Independent? *Front Physiol,* 9**,** 373.

BURTON, G. J., WATSON, A. L., HEMPSTOCK, J., SKEPPER, J. N. & JAUNIAUX, E. 2002. Uterine glands provide histiotrophic nutrition for the human fetus during the first trimester of pregnancy. *J Clin Endocrinol Metab,* 87**,** 2954-9.

CASANELLO, P., SCHNEIDER, D., HERRERA, E. A., UAUY, R. & KRAUSE, B. J. 2014. Endothelial heterogeneity in the umbilico-placental unit: DNA methylation as an innuendo of epigenetic diversity. *Front Pharmacol,* 5**,** 49.

CASTELLUCCI, M., KOSANKE, G., VERDENELLI, F., HUPPERTZ, B. & KAUFMANN, P. 2000. Villous sprouting: fundamental mechanisms of human placental development. *Hum Reprod Update,* 6**,** 485-94.

CASTELLUCCI, M., SCHEPER, M., SCHEFFEN, I., CELONA, A. & KAUFMANN, P. 1990a. The Development of the Human Placental Villous Tree. *Anatomy and Embryology,* 181**,** 117-128.

CASTELLUCCI, M., SCHEPER, M., SCHEFFEN, I., CELONA, A. & KAUFMANN, P. 1990b. The development of the human placental villous tree. *Anat Embryol (Berl),* 181**,** 117-28.

CHALLIER, J. C., GALTIER, M., KACEMI, A. & GUILLAUMIN, D. 1999. Pericytes of term human foeto-placental microvessels: ultrastructure and visualization. *Cell Mol Biol (Noisy-le-grand),* 45**,** 89-100.

CHANG, F., FLAVAHAN, S. & FLAVAHAN, N. A. 2017. Impaired activity of adherens junctions contributes to endothelial dilator dysfunction in ageing rat arteries. *J Physiol,* 595**,** 5143-5158.

CHEN, C. P. & APLIN, J. D. 2003. Placental extracellular matrix: gene expression, deposition by placental fibroblasts and the effect of oxygen. *Placenta,* 24**,** 316-25.

CHEN, C. P., BAJORIA, R. & APLIN, J. D. 2002. Decreased vascularization and cell proliferation in placentas of intrauterine growth-restricted fetuses with abnormal umbilical artery flow velocity waveforms. *Am J Obstet Gynecol,* 187**,** 764-9.

CHIRILA, F. V., KHAN, T. K. & ALKON, D. L. 2013. Spatiotemporal complexity of fibroblast networks screens for Alzheimer's disease. *J Alzheimers Dis,* 33**,** 165-76.

CLAYTON, P. E., CIANFARANI, S., CZERNICHOW, P., JOHANNSSON, G., RAPAPORT, R. & ROGOL, A. 2007. Management of the child born small for gestational age through to adulthood: a consensus statement of the International Societies of Pediatric Endocrinology and the Growth Hormone Research Society. *J Clin Endocrinol Metab,* 92**,** 804-10.

CLEAL, J. K., LOFTHOUSE, E. M., SENGERS, B. G. & LEWIS, R. M. 2018a. A systems perspective on placental amino acid transport. *J Physiol,* 596**,** 5511-5522.

CLEAL, J. K., LOFTHOUSE, E. M., SENGERS, B. G. & LEWIS, R. M. 2018b. A systems perspective on placental amino acid transport. *J Physiol*.

COSTA, M. A. 2016. The endocrine function of human placenta: an overview. *Reprod Biomed Online,* 32**,** 14-43.

CRAWFORD, C., KENNEDY-LYDON, T., SPROTT, C., DESAI, T., SAWBRIDGE, L., MUNDAY, J., UNWIN, R. J., WILDMAN, S. S. & PEPPIATT-WILDMAN, C. M. 2012. An intact kidney slice model to investigate vasa recta properties and function in situ. *Nephron Physiol,* 120**,** p17-31.

CROCKER, I. P., TANSINDA, D. M. & BAKER, P. N. 2004. Altered cell kinetics in cultured placental villous explants in pregnancies complicated by pre-eclampsia and intrauterine growth restriction. *J Pathol,* 204**,** 11-8.

DAWE, G. S., TAN, X. W. & XIAO, Z. C. 2007. Cell migration from baby to mother. *Cell Adh Migr,* 1**,** 19-27.

DE RIDDER, M. A., ENGELS, M. A., STIJNEN, T. & HOKKEN-KOELEGA, A. C. 2008. Small for gestational age children without early catch-up growth: spontaneous growth and prediction of height at 8 years. *Horm Res,* 70**,** 203-8.

DEERINCK, T. J., BUSHONG, E. A., LEV-RAM, V., SHU, X., TSIEN, R. Y. & ELLISMAN, M. H. 2010. Enhancing serial block-face scanning electronmicroscopy toenablehighresolution3-Dnanohistologyofcellsandtissues. . *Microsc. Microanal.,* 16**,** 1138–1139.

DEJANA, E., TOURNIER-LASSERVE, E. & WEINSTEIN, B. M. 2009a. The control of vascular integrity by endothelial cell junctions: molecular basis and pathological implications. *Dev Cell,* 16**,** 209-21.

DEJANA, E., TOURNIER-LASSERVE, E. & WEINSTEIN, B. M. 2009b. The Control of Vascular Integrity by Endothelial Cell Junctions: Molecular Basis and Pathological Implications. *Developmental Cell,* 16**,** 209-221.

DEMIR, R., KAUFMANN, P., CASTELLUCCI, M., ERBENGI, T. & KOTOWSKI, A. 1989. Fetal vasculogenesis and angiogenesis in human placental villi. *Acta Anat (Basel),* 136**,** 190-203.

DENK, W. & HORSTMANN, H. 2004. Serial block-face scanning electron microscopy to reconstruct three-dimensional tissue nanostructure. *PLoS Biol,* 2**,** e329.

DEVITT, G., HOWARD, K., MUDHER, A. & MAHAJAN, S. 2018. Raman Spectroscopy: An Emerging Tool in Neurodegenerative Disease Research and Diagnosis. *ACS Chem Neurosci,* 9**,** 404-420.

DIAZ-FLORES, L., GUTIERREZ, R., MADRID, J. F., VARELA, H., VALLADARES, F., ACOSTA, E., MARTIN-VASALLO, P. & DIAZ-FLORES, L., JR. 2009. Pericytes. Morphofunction, interactions and pathology in a quiescent and activated mesenchymal cell niche. *Histol Histopathol,* 24**,** 909-69.

DOROVINI-ZIS, K., PRAMEYA, R. & HUYNH, H. 2003. Isolation and characterization of human brain endothelial cells. *Methods Mol Med,* 89**,** 325-36.

DUASO, J., YANEZ, E., CASTILLO, C., GALANTI, N., CABRERA, G., CORRAL, G., MAYA, J. D., ZULANTAY, I., APT, W. & KEMMERLING, U. 2012.

Reorganization of extracellular matrix in placentas from women with asymptomatic chagas disease: mechanism of parasite invasion or local placental defense? *J Trop Med,* 2012**,** 758357.

EATON, B. M., LEACH, L. & FIRTH, J. A. 1993. Permeability of the fetal villous microvasculature in the isolated perfused term human placenta. *J Physiol,* 463**,** 141-55.

ERIKSSON, J. G., KAJANTIE, E., THORNBURG, K. L., OSMOND, C. & BARKER, D. J. 2011. Mother's body size and placental size predict coronary heart disease in men. *Eur Heart J,* 32**,** 2297-303.

FAKHREJAHANI, E. & TOI, M. 2012. Tumor angiogenesis: pericytes and maturation are not to be ignored. *J Oncol,* 2012**,** 261750.

FARLEY, A. E., GRAHAM, C. H. & SMITH, G. N. 2004. Contractile properties of human placental anchoring villi. *Am J Physiol Regul Integr Comp Physiol,* 287**,** R680-5.

FERREIRA, A. D. F., CUNHA, P. D. S., CARREGAL, V. M., DA SILVA, P. C., DE MIRANDA, M. C., KUNRATH-LIMA, M., DE MELO, M. I. A., FARACO, C. C. F., BARBOSA, J. L., FREZARD, F., RESENDE, V., RODRIGUES, M. A., DE GOES, A. M. & GOMES, D. A. 2017. Extracellular Vesicles from Adipose-Derived Mesenchymal Stem/Stromal Cells Accelerate Migration and Activate AKT Pathway in Human Keratinocytes and Fibroblasts Independently of miR-205 Activity. *Stem Cells Int,* 2017**,** 9841035.

FIRTH, J. A. 2002. Endothelial barriers: from hypothetical pores to membrane proteins. *J Anat,* 200**,** 541-8.

FORGÁCS, G. & NEWMAN, S. 2005. *Biological physics of the developing embryo,* Cambridge, UK ; New York, Cambridge University Press.

FOUDA, G. G., MARTINEZ, D. R., SWAMY, G. K. & PERMAR, S. R. 2018. The Impact of IgG transplacental transfer on early life immunity. *Immunohorizons,* 2**,** 14-25.

FRANCO, M., ROSWALL, P., CORTEZ, E., HANAHAN, D. & PIETRAS, K. 2011. Pericytes promote endothelial cell survival through induction of autocrine VEGF-A signaling and Bcl-w expression. *Blood,* 118**,** 2906-17.

FROEN, J. F., GARDOSI, J. O., THURMANN, A., FRANCIS, A. & STRAY-PEDERSEN, B. 2004. Restricted fetal growth in sudden intrauterine unexplained death. *Acta Obstet Gynecol Scand,* 83**,** 801-7.

GLUCKMAN, P. D., HANSON, M. A., COOPER, C. & THORNBURG, K. L. 2008. Effect of in utero and early-life conditions on adult health and disease. *N Engl J Med,* 359**,** 61-73.

GLYN, M. C. & WARD, B. J. 2000. Contraction in cardiac endothelial cells contributes to changes in capillary dimensions following ischaemia and reperfusion. *Cardiovasc Res,* 48**,** 346-56.

GODFREY, K. M. 2002. The role of the placenta in fetal programming-a review. *Placenta,* 23 Suppl A**,** S20-7.

GOGGIN, P. M., ZYGALAKIS, K. C., OREFFO, R. O. & SCHNEIDER, P. 2016. High-resolution 3D imaging of osteocytes and computational modelling in mechanobiology: insights on bone development, ageing, health and disease. *Eur Cell Mater,* 31**,** 264-95.

GUDE, N. M., ROBERTS, C. T., KALIONIS, B. & KING, R. G. 2004. Growth and function of the normal human placenta. *Thromb Res,* 114**,** 397-407.

HAEUSSNER, E., ASCHAUER, B., BURTON, G. J., HUPPERTZ, B., EDLER VON KOCH, F., MULLER-STARCK, J., SALAFIA, C., SCHMITZ, C. & FRANK, H. G. 2015. Does 2D-Histologic identification of villous types of human placentas at birth enable sensitive and reliable interpretation of 3D structure? *Placenta,* 36**,** 1425-32.

HALL, A. P. 2006. Review of the pericyte during angiogenesis and its role in cancer and diabetic retinopathy. *Toxicol Pathol,* 34**,** 763-75.

HARRIS, J. R. 2000. The future of transmission electron microscopy (TEM) in biology and medicine. *Micron,* 31**,** 1-3.

HAYWORTH, K. J., MORGAN, J. L., SCHALEK, R., BERGER, D. R., HILDEBRAND, D. G. & LICHTMAN, J. W. 2014. Imaging ATUM ultrathin section libraries with WaferMapper: a multi-scale approach to EM reconstruction of neural circuits. *Front Neural Circuits,* 8**,** 68.

HEMACHANDRA, A. H., KLEBANOFF, M. A., DUGGAN, A. K., HARDY, J. B. & FURTH, S. L. 2006. The association between intrauterine growth restriction in the full-term infant and high blood pressure at age 7 years: results from the Collaborative Perinatal Project. *Int J Epidemiol,* 35**,** 871-7.

HEPPELMANN, B., MESSLINGER, K. & SCHMIDT, R. F. 1989. Serial sectioning, electron microscopy, and three-dimensional reconstruction of fine nerve fibres and other extended objects. *J Microsc,* 156**,** 163-72.

HUNG, T. H., SKEPPER, J. N. & BURTON, G. J. 2001. In vitro ischemia-reperfusion injury in term human placenta as a model for oxidative stress in pathological pregnancies. *Am J Pathol,* 159**,** 1031-43.

ICHIMURA, K., MIYAZAKI, N., SADAYAMA, S., MURATA, K., KOIKE, M., NAKAMURA, K., OHTA, K. & SAKAI, T. 2015. Three-dimensional architecture of podocytes revealed by block-face scanning electron microscopy. *Sci Rep,* 5**,** 8993.

ILIC, D., KAPIDZIC, M. & GENBACEV, O. 2008. Isolation of human placental fibroblasts. *Curr Protoc Stem Cell Biol,* Chapter 1**,** Unit 1C 6.

INGMAN, K., COOKSON, V. J., JONES, C. J. & APLIN, J. D. 2010. Characterisation of Hofbauer cells in first and second trimester placenta: incidence, phenotype, survival in vitro and motility. *Placenta,* 31**,** 535-44.

IRIE, K., SHIMIZU, K., SAKISAKA, T., IKEDA, W. & TAKAI, Y. 2004. Roles and modes of action of nectins in cell-cell adhesion. *Semin Cell Dev Biol,* 15**,** 643-56.

JAUNIAUX, E., GULBIS, B. & BURTON, G. J. 2003. Physiological implications of the materno-fetal oxygen gradient in human early pregnancy. *Reprod Biomed Online,* 7**,** 250-3.

JONES, C. J., CHOUDHURY, R. H. & APLIN, J. D. 2015a. Functional changes in Hofbauer cell glycobiology during human pregnancy. *Placenta,* 36**,** 1130-7.

JONES, C. J. & DESOYE, G. 2011. A new possible function for placental pericytes. *Cells Tissues Organs,* 194**,** 76-84.

JONES, C. J. & FOX, H. 1991. Ultrastructure of the normal human placenta. *Electron Microsc Rev,* 4**,** 129-78.

JONES, C. J., HARRIS, L. K., WHITTINGHAM, J., APLIN, J. D. & MAYHEW, T. M. 2008. A re-appraisal of the morphophenotype and basal lamina coverage of cytotrophoblasts in human term placenta. *Placenta,* 29**,** 215-9.

JONES, S., BISCHOF, H., LANG, I., DESOYE, G., GREENWOOD, S. L., JOHNSTONE, E. D., WAREING, M., SIBLEY, C. P. & BROWNBILL, P. 2015b. Dysregulated flow-mediated vasodilatation in the human placenta in fetal growth restriction. *J Physiol,* 593**,** 3077-92.

JONKMAN, J. & BROWN, C. M. 2015. Any Way You Slice It-A Comparison of Confocal Microscopy Techniques. *J Biomol Tech,* 26**,** 54-65.

JOSEPH, O. 2017. *Embryology and Histology of Blood vessels* [Online]. Available: https://www.slideshare.net/OrlandoJoseph1/embryology-and-histology-of-bloodvessels [Accessed 1/02/2019 2019].

JUNAID, T. O., BROWNBILL, P., CHALMERS, N., JOHNSTONE, E. D. & APLIN, J. D. 2014. Fetoplacental vascular alterations associated with fetal growth restriction. *Placenta,* 35**,** 808-15.

KARIMU, A. L. & BURTON, G. J. 1995. Human term placental capillary endothelial cell specialization: a morphometric study. *Placenta,* 16**,** 93-9.

KAUFMANN A., L. M., MATERN P., MORRISON-GRAHAM K., QUICK D., RUNYEON J. 2019. The Cardiovascular System: Blood Vessels and Circulation. *In:* BIGA, L. M., DAWSON, S. HARWELL A., HOPKINS R. (ed.) *Anatomy and Physiology.* 2019 ed. Simple Book Production: Pressbooks.com.

KAUFMANN, P., MAYHEW, T. M. & CHARNOCK-JONES, D. S. 2004. Aspects of human fetoplacental vasculogenesis and angiogenesis. II. Changes during normal pregnancy. *Placenta,* 25**,** 114-26.

KAUFMANN, P., SEN, D. K. & SCHWEIKHART, G. 1979. Classification of human placental villi. I. Histology. *Cell Tissue Res,* 200**,** 409-23.

KAUFMANN, P., STARK, J. & STEGNER, H. E. 1977. The villous stroma of the human placenta. I. The ultrastructure of fixed connective tissue cells. *Cell Tissue Res,* 177**,** 105-21.

KESSLER, D., DETHLEFSEN, S., HAASE, I., PLOMANN, M., HIRCHE, F., KRIEG, T. & ECKES, B. 2001. Fibroblasts in mechanically stressed collagen lattices assume a "synthetic" phenotype. *Journal of Biological Chemistry,* 276**,** 36575-36585.

KNOTT, G., MARCHMAN, H., WALL, D. & LICH, B. 2008. Serial section scanning electron microscopy of adult brain tissue using focused ion beam milling. *J Neurosci,* 28**,** 2959-64.

KOHNEN, G., KERTSCHANSKA, S., DEMIR, R. & KAUFMANN, P. 1996. Placental villous stroma as a model system for myofibroblast differentiation. *Histochem Cell Biol,* 105**,** 415-29.

KOLKA, C. M. & BERGMAN, R. N. 2012. The Barrier Within: Endothelial Transport of Hormones. *Physiology,* 27**,** 237-247.

KURZEN, H., MANNS, S., DANDEKAR, G., SCHMIDT, T., PRATZEL, S. & KRALING, B. M. 2002. sync. *J Invest Dermatol,* 119**,** 143-53.

LAFONTANT, P. J., BEHZAD, A. R., BROWN, E., LANDRY, P., HU, N. & BURNS, A. R. 2013. Cardiac myocyte diversity and a fibroblast network in the junctional region of the zebrafish heart revealed by transmission and serial block-face scanning electron microscopy. *PLoS One,* 8**,** e72388.

LAMPUGNANI, M. G. 2012. Endothelial cell-to-cell junctions: adhesion and signaling in physiology and pathology. *Cold Spring Harb Perspect Med,* 2.

LAMPUGNANI, M. G., CORADA, M., CAVEDA, L., BREVIARIO, F., AYALON, O., GEIGER, B. & DEJANA, E. 1995. The molecular organization of endothelial cell to cell junctions: differential association of plakoglobin, beta-catenin, and alpha-catenin with vascular endothelial cadherin (VE-cadherin). *J Cell Biol,* 129**,** 203-17.

LANG, I., HARTMANN, M., BLASCHITZ, A., DOHR, G., SKOFITSCH, G. & DESOYE, G. 1993. Immunohistochemical evidence for the heterogeneity of maternal and fetal vascular endothelial cells in human full-term placenta. *Cell Tissue Res,* 274**,** 211-8.

LANG, I., PABST, M. A., HIDEN, U., BLASCHITZ, A., DOHR, G., HAHN, T. & DESOYE, G. 2003. Heterogeneity of microvascular endothelial cells isolated from human term placenta and macrovascular umbilical vein endothelial cells. *Eur J Cell Biol,* 82**,** 163-73.

LANGEVIN, H. M., CORNBROOKS, C. J. & TAATJES, D. J. 2004. Fibroblasts form a body-wide cellular network. *Histochem Cell Biol,* 122**,** 7-15.

LAWN, J. E., COUSENS, S., ZUPAN, J. & LANCET NEONATAL SURVIVAL STEERING, T. 2005. 4 million neonatal deaths: when? Where? Why? *Lancet,* 365**,** 891-900.

LE BIHAN, O., DECOSSAS, M., GONTIER, E., GERBOD-GIANNONE, M. C. & LAMBERT, O. 2015. Visualization of adherent cell monolayers by cryo-electron microscopy: A snapshot of endothelial adherens junctions. *J Struct Biol,* 192**,** 470-477.

LEACH, L. 2002. The phenotype of the human materno-fetal endothelial barrier: molecular occupancy of paracellular junctions dictate permeability and angiogenic plasticity. *J Anat,* 200**,** 599-606.

LEACH, L. & FIRTH, J. A. 1992. Fine structure of the paracellular junctions of terminal villous capillaries in the perfused human placenta. *Cell Tissue Res,* 268**,** 447-52.

LEACH, L., LAMMIMAN, M. J., BABAWALE, M. O., HOBSON, S. A., BROMILOU, B., LOVAT, S. & SIMMONDS, M. J. 2000. Molecular organization of tight and adherens junctions in the human placental vascular tree. *Placenta,* 21**,** 547-57.

LEVIN, B. D., PADGETT, E., CHEN, C. C., SCOTT, M. C., XU, R., THEIS, W., JIANG, Y., YANG, Y., OPHUS, C., ZHANG, H., HA, D. H., WANG, D., YU, Y., ABRUNA, H. D., ROBINSON, R. D., ERCIUS, P., KOURKOUTIS, L. F., MIAO, J., MULLER, D. A. & HOVDEN, R. 2016. Nanomaterial datasets to advance tomography in scanning transmission electron microscopy. *Sci Data,* 3**,** 160041.

LEWIS, R. M., BROOKS, S., CROCKER, I. P., GLAZIER, J., HANSON, M. A., JOHNSTONE, E. D., PANITCHOB, N., PLEASE, C. P., SIBLEY, C. P., WIDDOWS, K. L. & SENGERS, B. G. 2013. Review: Modelling placental amino acid transfer--from transporters to placental function. *Placenta,* 34 Suppl**,** S46-51.

LICHTMAN, J. W. & DENK, W. 2011. The big and the small: challenges of imaging the brain's circuits. *Science,* 334**,** 618-23.

LIEVANO, S., ALARCON, L., CHAVEZ-MUNGUIA, B. & GONZALEZ-MARISCAL, L. 2006. Endothelia of term human placentae display diminished expression of tight junction proteins during preeclampsia. *Cell Tissue Res,* 324**,** 433-48.

MARCOS, R., BRAGANCA, B. & FONTES-SOUSA, A. P. 2015. Image Analysis or Stereology: Which to Choose for Quantifying Fibrosis? *J Histochem Cytochem,* 63**,** 734-6.

MARCU, R., CHOI, Y. J., XUE, J., FORTIN, C. L., WANG, Y., NAGAO, R. J., XU, J., MACDONALD, J. W., BAMMLER, T. K., MURRY, C. E., MUCZYNSKI, K., STEVENS, K. R., HIMMELFARB, J., SCHWARTZ, S. M. & ZHENG, Y. 2018. Human Organ-Specific Endothelial Cell Heterogeneity. *iScience,* 4**,** 20-35.

MARTINEZ-LEMUS, L. A. 2012. The dynamic structure of arterioles. *Basic Clin Pharmacol Toxicol,* 110**,** 5-11.

MASTERSON, E., EDELHAUSER, H. F. & VAN HORN, D. L. 1977. The role of thyroid hormone in the development of the chick corneal endothelium and epithelium. *Invest Ophthalmol Vis Sci,* 16**,** 105-15.

MATHIISEN, T. M., LEHRE, K. P., DANBOLT, N. C. & OTTERSEN, O. P. 2010. The perivascular astroglial sheath provides a complete covering of the brain microvessels: an electron microscopic 3D reconstruction. *Glia,* 58**,** 1094-103.

MATSUDA, Y., OGAWA, M., NAKAI, A., HAYASHI, M., SATOH, S. & MATSUBARA, S. 2015. Fetal/Placental weight ratio in term Japanese pregnancy: its difference among gender, parity, and infant growth. *Int J Med Sci,* 12**,** 301-5.

MAYHEW, T. M. 2006. Stereology and the placenta: where's the point? -- a review. *Placenta,* 27 Suppl A**,** S17-25.

MAYHEW, T. M. 2009. A stereological perspective on placental morphology in normal and complicated pregnancies. *J Anat,* 215**,** 77-90.

MAYHEW, T. M., JENKINS, H., TODD, B. & CLIFTON, V. L. 2008. Maternal asthma and placental morphometry: effects of severity, treatment and fetal sex. *Placenta,* 29**,** 366-73.

MAYHEW, T. M., WIJESEKARA, J., BAKER, P. N. & ONG, S. S. 2004. Morphometric evidence that villous development and fetoplacental angiogenesis are compromised by intrauterine growth restriction but not by pre-eclampsia. *Placenta,* 25**,** 829-33.

MCNEILLY, C. M., BANES, A. J., BENJAMIN, M. & RALPHS, J. R. 1996. Tendon cells in vivo form a three dimensional network of cell processes linked by gap junctions. *J Anat,* 189 (Pt 3)**,** 593-600.

MILLER, R. K., GENBACEV, O., TURNER, M. A., APLIN, J. D., CANIGGIA, I. & HUPPERTZ, B. 2005. Human placental explants in culture: approaches and assessments. *Placenta,* 26**,** 439-48.

MORI, M., ISHIKAWA, G., LUO, S. S., MISHIMA, T., GOTO, T., ROBINSON, J. A., MATSUBARA, S., TAKESHITA, T., KATAOKA, H. & TAKIZAWA, T. 2007a. The cytotrophoblast layer of human chorionic villi becomes thinner but maintains its structural integrity during gestation. *Biology of Reproduction,* 76**,** 164-172.

MORI, M., ISHIKAWA, G., LUO, S. S., MISHIMA, T., GOTO, T., ROBINSON, J. M., MATSUBARA, S., TAKESHITA, T., KATAOKA, H. & TAKIZAWA, T. 2007b. The cytotrophoblast layer of human chorionic villi becomes thinner but maintains its structural integrity during gestation. *Biol Reprod,* 76**,** 164-72.

MOUTON, P. R. 2002. *Principles and practices of unbiased stereology : an introduction for bioscientists,* Baltimore, Johns Hopkins University Press.

MULLER, W. A. 2014. How endothelial cells regulate transmigration of leukocytes in the inflammatory response. *Am J Pathol,* 184**,** 886-96.

MYREN, M., MOSE, T., MATHIESEN, L. & KNUDSEN, L. E. 2007. The human placenta--an alternative for studying foetal exposure. *Toxicol In Vitro,* 21**,** 1332-40.

NAKAJIMA, A., KURIHARA, H., YAGITA, H., OKUMURA, K. & NAKANO, H. 2008. Mitochondrial Extrusion through the cytoplasmic vacuoles during cell death. *J Biol Chem,* 283**,** 24128-35.

NELSON, D. M., CROUCH, E. C., CURRAN, E. M. & FARMER, D. R. 1990. Trophoblast interaction with fibrin matrix. Epithelialization of perivillous fibrin deposits as a mechanism for villous repair in the human placenta. *Am J Pathol,* 136**,** 855-65.

NIKOLOV, S. D. & SCHIEBLER, T. H. 1973. [Fetal blood vessel system of the human full-term placenta]. *Z Zellforsch Mikrosk Anat,* 139**,** 333-50.

NORRIS, J. L. & CAPRIOLI, R. M. 2013. Analysis of tissue specimens by matrix-assisted laser desorption/ionization imaging mass spectrometry in biological and clinical research. *Chem Rev,* 113**,** 2309-42.

ODEGARD, R. A., VATTEN, L. J., NILSEN, S. T., SALVESEN, K. A. & AUSTGULEN, R. 2000. Preeclampsia and fetal growth. *Obstet Gynecol,* 96**,** 950-5.

OHLSSON, R., FALCK, P., HELLSTROM, M., LINDAHL, P., BOSTROM, H., FRANKLIN, G., AHRLUND-RICHTER, L., POLLARD, J., SORIANO, P. & BETSHOLTZ, C. 1999. PDGFB regulates the development of the labyrinthine layer of the mouse fetal placenta. *Dev Biol,* 212**,** 124-36.

OSMOND, C. & BARKER, D. J. 2000. Fetal, infant, and childhood growth are predictors of coronary heart disease, diabetes, and hypertension in adult men and women. *Environ Health Perspect,* 108 Suppl 3**,** 545-53.

PALAIOLOGOU, E., GOGGIN, P., CHATELET, D. S., LOFTHOUSE, E. M., TORRENS, C., SENGERS, B. G., CLEAL, J. K., PAGE, A. & LEWIS, R. M. 2017. Serial block-face scanning electron microscopy of erythrocytes protruding through the human placental syncytiotrophoblast. *J Anat,* 231**,** 634-637.

RACUSEN, L. C. 1998. Epithelial cell shedding in acute renal injury. *Clin Exp Pharmacol Physiol,* 25**,** 273-5.

RANDLES, M. J., COLLINSON, S., STARBORG, T., MIRONOV, A., KRENDEL, M., KONIGSHAUSEN, E., SELLIN, L., ROBERTS, I. S., KADLER, K. E., MINER, J. H. & LENNON, R. 2016. Three-dimensional electron microscopy reveals the evolution of glomerular barrier injury. *Sci Rep,* 6**,** 35068.

RAVIKANTH, M., SOUJANYA, P., MANJUNATH, K., SARASWATHI, T. R. & RAMACHANDRAN, C. R. 2011. Heterogenecity of fibroblasts. *J Oral Maxillofac Pathol,* 15**,** 247-50.

REGLERO-REAL, N., COLOM, B., BODKIN, J. V. & NOURSHARGH, S. 2016. Endothelial Cell Junctional Adhesion Molecules: Role and Regulation of Expression in Inflammation. *Arterioscler Thromb Vasc Biol,* 36**,** 2048-57.

RESNIK, R. 2002. Intrauterine growth restriction. *Obstet Gynecol,* 99**,** 490-6.

REVEL, J. P., NAPOLITANO, L. & FAWCETT, D. W. 1960. Identification of glycogen in electron micrographs of thin tissue sections. *J Biophys Biochem Cytol,* 8**,** 575-89.

RILLA, K., MUSTONEN, A. M., ARASU, U. T., HARKONEN, K., MATILAINEN, J. & NIEMINEN, P. 2019. Extracellular vesicles are integral and functional components of the extracellular matrix. *Matrix Biol,* 75-76**,** 201-219.

ROBIN, C., BOLLEROT, K., MENDES, S., HAAK, E., CRISAN, M., CERISOLI, F., LAUW, I., KAIMAKIS, P., JORNA, R., VERMEULEN, M., KAYSER, M., VAN DER LINDEN, R., IMANIRAD, P., VERSTEGEN, M., NAWAZ-YOUSAF, H., PAPAZIAN, N., STEEGERS, E., CUPEDO, T. & DZIERZAK, E. 2009. Human placenta is a potent hematopoietic niche containing hematopoietic stem and progenitor cells throughout development. *Cell Stem Cell,* 5**,** 385-95.

RONNEBERGER, O., FISCHER, P. & BROX, T. 2015. U-Net: Convolutional Networks for Biomedical Image Segmentation. *Medical Image Computing and Computer-Assisted Intervention, Pt Iii,* 9351**,** 234-241.

ROSEBOOM, T. J., VAN DER MEULEN, J. H., RAVELLI, A. C., OSMOND, C., BARKER, D. J. & BLEKER, O. P. 2001. Effects of prenatal exposure to the Dutch famine on adult disease in later life: an overview. *Twin Res,* 4**,** 293-8.

ROSEN, S. & STILLMAN, I. E. 2008. Acute tubular necrosis is a syndrome of physiologic and pathologic dissociation. *J Am Soc Nephrol,* 19**,** 871-5.

RUSKA, E. 1980. The early development of electron lenses and electron microscopy. *Microsc Acta Suppl***,** 1-140.

SATI, L., DEMIR, A. Y., SARIKCIOGLU, L. & DEMIR, R. 2008. Arrangement of collagen fibers in human placental stem villi. *Acta Histochem,* 110**,** 371-9.

SCHINDELIN, J., ARGANDA-CARRERAS, I., FRISE, E., KAYNIG, V., LONGAIR, M., PIETZSCH, T., PREIBISCH, S., RUEDEN, C., SAALFELD, S., SCHMID, B., TINEVEZ, J. Y., WHITE, D. J., HARTENSTEIN, V., ELICEIRI, K., TOMANCAK, P. & CARDONA, A. 2012. Fiji: an open-source platform for biological-image analysis. *Nat Methods,* 9**,** 676-82.

SCHNEIDER, H. 1996. Ontogenic changes in the nutritive function of the placenta. *Placenta,* 17**,** 15-26.

SCHRODER, J. 1975. Transplacental passage of blood cells. *J Med Genet,* 12**,** 230-42.

SEN, D. K., KAUFMANN, P. & SCHWEIKHART, G. 1979. Classification of human placental villi. II. Morphometry. *Cell Tissue Res,* 200**,** 425-34.

SEVAL, Y., KORGUN, E. T. & DEMIR, R. 2007. Hofbauer cells in early human placenta: possible implications in vasculogenesis and angiogenesis. *Placenta,* 28**,** 841-5.

SHAMI, G. J., CHENG, D., HUYNH, M., VREULS, C., WISSE, E. & BRAET, F. 2016. 3-D EM exploration of the hepatic microarchitecture - lessons learned from large-volume in situ serial sectioning. *Sci Rep,* 6**,** 36744.

SHINDO, S., TAKAGI, A. & WHITTEMORE, A. D. 1987. Improved patency of collagen-impregnated grafts after in vitro autogenous endothelial cell seeding. *J Vasc Surg,* 6**,** 325-32.

SIAUVE, N., CHALOUHI, G. E., DELOISON, B., ALISON, M., CLEMENT, O., VILLE, Y. & SALOMON, L. J. 2015. Functional imaging of the human placenta with magnetic resonance. *Am J Obstet Gynecol,* 213**,** S103-14.

SIBLEY, C. P. 2009. Understanding placental nutrient transfer--why bother? New biomarkers of fetal growth. *J Physiol,* 587**,** 3431-40.

SIBLEY, C. P., COAN, P. M., FERGUSON-SMITH, A. C., DEAN, W., HUGHES, J., SMITH, P., REIK, W., BURTON, G. J., FOWDEN, A. L. & CONSTANCIA, M. 2004. Placental-specific insulin-like growth factor 2 (Igf2) regulates the diffusional exchange characteristics of the mouse placenta. *Proc Natl Acad Sci U S A,* 101**,** 8204-8.

SIMNER, C., NOVAKOVIC, B., LILLYCROP, K. A., BELL, C. G., HARVEY, N. C., COOPER, C., SAFFERY, R., LEWIS, R. M. & CLEAL, J. K. 2017. DNA methylation of amino acid transporter genes in the human placenta. *Placenta,* 60**,** 64-73.

SIMS, D. E. 1986. The pericyte--a review. *Tissue Cell,* 18**,** 153-74.

STANIROWSKI, P. J., SZUKIEWICZ, D., PYZLAK, M., ABDALLA, N., SAWICKI, W. & CENDROWSKI, K. 2017. Impact of pre-gestational and gestational diabetes mellitus on the expression of glucose transporters GLUT-1, GLUT-4 and GLUT-9 in human term placenta. *Endocrine,* 55**,** 799-808.

STIK, G., CREQUIT, S., PETIT, L., DURANT, J., CHARBORD, P., JAFFREDO, T. & DURAND, C. 2017. Extracellular vesicles of stromal origin target and support hematopoietic stem and progenitor cells. *J Cell Biol,* 216**,** 2217-2230.

STRID, H., BUCHT, E., JANSSON, T., WENNERGREN, M. & POWELL, T. L. 2003. ATP dependent Ca2+ transport across basal membrane of human syncytiotrophoblast in pregnancies complicated by intrauterine growth restriction or diabetes. *Placenta,* 24**,** 445-52.

TAKEMURA, S. Y., BHARIOKE, A., LU, Z., NERN, A., VITALADEVUNI, S., RIVLIN, P. K., KATZ, W. T., OLBRIS, D. J., PLAZA, S. M., WINSTON, P., ZHAO, T., HORNE, J. A., FETTER, R. D., TAKEMURA, S., BLAZEK, K., CHANG, L. A., OGUNDEYI, O., SAUNDERS, M. A., SHAPIRO, V., SIGMUND, C., RUBIN, G. M., SCHEFFER, L. K., MEINERTZHAGEN, I. A. & CHKLOVSKII, D. B. 2013. A visual motion detection circuit suggested by Drosophila connectomics. *Nature,* 500**,** 175-81.

TAKIZAWA, T. & ROBINSON, J. M. 2006. Correlative microscopy of ultrathin cryosections in placental research. *Methods Mol Med,* 121**,** 351-69.

TEASDALE, F. & JEAN-JACQUES, G. 1985. Morphometric evaluation of the microvillous surface enlargement factor in the human placenta from mid-gestation to term. *Placenta,* 6**,** 375-81.

THOMPSON, L. P., PENCE, L., PINKAS, G., SONG, H. & TELUGU, B. P. 2016. Placental Hypoxia During Early Pregnancy Causes Maternal Hypertension and Placental Insufficiency in the Hypoxic Guinea Pig Model. *Biol Reprod,* 95**,** 128.

THORNBURG, K. L., KOLAHI, K., PIERCE, M., VALENT, A., DRAKE, R. & LOUEY, S. 2016. Biological features of placental programming. *Placenta,* 48 Suppl 1**,** S47-S53.

TONG, M. & CHAMLEY, L. W. 2015. Placental extracellular vesicles and feto-maternal communication. *Cold Spring Harb Perspect Med,* 5**,** a023028.

TURCO, M. Y., GARDNER, L., KAY, R. G., HAMILTON, R. S., PRATER, M., HOLLINSHEAD, M. S., MCWHINNIE, A., ESPOSITO, L., FERNANDO, R.,

SKELTON, H., REIMANN, F., GRIBBLE, F. M., SHARKEY, A., MARSH, S. G. E., O'RAHILLY, S., HEMBERGER, M., BURTON, G. J. & MOFFETT, A. 2018. Trophoblast organoids as a model for maternal-fetal interactions during human placentation. *Nature,* 564**,** 263-267.

TZIMA, E., IRANI-TEHRANI, M., KIOSSES, W. B., DEJANA, E., SCHULTZ, D. A., ENGELHARDT, B., CAO, G., DELISSER, H. & SCHWARTZ, M. A. 2005. A mechanosensory complex that mediates the endothelial cell response to fluid shear stress. *Nature,* 437**,** 426-31.

UGELE, B. & LANGE, F. 2001. Isolation of endothelial cells from human placental microvessels: effect of different proteolytic enzymes on releasing endothelial cells from villous tissue. *In Vitro Cell Dev Biol Anim,* 37**,** 408-13.

VAILLANCOURT, C. & LAFOND, J. 2009. Human embryogenesis: overview. *Methods Mol Biol,* 550**,** 3-7.

VANNI, S. 2017. Intracellular Lipid Droplets: From Structure to Function. *Lipid Insights,* 10**,** 1178635317745518.

VEDMEDOVSKA, N., REZEBERGA, D., TEIBE, U., MELDERIS, I. & DONDERS, G. G. 2011. Placental pathology in fetal growth restriction. *Eur J Obstet Gynecol Reprod Biol,* 155**,** 36-40.

WALKER, N., FILIS, P., O'SHAUGHNESSY, P. J., BELLINGHAM, M. & FOWLER, P. A. 2019. Nutrient transporter expression in both the placenta and fetal liver are affected by maternal smoking. *Placenta,* 78**,** 10-17.

WALLACE, J. M., BHATTACHARYA, S. & HORGAN, G. W. 2013. Gestational age, gender and parity specific centile charts for placental weight for singleton deliveries in Aberdeen, UK. *Placenta,* 34**,** 269-74.

WALLEZ, Y. & HUBER, P. 2008. Endothelial adherens and tight junctions in vascular homeostasis, inflammation and angiogenesis. *Biochim Biophys Acta,* 1778**,** 794-809.

WELSH, J. A., SCORLETTI, E., CLOUGH, G. F., ENGLYST, N. A. & BYRNE, C. D. 2018. Leukocyte extracellular vesicle concentration is inversely associated with liver fibrosis severity in NAFLD. *J Leukoc Biol*.

WILCOX, A. J., BAIRD, D. D. & WEINBERG, C. R. 1999. Time of implantation of the conceptus and loss of pregnancy. *N Engl J Med,* 340**,** 1796-9.

WOLBURG, H., NOELL, S., MACK, A., WOLBURG-BUCHHOLZ, K. & FALLIER-BECKER, P. 2009. Brain endothelial cells and the glio-vascular complex. *Cell Tissue Res,* 335**,** 75-96.

WRIGHT, S. J. & WRIGHT, D. J. 2002. Introduction to confocal microscopy. *Methods Cell Biol,* 70**,** 1-85.

XU, H., SIMONET, F. & LUO, Z. C. 2010. Optimal birth weight percentile cut-offs in defining small- or large-for-gestational-age. *Acta Paediatr,* 99**,** 550-5.

YAMAZAKI, Y., SHINOHARA, M., SHINOHARA, M., YAMAZAKI, A., MURRAY, M. E., LIESINGER, A. M., HECKMAN, M. G., LESSER, E. R., PARISI, J. E., PETERSEN, R. C., DICKSON, D. W., KANEKIYO, T. & BU, G. 2019. Selective loss of cortical endothelial tight junction proteins during Alzheimer's disease progression. *Brain,* 142**,** 1077-1092.

YANG, X., CHANG, Y. & WEI, W. 2016. Endothelial Dysfunction and Inflammation: Immunity in Rheumatoid Arthritis. *Mediators Inflamm,* 2016**,** 6813016.

YUE, B. 2014. Biology of the extracellular matrix: an overview. *J Glaucoma,* 23**,** S20-3.

Online resources
https://www1.udel.edu/biology/Wags/histopage/empage/ecu/ecu.htm   (Accessed: 26/01/2019)